

学 位 論 文

Origin of HIMU and EM Sources
in the Polynesian Plume Province
Inferred from Elemental and Isotopic Studies

化学・同位体組成に基づいたHIMU及びEM

マグマ源の成因に関する研究

— ポリネシア地域のホットスポット火山を例として

平成8年12月博士(理学)申請

東京大学大学院理学系研究科

地球惑星物理学専攻

羽 生 毅

学位論文

Origin of HIMU and EM Sources
in the Polynesian Plume Province
Inferred from Elemental and Isotopic Studies

化学・同位体組成に基づいた HIMU 及び EM
マグマ源の成因に関する研究
—ポリネシア地域のホットスポット火山を例として—

平成 8 年 12 月博士（理学）申請

東京大学大学院理学系研究科
地球惑星物理学専攻
羽生 毅

Abstract

Sr and Nd isotopes, trace and rare earth elements and noble gas isotopes for hotspot magmas in the Polynesian region were analyzed in order to investigate the origin of HIMU and EM sources. HIMU and EM are defined by their Sr, Nd and Pb isotope ratios and they have been considered to be distinct mantle components from the upper mantle material. What to be solved about the problems on HIMU and EM sources are the origin and time of their formation, their location in the mantle, and their survival for long period in the stirring mantle.

For this purpose, I analyzed noble gas isotopes for HIMU and EM magmas from the Polynesian Islands in the South Pacific, which have not been studied in detail before, together with the analyses of Sr and Nd isotopes, trace and rare earth elements by using cpx phenocrysts and some whole rock samples. This is the first attempt to analyze both solid and noble gas isotopes by using the same phenocryst samples in order to study HIMU and EM sources, which makes it possible to interpret their relationships more clearly.

It has been revealed from noble gas analyses that $^3\text{He}/^4\text{He}$ ratios of HIMU samples (6.8Ra) are quite uniform and slightly lower than that of MORB (around 8.6Ra). On the other hand, $^3\text{He}/^4\text{He}$ of EM samples in the Polynesian region is variable and higher than that of MORB. Anomalous noble gas abundance patterns have been found from HIMU samples. It is noteworthy that HIMU samples show He and Ne depletion and Kr and Xe enrichment relative to those of the atmosphere, which provides another key to infer the origin of the HIMU source.

By using cpx samples, it is possible to analyze both noble gas isotopes and Sr and Nd isotopes. Further, it makes it possible to obtain essential magmatic information on Sr and Nd isotopes with least secondary effects such as seawater contamination to magmas. It has been revealed that $^{87}\text{Sr}/^{86}\text{Sr}$ ratios of HIMU samples are similar to MORB and they are quite uniform. The small variation of $^{143}\text{Nd}/^{144}\text{Nd}$ among HIMU

samples is explained by mixing of the HIMU end-member and the MORB source. ϵ_{Nd} of the HIMU end-member is constrained to be less than +3.3. The correlation between ϵ_{Nd} and trace elemental ratios such as Pb/Ta gives further information on HIMU and EM sources.

The origin of HIMU and EM sources has been discussed by using the data obtained in this study combined together with the constraint derived from the Pb isotope data so far reported. Lower $^3\text{He}/^4\text{He}$ of HIMU than that of MORB requires relatively high time-integrated $(\text{U}+\text{Th})/^3\text{He}$ for the HIMU source, which suggests that the HIMU source was related to recycled materials which were once located near the Earth's surface. The Sr isotope signature of HIMU requires uniform and relatively low time-integrated Rb/Sr, while very high Pb isotope ratios (e.g., $^{206}\text{Pb}/^{204}\text{Pb} > 21.0$) indicate elevated $(\text{U}+\text{Th})/\text{Pb}$ ratios for HIMU sources. Correlation between Pb/Ta and ϵ_{Nd} indicates that Pb is more depleted than Ta in HIMU samples.

Such elemental fractionation would occur by high temperature hydrothermal effects. Studies of hydrothermal fluids and ophiolites suggest that Pb would be dramatically leached from oceanic crusts by high temperature hydrothermal fluids comparing other elements. Combining the constraints of Sr, Pb isotopes with those derived from some trace elements, the preferred model proposed in this study is that the HIMU source was the ancient less-altered oceanic crusts which suffered only from high temperature hydrothermal circulation and subducted without dehydration. This model is consistent with the unique feature of noble gas abundance patterns found in HIMU samples because, Ne depletion and Kr, Xe enrichment are usually found in abyssal basalts and sediments.

The problem of decoupling between ϵ_{Nd} and $^{87}\text{Sr}/^{86}\text{Sr}$ which is characteristic for HIMU magmas can not be explained by the model described above alone. This requires that the ancient MORB source in the upper mantle at the time of the HIMU source formation was more enriched than the present one regarding Sm/Nd. Based on the first-

order transport model to express the depletion history of the upper mantle, the age of HIMU source formation has been estimated to be around 2Ga or older.

To explain the value of $^3\text{He}/^4\text{He}$ for HIMU samples (6.8Ra) observed in this study, the He open system model is introduced which includes the effects of ^4He production and diffusion between HIMU source rock and surrounding mantle. As a result for this model, the thickness of the HIMU source rock layer has been estimated to be in the order of 1km.

Contents

1. Introduction	
1. HIMU and EM in ocean island basalts	1
2. Previous models of HIMU and EM based on solid isotopes and trace elements	3
3. Previous noble gas studies of ocean island basalts	4
4. Aim of this study	6
2. Samples and Experiments	
1. Geological and geochemical background	7
2. Trace elements and REEs analyses	11
3. Sr and Nd isotope analyses	12
4. Noble gas analyses	13
3. Results	
1. Cpx zoning	16
2. Trace elements and REEs	16
3. Sr and Nd isotopes	28
4. Noble gases	32
4. Discussion	
1. Constraints to the origin of HIMU and EM	53
2. Origin of HIMU	54
3. Relation between HIMU and EM	57
4. Nd isotope problem for HIMU	58
5. Noble gas elemental patterns	68
6. He open system	73
5. Summary	81
Acknowledgments	83
References	84
Appendix	
A. Setting up of the noble gas mass spectrometry system at Earthquake Research Institute, University of Tokyo	93
B. Secondary effect - radiogenic, nucleogenic, fissionogenic and cosmogenic components	104
C. He open system model	109
D. Data Table	112

1. Introduction

HIMU and EM components in ocean island basalts

Ocean island basalts (OIBs) are the representative of intra-plate volcanism which is one of the igneous activities found on the earth's surface. In many cases, ocean islands form chain tracks which are parallel to the movement of the plate. Their ages are consistent with the "hotspot hypothesis" that they are formed by stationary magma sources below constantly moving oceanic plates (Wilson, 1965; Morgan, 1971). Thus, many OIBs are believed to be the products of hotspot activities. Since the upper mantle is considered to be stirred, the roots of stationary hotspots would be located in the deep mantle. Here, the deep mantle indicates the lower mantle and around the upper and lower mantle boundary region. This idea suggests that OIBs give us information about the deep mantle situation.

Previous geochemical studies of OIBs have revealed that the deep mantle is rather heterogeneous compared to the upper mantle (Fig. 1-1). On the basis of Sr, Nd and Pb isotope studies, at least four end-member components have been proposed; DM, EM1, EM2 and HIMU (e.g., Zindler and Hart, 1986). DM (depleted mantle) corresponds to the end-member of the upper mantle material. It is characterized by lower $^{87}\text{Sr}/^{86}\text{Sr}$ and higher $^{143}\text{Nd}/^{144}\text{Nd}$ than those of any other components, which indicates that DM component has low time-integrated Rb/Sr and high time-integrated Sm/Nd. On the contrary, EM1 and EM2 (Enriched Mantle) are the end-members with low $^{143}\text{Nd}/^{144}\text{Nd}$ and variable $^{87}\text{Sr}/^{86}\text{Sr}$.

Although ranges of Pb isotope ratios of most OIBs overlap those of MORB, quite high Pb isotope ratios (e.g., $^{206}\text{Pb}/^{204}\text{Pb} > 21.0$) have been found from five ocean islands; St. Helena Island in the Atlantic Ocean and four islands in the Cook-Austral Archipelago in the southern Pacific Ocean (Zindler and Hart, 1986). The end-member with quite high Pb isotope ratios has been named as HIMU, because it requires a high

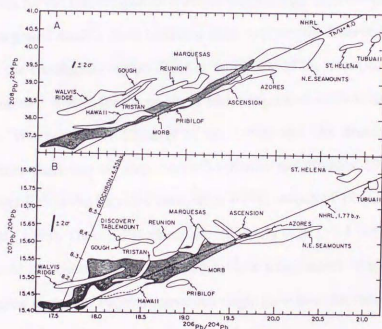
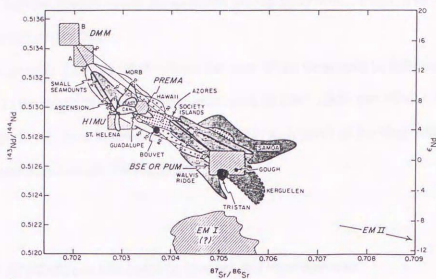


Fig. 1-1. Sr-Nd-Pb isotope systematics of MORBs and OIBs (after Zindler and Hart (1986)). At least four end-members (DM, HIMU, EM1, EM2) are required for the variation of isotope ratios.

time-integrated μ value ($\mu=^{238}\text{U}/^{204}\text{Pb}$). Sr and Nd isotope signatures of HIMU are noteworthy that they are plotted below the so-called mantle array which consists of the data for MORBs and most OIBs.

If such a heterogeneity found in OIBs reflects the state of the deep mantle, following problems arise (1) the origin of several components such as EM1, EM2 and HIMU, (2) depth and distribution of them in the deep mantle, and (3) their survival for long period in the mantle to produce isotopic heterogeneity.

Previous models of HIMU and EM based on isotopes and trace elements

The end-member for the EM component material requires high time-integrated Rb/Sr and low time-integrated Sm/Nd. Such feature is alike to presently observed sediments and rocks from the continental region (Zindler and Hart, 1986; Ben Othman et al., 1989). Thus, proposed models for the origin of EM components include the sediment recycling (e.g., Weaver, 1991; Chauvel et al., 1992) and the delamination of subcontinental lithosphere into the deep mantle (McKenzie and O'Nions, 1983). One of the evidences that EM is the recycled material is $\delta^{18}\text{O}$ values of Pitcairn magmas (Woodhead et al., 1993). Their $\delta^{18}\text{O}$ values are relatively high (>7.4 per mil). Since high $\delta^{18}\text{O}$ would be related to the alteration by low temperature fluids, it would suggest that magma sources of Pitcairn seamounts might have been the recycled altered materials which were located once on the Earth's surface.

On the other hand, it is more difficult to infer the origin for the HIMU source, because no material has been found which has the same isotopic signatures as HIMU. Many previous studies tried to explain the processes to produce its high Pb isotope ratios or high time-integrated $(\text{U}+\text{Th})/\text{Pb}$. One of the models is that the HIMU source was produced by the reaction with the core (e.g., Allègre et al., 1982). Selective transportation of Pb to the core might have elevated $(\text{U}+\text{Th})/\text{Pb}$ in the silicate portion,

which would become the HIMU source. However, the evidence that no systematic depletion of siderophile and chalcophile elements in HIMU magmas has been found, which argues against the model (Newsom et al., 1986).

Other proposed mechanism is the recycling of altered and dehydrated MORB (Hofmann and White, 1982; Weaver, 1991; Chauvel et al., 1992; Chauvel et al., 1995). Alteration by hydrothermal fluids may increase (U+Th)/Pb of MORB. Experiments of dehydration during subduction of slabs suggest that Pb would be selectively leached from altered MORB and sediments than U and Th during dehydration (Brenan et al., 1995; Kogiso, 1995; Keppler, 1996). This mechanism is compatible with the model of arc magmatism. It is widely accepted that dehydrated fluids from a subducting material would play a great role for generation of arc magmas (e.g., Tatsumi and Eggins, 1995). Dupuy et al. (1988) have argued that concentration patterns of trace elements show mirror images between arc magmas and HIMU. It is consistent with a model that the HIMU source was the remnant of subducting material after dehydration.

These models apparently succeed in explaining the differentiation of (U+Th)/Pb of the HIMU source. However, Sr and Nd isotopic information has not been taken into accounts in the previous studies. Further information such as $\delta^{18}\text{O}$ evidence, osmium isotopes (Roy-Barman and Allègre, 1995) and noble gas isotopes would provide more strong constraints to infer the origin of HIMU and EM sources.

Previous noble gas studies of ocean island basalts

OIBs have been separated into two categories by their helium isotope ratios ($^3\text{He}/^4\text{He}$); so-called "high- ^3He " and "low- ^3He " hotspots. "High- ^3He " and "low- ^3He " hotspots are defined by their $^3\text{He}/^4\text{He}$ values which are higher and lower than that of MORB (around 8Ra; 1Ra is the $^3\text{He}/^4\text{He}$ of the atmosphere.), respectively.

"High- ^3He " signature is found from typical hotspots such as Hawaii (e.g., Kaneoka et al., 1983; Kurz et al., 1983; Hiyagon et al., 1992), Iceland (Kurz et al., 1985; Poreda et al., 1986) and Réunion (e.g., Graham et al., 1990; Staudacher et al., 1990). Such signature is interpreted to be the contribution of less-degassed or primitive mantle material into their magma sources. Although its locality in the mantle is not well known, it would reside in the deeper part than where MORBs are produced (e.g., Kaneoka and Takaoka, 1985). Note that magmas of Hawaii, Iceland and Réunion are not accompanied by the signatures of HIMU and EM on Sr, Nd and Pb isotope ratios.

Most EM OIBs show relatively low $^3\text{He}/^4\text{He}$ ratios (e.g., Kurz et al., 1982, Vance et al., 1989) except for Samoa (Poreda and Farley, 1992) and Heard Island (Hilton et al., 1995). $^3\text{He}/^4\text{He}$ of HIMU, which are previously available for only three samples from St. Helena Island and one sample from Tubuai Island, also show the "low- ^3He " signature (Graham et al., 1992). Since their $^3\text{He}/^4\text{He}$ is less than those of MORB or the upper mantle which was extensively degassed early in the Earth's evolution, "low- ^3He " hotspot sources should have higher $(\text{U}+\text{Th})/^3\text{He}$ than the upper mantle. One of the processes to increase $(\text{U}+\text{Th})/^3\text{He}$ has been considered to be the introduction of surface materials by recycling.

The argument against the above discussion was raised by Hilton et al. (1995). They showed that contamination of crustal material could decrease apparent $^3\text{He}/^4\text{He}$ in case of Heard Island. Since previous helium studies have provided data from few samples for each island, Hilton et al. (1995) have insisted that uniform $^3\text{He}/^4\text{He}$ from large number of samples for each island should be guaranteed in order to presume "low- ^3He " hotspots.

So far, Ne, Ar, Kr and Xe isotope data obtained for HIMU and EM are rather limited. Poreda and Farley (1992) provided all noble gas isotope data from the Samoa Island. They found Ne and Xe anomalies accompanied by high $^3\text{He}/^4\text{He}$, which suggests contribution of less-degassed mantle material into the Samoan magmas at least

for He and Ne isotopes. Any other information for HIMU and EM have not yet been reported from noble gas studies.

Aim of this study

The lack of data for noble gas isotopes has precluded a contribution to studies for HIMU and EM. This study provides large data set of noble gases regarding hotspot magmas in the Polynesian region. Since noble gases are measured for phenocrysts coexisting with a melt (or whole rock), phenocryst samples are also used for analyses of Sr and Nd isotopes, trace and rare earth elements. It would be the first attempt to analyze both solid and noble gas isotopes by using the same phenocryst samples, which will clarify correlation and/or decoupling among both isotope systematics. Since noble gases would behave in a different way from other solid isotopes during the formation of HIMU and EM sources, coupled data of noble gases and solid isotopes will give strong constraints to infer the origin for HIMU and EM sources.

2. Samples and Experiments

Geological and geochemical background

There are five volcanic island chains in the Polynesian region; Marquesas, Tuamotu, Gambier, Society and Cook-Austral Archipelagoes (Fig. 2-1). The ages of rocks from these islands are consistent with the "hotspot hypothesis" that they would be the products of active hotspot volcanism which is fixed under the constantly moving Pacific plate (Duncan and McDougall, 1976). The dense distribution of hotspot volcanism in the Polynesian region may be related to so-called "Superswell" which is characterized by elevated topography (McNutt and Judge, 1990). It is accompanied by negative geoid anomaly and slow seismic velocity under the region (McNutt and Judge, 1990). Cazenave and Thoraval(1994) have discussed that the "Superswell" is generated by the degree 6 flow of the mantle circulation. Seismic velocity anomaly in the lower mantle would be linked to the upwelling of the mantle material (Dziewonski, 1984; Fukao, 1992).

Volcanic rocks in the Polynesian region show large variety of Sr, Nd, Pb isotope ratios, such as EM1, EM2 and HIMU (Palacz and Saunders, 1986; Nakamura and Tatsumoto, 1988; Chauvel et al., 1992; Hemond et al., 1994). It indicates that their magma sources are heterogeneous; their variation in the Polynesian region is comparable to that in OIBs in the world (e.g., Zindler and Hart, 1986).

Cook-Austral Archipelago consists of more than 10 islands and some seamounts. Among them, four islands (Mangaia, Rurutu, Tubuai and Rimatara) are classified in the category of HIMU, while the other islands show the character of EM1(Palacz and Saunders, 1986; Nakamura and Tatsumoto, 1988; Chauvel et al., 1992). Combining the dating result of the islands, the ages of HIMU islands are consistent with the "hotspot hypothesis" that they are the products of a fixed hotspot volcanism (Duncan and McDougall, 1976; Turner and Jarrard, 1982). However, the "hotspot hypothesis"

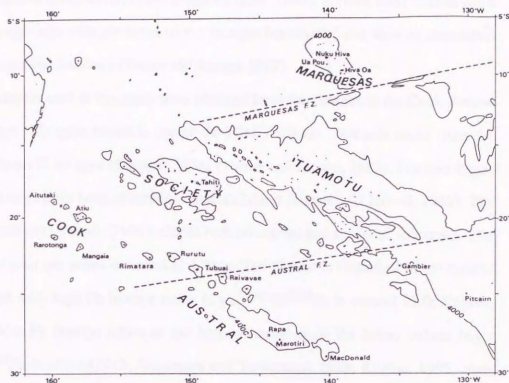


Fig. 2-1. Map of five island chains in the Polynesian plume province in the Southern Pacific Ocean (after Dupuy et al. (1989)).

includes some problems. Lavas of the presently active hotspot, MacDonald Seamount, is not classified in HIMU, but EM1 (Hémond et al., 1994). Further, EM1 islands show much younger ages than predicted by the "hotspot hypothesis" and have no correlation between ages and locations (Turner and Jarrard, 1982).

Rock samples used in this study were obtained from four islands in the Cook-Austral Archipelago. Mangaia Island is one of the HIMU islands. Volcanic rocks from the island indicate K-Ar ages of around 18Ma (Turner and Jarrard, 1982). The two stages of the activities have been observed in Rurutu Island (Turner and Jarrard, 1982). The old stage activity (around 12Ma) includes both submarine and subaerial volcanism. The activity of younger series occurred at 1-2Ma. The former is classified in the typical HIMU with very high Pb isotope ratios (e.g., $^{206}\text{Pb}/^{204}\text{Pb}$ is around 21.0; Kogiso, 1995), while Pb isotope ratios of the latter activity show the lower values (e.g., $^{206}\text{Pb}/^{204}\text{Pb}$ is around 20.3; Nakamura and Tatsumoto, 1988; Kogiso, 1995) than Rurutu old series. Rocks from Tubuai Island also have the character of HIMU (Nakamura and Tatsumoto, 1988; Chauvel et al., 1992). In Tubuai Island, binary activities have been observed; the earlier one from 12Ma to 9.4Ma and the later one from 6.8Ma to 5.7Ma (Chauvel et al., 1992). The ages of rocks from Rarotonga Island are 1-2Ma (Turner and Jarrard, 1982). Rocks of Rarotonga Island are classified into EM1 (Nakamura and Tatsumoto, 1988).

I analysed samples from two islands in the Society Archipelago to compare rocks from the Cook-Austral Islands. One is the Tahiti Island which is the biggest island in the Polynesian region, and the other is the neighbor island, Moorea. Rocks of the Society Archipelago are characterized in EM2 (Zindler and Hart, 1986). K-Ar ages of volcanic rocks from Tahiti and Moorea Islands are 0.5-1.2Ma and around 1.5Ma, respectively.

Samples analyzed in this study are listed in Table 2-1. Rock types of most samples are olivine and clinopyroxene (cpx) phyric alkali basalts such as ankaramite and olivine basalt. The result of mode counting is also shown in Table 2-1. I selected phenocryst-

Table 2-1. List of samples.

Sample	Rock Type	Mode (volume %)			Analyses		Sr, Nd cpx	noble gas	
		olivine	cpx	groundmass	trace elements, REEs whole rock	cpx		heating	crushing
Cook-Austral Archipelago									
Rarotonga									
RTG-C4	ankaramite	29	18	53	O	O	O	-	cpx
RTG-C5	ankaramite	8	17	75	O	O	O	ol	ol, cpx
RTG-C8	olivine basalt	1	7	92	O	O	O	-	cpx
RTG-C10	ankaramite	6	28	66	O	O(*)	O(*)	ol, cpx(*)	cpx
Mangaia									
MGA-C8	ankaramite	30	19	51	O	O	O	ol	
MGA-C12	ankaramite	29	27	45	O	O	O	ol, cpx	ol, cpx
MGA-C23	ankaramite	29	22	49	O	O	O	-	cpx
MGA-C29	ankaramite	16	20	64	O	O	O	cpx	ol
Tubuai									
TU01-01	ankaramite	18	16	67	O	O(*)	O(*)	ol, cpx(*)	cpx
TU04-01	aphyric phonolite	0	0	100	O	-	-	-	-
TU09-01	ankaramite	12	22	66	O	O	O	ol	cpx
TU12-01	ankaramite	17	13	70	O	O	O	ol	cpx
TBA-C25	olivine nephelinite	8	1	91	O	-	-	-	-
Rurutu (ancient series)									
RU01-01	olivine basalt	23	0	77	O	O	O	ol	ol
RU02-01	ankaramite	15	8	77	O	O	O	ol	cpx
RU09-01	ankaramite	23	4	73	O	O	O	ol	ol
Rurutu (recent series)									
RU08-01	aphyric alkali basalt	0	0	100	O	-	-	-	-
RRT-C31	olivine basalt	13	0	87	O	-	-	ol	ol
RRT-C33	olivine-basalt	11	0	89	O	-	-	-	ol
Society Archipelago									
Moorea									
MO01-01	ankaramite	16	12	73	-	-	-	ol	ol
Tahiti									
TA01-02	ankaramite	9	18	73	-	-	-	cpx	cpx

Abbreviations; O, samples analyzed; -, not analyzed; ol, olivine samples analyzed; cpx, clinopyroxene samples analyzed; (*), rim-core test was performed.

rich basalts because I used olivine and cpx phenocrysts as samples for analyses (see below). Least altered rocks were selected for the analyses. Especially, olivines replaced by iddingsite at the surface and along the veins were excluded. Strongly differentiated rocks as phonolites and nephelinites have been exposed in Rurutu and Tubuai Islands. They were also analyzed for comparison.

Trace elements and REEs analyses

One of the characteristics in this study is to measure Sr, Nd and noble gas isotopes using same cpx samples. In this case, it is requested to check chemical equilibrium between cpx and whole rock (melt). Then, samples of both whole rock and cpx were used for trace elements and REEs for the purpose.

Large rocks were chopped by a hammer or cut by a rock cutter, following crushed by a jaw crusher. Pieces with cutting sections were carefully removed and then washed by distilled water. After drying them, part of them was ground into powder by a mill. The rest was further crushed in the iron mortar into the mesh size of #60-#80. Cpx samples were collected using a magnetic separator. In case of bad purity of cpx, they were leached by hot 2N-HCl and purified by magnetic separator again.

Because cpx had the normal zoning as described in the following section (Fig. 3-1), rim and core of cpx were separated to check the difference of elemental and isotopic compositions between them for selected samples (RTG-C10 and TU01-01). Cpx with the mesh size of #100-#200 were used for this purpose. First, purified cpx including both rim and core parts were leached by hot 2N-HCl. Then, magnetic separation was carefully carried out for them. They were separated into rim-rich part, core-rich part and mixture of them due to the difference of Fe content. Repeated separation raised the purity of rim-rich part and core-rich part. Because the colors of rim and core were different due to the contents of Ti and Cr, they could be roughly checked under a

binocular. Further check was performed by the EPMA analysis for randomly picked grains of them. The rim-rich part and core-rich part were estimated to include more than 80% of rim and core, respectively.

Trace elements and REEs were analyzed by the inductivity coupled plasma-mass spectrometry (ICP-MS) in the Pheasant Memorial Laboratory (PML) in the Institute for Study of the Earth's Interior (ISEI), Okayama University. The chemical treatments and mass spectrometric procedures were carried out according to the techniques in PML (Makishima et al., 1995). Samples were weighed in teflon beakers. They were decomposed by HF and HClO₄. Then, sample solutions were induced in the ICP-MS. The accuracy is within 7% (2σ) (Makishima et al., 1995). Some samples were selected for duplicate analyses.

Sr and Nd isotope analyses

Sr and Nd isotopic analyses were carried out using cpx samples. The samples were the same as those used for analyses of trace elements and REEs. Measurement of them was performed by the thermal ionization mass spectrometer (TIMS) in PML in ISEI, Okayama University. The chemical treatments and mass spectrometric procedures were carried out according to the techniques in PML (Shibata et al., 1989; Yoshikawa and Nakamura, 1993). After samples were weighed in teflon beakers, they were decomposed by HF and HClO₄. Sr and Nd were chemically separated by cation-exchange chromatography. Separated Sr and Nd were loaded on filaments and set in TIMS for isotope analyses. Procedural total blanks of Sr and Nd (handled by T. Hanyu) were 34pg and 73pg, respectively.

Cpx and olivine phenocrysts were used for noble gas analyses. Rocks were crushed into the mesh size of #30-60. Cpx and olivine were handpicked under a binocular. Phenocrysts stuck by small amounts of groundmass and altered parts were carefully excluded because noble gases of secondary origin were highly concentrated in them. To check the purity of sampled phenocrysts, some samples were selected for leaching test; a part of phenocrysts was leached by hot 2N-HNO₃ and noble gas compositions of them were compared to those of unleached samples.

Cpx and olivine samples were washed by acetone, ethanol and distilled water. After drying them, they were weighed. For heating experiments, they were wrapped by thin aluminium foil and loaded into the sample holder of the vacuum line. They were directly loaded in the crusher for crushing experiments.

Noble gas analyses were carried out in two laboratories. Heating experiments were done using modified VG-5400 in ISEI, Okayama University. Details of the mass spectrometric technique were referred elsewhere (Miura and Nagao, 1991; Nagao et al., 1996). Both heating and crushing experiments were performed by VG-5400 at Earthquake Research Institute (ERI), University of Tokyo. Details of MS at ERI are described in the Appendix-A.

I mention the outline of the experimental procedures here. Gas extraction and purification lines were baked at 150-200°C for more than 8 hours. Samples were preheated at 160°C during baking. For heating experiments, crucible was degassed at more than 1900°C for more than 4 hours to reduce the hot blank. Two stage stepwise heating was applied to extract noble gases for heating experiments. Stepwise temperatures were determined by the pre-analyses of investigating gas release patterns. Possible air contamination on the sample surface is expected to be removed in the low temperature fraction (700 or 800°C). Noble gases with more magmatic information would be released by the high temperature fraction at 1700°C and 1850°C for cpx and

olivine, respectively. Duration of heating is 40-60 minutes and 20 minutes for the low temperature fraction and the high temperature fraction, respectively.

For crushing experiments, samples were crushed by pressing-type crusher (Fig. A-2). It was heated at 120°C, and a charcoal trap cooled by liquid nitrogen was used during crushing to avoid adsorption of heavy noble gases on the fresh surfaces produced by crushing samples (see Appendix-A).

Noble gases extracted by both heating and crushing methods were purified by two or three titanium-zirconium getters heated at 700-800°C. Five noble gases (He, Ne, Ar, Kr, Xe) were separated each other using cold traps with activated charcoal and cryogenic pump.

Noble gas isotopic measurements were performed by a sector-type mass spectrometer (VG-5400). Induced noble gases into the mass spectrometer are ionized by the Nier-type ion source. Three collectors, Faraday cup, Daly multiplier and electron multiplier-ion counting system, are equipped on the mass spectrometer. A peak jumping method is applied to the isotopic measurements. The resolution power of MS is more than 600 ($M/\Delta M$) which is enough to separate the $^3\text{He}^+$ peak from HD^+ and $^3\text{H}^+$ peaks for helium measurement. Helium isotope ratio was calibrated by repeated measurements of the standard gases ($^3\text{He}/^4\text{He} = 6.04 \pm 0.29$ Ra) from Kaminoyama well, Yamagata, Japan, during a series of experiment. For neon analyses, peak heights of $^{20}\text{Ne}^+$ and $^{22}\text{Ne}^+$ were corrected for interferences of doubly charged $^{40}\text{Ar}^{++}$ and $^{44}\text{CO}_2^{++}$, respectively. Production rates of $^{40}\text{Ar}^{++}/^{40}\text{Ar}^+$ and $^{44}\text{CO}_2^{++}/^{44}\text{CO}_2^+$ during measurements were 0.25 and 0.008 for MS in ERI and 0.2 and 0.01 for MS in ISEI, respectively. For Ne, Ar, Kr and Xe analyses, measured isotope ratios were calibrated by repeated measurements of standard gases of diluted air.

For noble gas abundance measurement, the absolute sensitivity of Ar was determined by measuring standard samples of MMhb-1 and JG-1 (biotite). The relative sensitivities of He/Ar, Ne/Ar, Kr/Ar and Xe/Ar were determined by measuring standard gases of diluted air. The error for the noble gas abundance was about 5% for all noble gases.

Mass fractionation factors were often checked by standard gases. Hot blanks and crushing blanks were measured in the same way as sample runs. Corrections of blanks were carried out for all data of sample runs. Typical hot blanks and crushing blanks are listed in Table D-9.

3. Results

Cpx zoning

Cpx in all samples analysed in the present study have the normal zoning. Two cpx samples, RTG-C10 and TU01-01, were selected for checking the effects of zoning on elemental and isotopic compositions (rim-core test). The patterns of zoning were investigated by EPMA analyses at ERI.

Most cpx have the zoning pattern represented by cpx of TU01-01 (Fig. 3-1). They have the continuous zoning with thin rims ($<100\mu\text{m}$). Both rim and core are classified as Ti-augite, but the major element composition of rim is different from that of core (Fig. 3-2). The difference of Fe content between rim and core enables the separation of rim-rich part and core-rich part of cpx by magnetic separation for the rim-core test.

Only cpx of RTG-C10 has the dissimilar zoning pattern to the others. It has discontinuous zoning with thicker rim (Figs. 3-1 and 3-2). Rim and core are classified as Ti-augite and Cr-diopside, respectively.

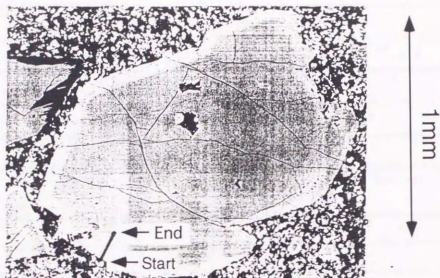
The depth of cpx formation was estimated using clinopyroxene geobarometer (Nimis, 1995). Pressures that core and rim of cpx were formed are simulated to be 1.1 and 1.4 kbar, respectively (error; $\pm 2\text{kbar}$). Accordingly, both core and rim of cpx would have been formed in the shallow magma chamber.

Trace elements and REEs

Concentrations of trace elements and REEs of whole rock and cpx samples are listed in Tables D-1 and D-2. Fig. 3-3 shows the trace element concentrations of whole rock samples except for the Rurutu recent series and evolved rocks in the Tubuai Island (See caption for more details.). Highly fractionated pattern of REE is usually found in OIB,

(a) TU01-01

17



(b) RTG-C10

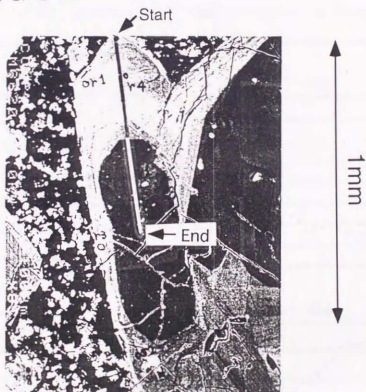


Fig. 3-1. Cpx samples with zoning. (a) Cpx of TU01-01; (b) cpx of RTG-C10. The line analyses for major elements (Fig. 3-2) were performed by EPMA along the lines from rim ("Start") to core ("End") shown in the figures.

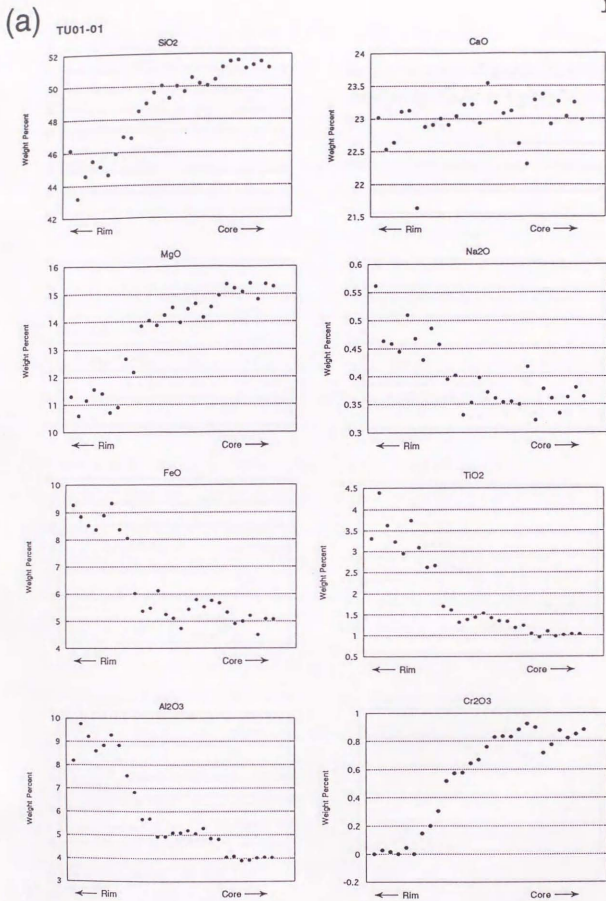


Fig. 3-2. Major element profiles of cpx with zoning. (a) Cpx of TU01-01, (b) cpx of RTG-C10. Analyses were performed along the lines shown in Fig. 3-1.

(b)

RTG-C10

19

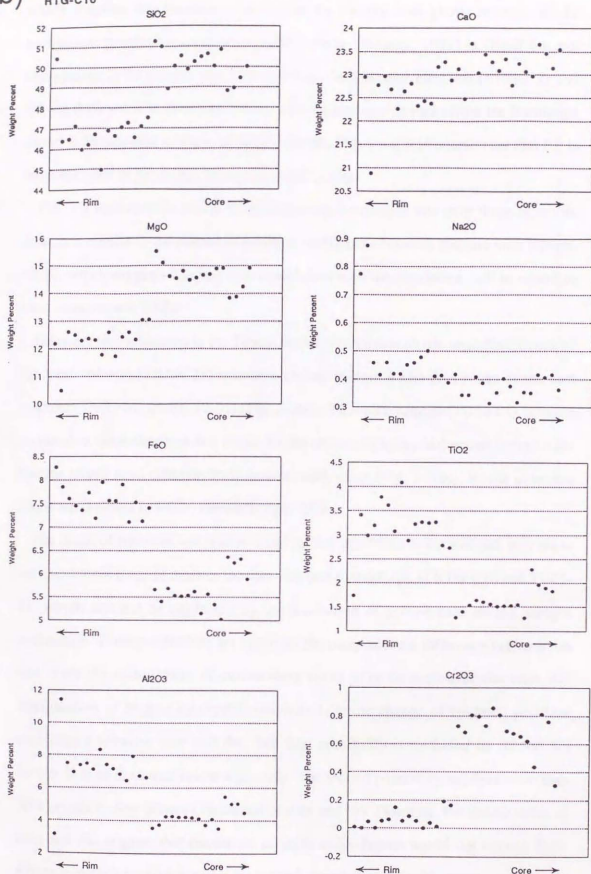


Fig. 3-2. (Continued)

which suggests that magmas were formed by melting with garnet residue. Nb-Ta enrichment previously reported in HIMU rocks (Weaver, 1991) is found but not conspicuous in the present data. The other high field strength elements (HFSE), Zr and Hf, are depleted. The elemental pattern of trace elements in rocks from the Rarotonga Island is almost akin to those of HIMU islands. However, it is noteworthy that Rb is more enriched in Rarotonga rocks than HIMU rocks.

Fig. 3-4 indicates the ratios of element concentrations in cpx over those of whole rock. It is similar to the pattern of partition coefficients between cpx and melt (Green, 1994), which suggests that cpx is in equilibrium with the coexisting melt in regard to trace elements and REEs.

There are two volcanoes in the Tubuai Island. The olivine phyric nephelinitic rock of the west volcano (TBA-C25) is more enriched in light REEs than rocks of the east volcano (TU01-01, 09-01, 12-01) (Fig. 3-5(a)). Phonolite sample (TU04-01) is much enriched in trace elements and REEs. Rocks of ancient series and recent series in the Rurutu Island have different REE patterns each other (Fig. 3-5(b)). Rocks of recent series are enriched in REEs, especially light REEs.

The result of rim-core test is shown in Fig. 3-6. All REEs in the rim-rich part show the enrichment twice of those in the core-rich part for both cpx of RTG-C10 and TU01-01, which can not be explained by contamination of groundmass during sample preparation. Three possibilities are raised for the compositional difference between rim and core; (1) assimilation of surrounding rocks after formation of the core, (2) fractionation of magma by crystallization and (3) the change of cpx/melt partition coefficients between core and rim. The first possibility is excluded by Sr and Nd isotope data as discussed below separately. The second possibility requires more than 50% crystallization between formation of core and rim. However, FeO/MgO ratios of core and rim suggest that maximum crystallization degree would not exceed 25%. Hence it can not be explained by the second possibility alone. The third possibility is based on the dependency of partitioning on pressure, temperature and compositional

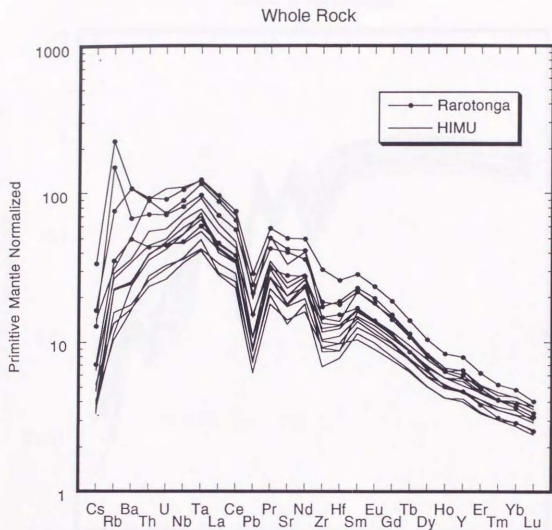


Fig. 3-3. Primitive mantle normalized abundance patterns of trace elements and REEs in the whole rock samples. Samples of phonolite (TU04-01), nephelinite (TBA-C25) and recent-series lavas from Rurutu Island are excluded in this figure. Normalized values of primitive mantle are taken from Sun and McDonough (1989).

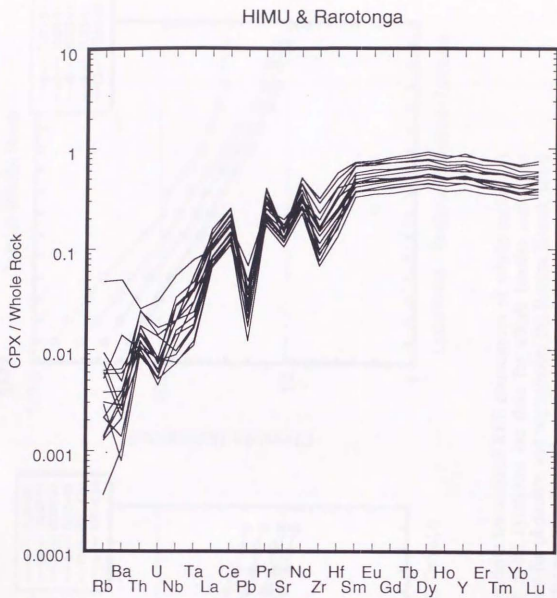


Fig. 3-4. Concentration ratios of cpx and whole rock for HIMU and Rarotonga samples.

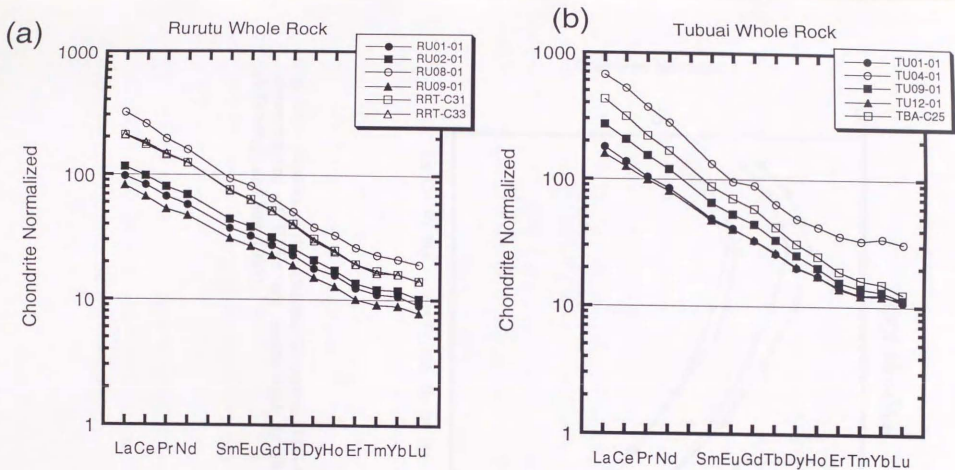


Fig. 3-5. Chondrite normalized REE abundances of whole rocks. (a) Tubuai Island; solid symbols are data for alkali basalts and open symbols are data for phonolite and nephelinite. (b) Rurutu Island; solid and open symbols are data for ancient-series and recent-series in Rurutu Island. Normalized values of chondrite are taken from McDonough and Sun (1995).

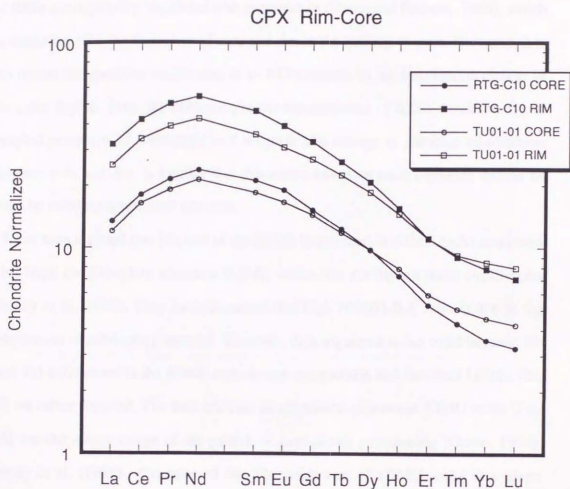


Fig. 3-6. Results of rim-core test for cpx of RTG-C10 and TU01-01. Concentrations of REEs are normalized by those of chondrite (McDonough and Sun, 1995).

effects. Since both core and rim are formed in the shallow magma chamber at around 1kbar, the pressure effect is not plausible. It has been known that partition coefficients of REEs are negatively correlated with temperature (Green and Pearson, 1985), which is consistent with the formation of core and rim in the cooling magma. However, it is not certain that partition coefficients of all REEs depend on the temperature change in the same degree. Thus, the difference in the concentration of REEs would be due to coupled processes of fractionation of magmas and change of partition coefficients between core and rim. It implies that discussion based on trace elements should be made by selecting appropriate elements.

It has been claimed that Nb, one of the HFSE, is enriched in HIMU rocks compared with large ion lithophile elements (LILE) which has similar partition coefficients (Dupuy et al., 1988). They have discussed that high HFSE/LILE ratio is due to the dehydration of subducting material. However, their argument is not valid because Nb (and Ta) enrichment in the HIMU rocks is not conspicuous and the other HFSEs (Zr, Hf) are rather depleted. The trace element concentration patterns of HIMU rocks (Fig. 3-3) are the mirror image of the pattern of garnet/melt partitioning (Green, 1994). Dupuy et al. (1988) also inferred the Nb enrichment of HIMU rocks at a given concentration of Zr. However, Nb-Zr is not a good indicator for the magma source because Zr/Nb would differentiate during melting and crystallization. Zr/Nb of HIMU is actually explained by melting with garnet residue.

The appropriate element pairs to be discussed should have the same incompatibility for garnet-melt and cpx-melt because both garnet and cpx are the key phases for partitioning during melting and crystallization. Considering the garnet/melt and cpx/melt partition (Fig. 3-4; Green, 1994), one of the recommended pairs is Pb-Ta. Pb/Ta is correlated with ϵ_{Nd} for HIMU samples (Fig. 3-7). Pb/Ta of HIMU end-member is less than 0.6. Samples from the Rarotonga Island show rather higher Pb/Ta. Depletion of Pb relative to Ta in HIMU rocks is one of the constraint for the origin of HIMU.

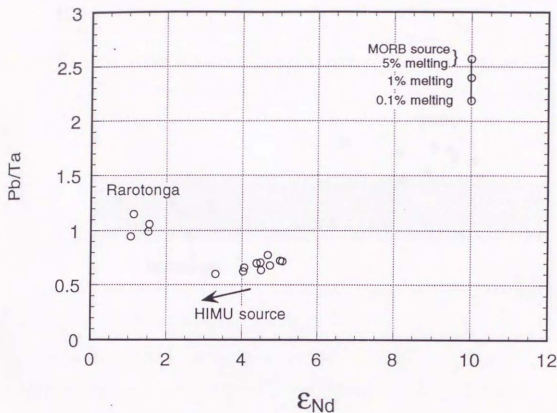


Fig. 3-7. ϵ_{Nd} - Pb/Ta diagram. For HIMU samples, correlation coefficient between Pb/Ta and ϵ_{Nd} is 0.77. Compositions of partial melt from MORB source are also shown. The starting compositions of MORB source are assumed as $\epsilon_{Nd}=+10$ and $Pb/Ta=2.6$. Partition coefficients of spinel peridotite (McKenzie and O'Nions, 1991) are used for the calculation of Pb/Ta of partial melt.

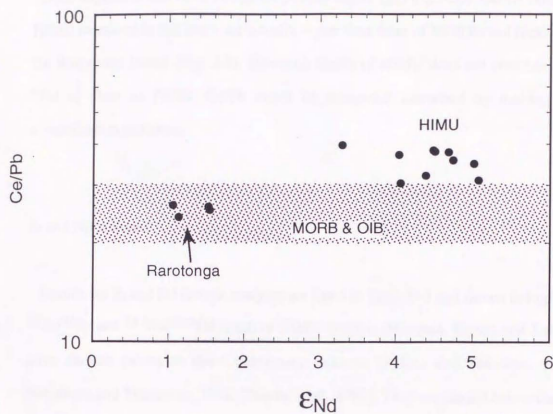


Fig. 3-8. ϵ_{Nd} - Ce/Pb diagram. Most samples from MORBs and OIBs are plotted in the hatched area (Hofmann et al., 1986).

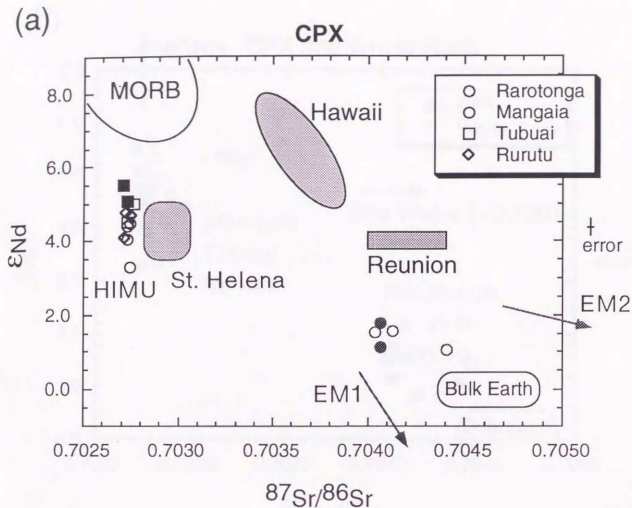
Ce/Pb is often used for source characterization. MORBs and most OIBs show uniform Ce/Pb of around 25 (Hofmann et al., 1986). On the other hand, Chauvel et al. (1992) suggested that HIMU magmas possess higher Ce/Pb (27-55). Ce/Pb values of HIMU measured in this study are actually higher than those of MORBs and rocks from the Rarotonga Island (Fig. 3-8). However, Ce/Pb of HIMU does not correlate with ϵ_{Nd} as clear as Pb/Ta. Ce/Pb might be somewhat disturbed by melting and crystallization processes.

Sr and Nd isotopes

Results for Sr and Nd isotope analyses are listed in Table D-3 and shown in Fig. 3-9. $^{87}\text{Sr}/^{86}\text{Sr}$ and $^{143}\text{Nd}/^{144}\text{Nd}$ (ϵ_{Nd}) of HIMU samples (Mangaia, Rurutu and Tubuai) have similar values to those previously reported (Palacz and Saunders, 1986; Nakamura and Tatsumoto, 1988; Chauvel et al., 1992). They are plotted below the so-called mantle array.

The rim-core test was performed for Sr and Nd isotope ratios. Both RTG-C10 and TU01-01 show indistinguishable isotope ratios between rim-rich part and core-rich part of cpx in the analytical error range (Fig. 3-9(a)). It excludes the contamination of exotic material into the magma during cpx formation.

HIMU data obtained in this study show quite uniform values of $^{87}\text{Sr}/^{86}\text{Sr}$ comparing with those of the previous data which are rather variable (Fig. 3-9(b)). Such difference might be caused due to the difference in phases used for analyses; cpx was used in this study while whole rock samples were used in the previous studies. Whole rock samples would suffer the secondary effects such as reaction with the seawater, contamination of crustal materials and alteration after eruption, for instance. Even if fresh rocks are selected and leached, complete removal of secondary effects is difficult for whole rock analyses. On the other hand, cpx would preserve more primitive



$$\epsilon_{Nd} = \left[\frac{\left(\frac{^{143}Nd}{^{144}Nd} \right)_{Sample}}{\left(\frac{^{143}Nd}{^{144}Nd} \right)_{CHUR}} - 1 \right] \times 10000$$

Fig. 3-9. $^{87}Sr/^{86}Sr$ - ϵ_{Nd} diagram for cpx data of HIMU and Rarotonga samples. (a) The solid symbols show the pairs of rim and core of cpx. Isotopic ranges of Hawaii, Réunion and St. Helena (e.g., White and Hoffman, 1982; Stille et al., 1986; Fisk et al., 1988) are indicated by hatches. (b) Comparison of cpx data from this study and whole rock data from previous studies (Palacz and Saunders, 1986; Nakamura and Tatsumoto, 1988; Chauvel et al., 1992). (c) ϵ_{Nd} of HIMU samples shifts according to the ages of islands.

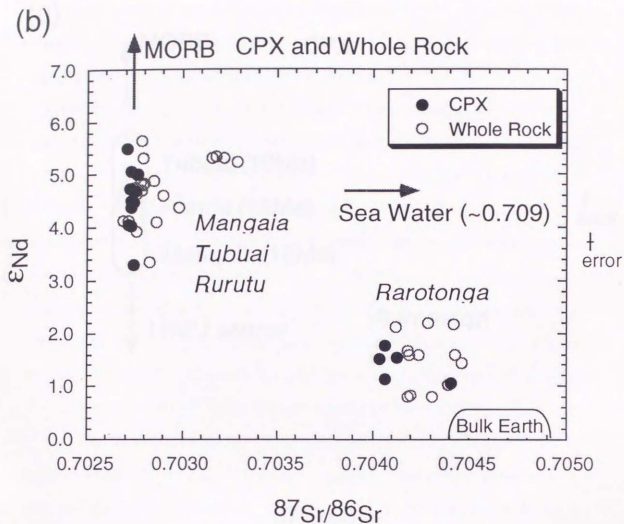


Fig. 3-9. (Continued)

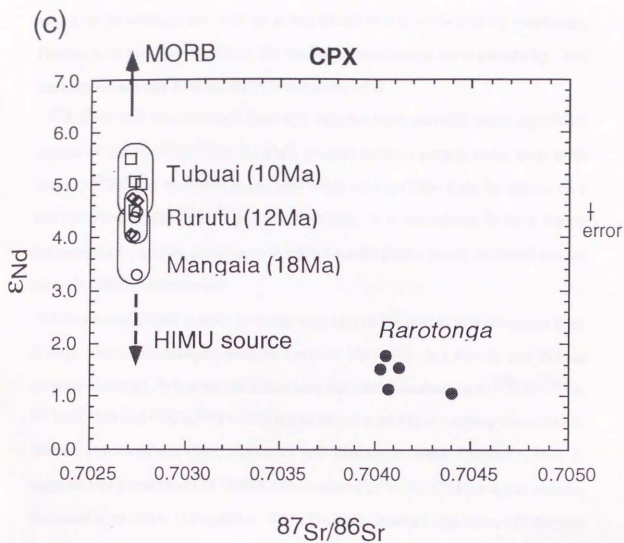


Fig. 3-9. (Continued)

isotopic information. Because secondary effects after cpx formation in the magma would not be added to cpx, and cpx is less altered than a whole rock by weathering. Further, it is possible to remove the surface contamination on a sample by acid leaching because cpx does not dissolve in a strong acid.

$^{87}\text{Sr}/^{86}\text{Sr}$ and ϵ_{Nd} obtained from cpx samples have revealed some significant aspects of HIMU. $^{87}\text{Sr}/^{86}\text{Sr}$ of HIMU is quite uniform among rocks from three islands. $^{87}\text{Sr}/^{86}\text{Sr}$ of HIMU is the least value among OIBs. Data lie almost on a straight trend in the $^{87}\text{Sr}/^{86}\text{Sr}$ - ϵ_{Nd} diagram. It is considered to be a binary component mixing; one end-member is MORB source (upper mantle material) and the other the HIMU end-member.

ϵ_{Nd} values of HIMU samples correlate with ages of the islands to some extent (Fig. 3-9(c)). The oldest Mangaia samples have the least ϵ_{Nd} than Rurutu and Tubuai samples. Reported Pb isotope ratios also have the similar tendency that $^{206}\text{Pb}/^{204}\text{Pb}$, $^{207}\text{Pb}/^{204}\text{Pb}$ and $^{208}\text{Pb}/^{204}\text{Pb}$ of Mangaia samples are highest among three islands (Palacz and Saunders, 1986; Nakamura and Tatsumoto, 1988; Chauvel, 1992). It suggests that entrainment of MORB-like components to the HIMU magma sources increased from 18Ma (Mangaia) to 10Ma (Tubuai). Isotopic signatures of Mangaia samples would be more close to the HIMU end-member composition.

Noble gases

Stepwise Test

The stepwise heating is a conventional method for extracting gases from rock samples. Atmospheric adsorption on the sample surface would not be completely removed even in the vacuum condition. The appropriate choice of stepwise temperature would make it possible to separate essential gases of magmatic origin from gases of

secondary origin. In the low temperature fractions, adsorptive gases would be removed from sample surfaces while magmatic gases would be trapped in the matrix and/or fluid inclusions. Then, they would be degassed from samples and analyzed at high temperatures.

The gas release pattern as a function of heating temperature was investigated for both olivine and cpx to determine appropriate stepwise temperatures. MGA-C12 and TU01-01 were selected for the test of cpx samples. The noble gas abundance, He isotope ratio ($^3\text{He}/^4\text{He}$) and Ar isotope ratios ($^{38}\text{Ar}/^{36}\text{Ar}$, $^{40}\text{Ar}/^{36}\text{Ar}$) were measured at each temperature step (600, 700, 800, 1000, 1200, 1400, 1600 and 1800°C). Results are listed in Table D-6 and shown in Fig. 3-10. To evaluate the efficiencies of leaching samples to remove secondary components, noble gases in leached cpx (by HNO_3) and unleached cpx were compared (see below).

No significant differences were observed between leached and unleached samples (Fig. 3-10). At 600°C, a low $^3\text{He}/^4\text{He}$ ($<1\text{Ra}$) and an $^{40}\text{Ar}/^{36}\text{Ar}$ of near the atmospheric value were observed. Hence, noble gases released at this step would represent those of the atmosphere adsorbed on the sample surface. At 1400°C, relatively high values of $^3\text{He}/^4\text{He}$ (about 3Ra for MGA-C12 and 6Ra for TU01-01) and $^{40}\text{Ar}/^{36}\text{Ar}$ (about 700 for MGA-C12 and 550 for TU01-01) were observed, which can be interpreted to be of magmatic origin. High $^3\text{He}/^4\text{He}$ values were seen at relatively lower temperature steps than Ar. It probably reflects the high diffusivity of helium than that of argon in phenocrysts. Gases were scarcely released in the 1600 and 1800°C fractions. Since liquidus of augite is around 1500°C, gases in cpx would have been mostly released below its liquidus. In this experiment, the heating temperature in the low temperature fraction was chosen to be 800°C to remove secondary noble gases completely. The high temperature fraction was set at 1700°C to guarantee complete melting and degassing from cpx sample.

The same experiments were carried out for olivine samples (MGA-C12, leached olivine). The results are listed in Table D-7 and shown in Fig. 3-11. The noble gas

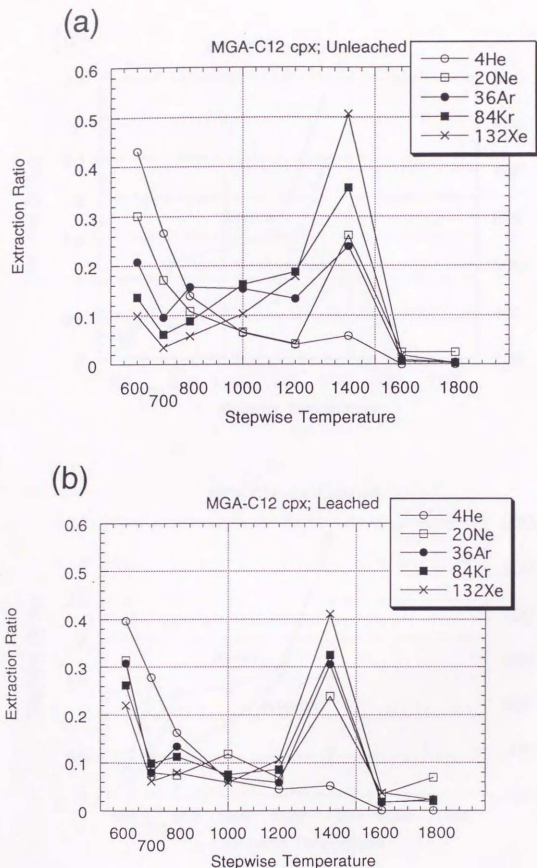


Fig. 3-10. Results of stepwise tests for noble gases. Gas release patterns (a,b,e,f) and $^3\text{He}/^4\text{He}$ and $^{40}\text{Ar}/^{36}\text{Ar}$ in each temperature step (c,d,g,h) are shown for samples of unleached and leached cpx of MGA-C12 and TU01-01. Extraction ratio (a,b,e,f) means a proportion of gases released at the temperature step compared to the total released gases.

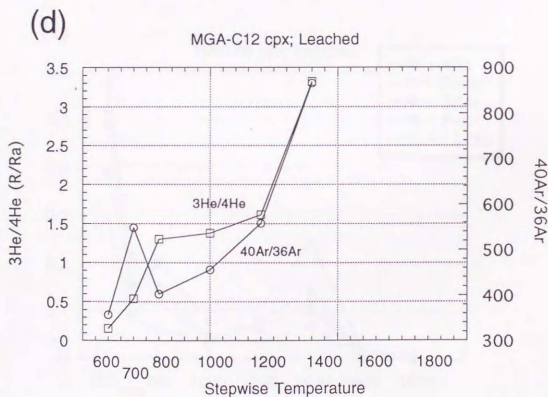
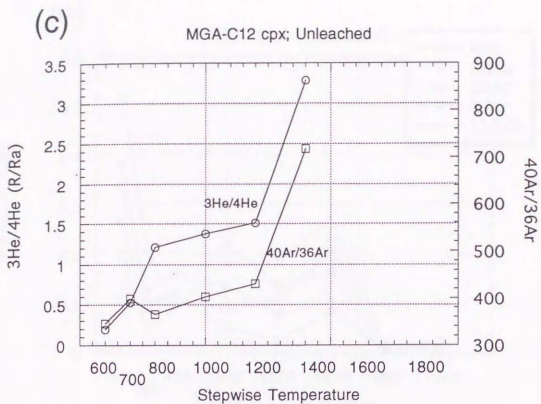


Fig. 3-10. (Continued)

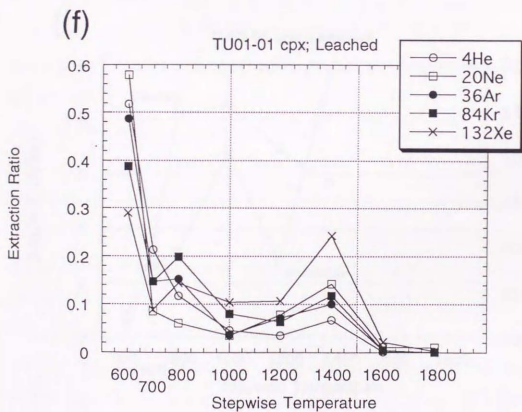
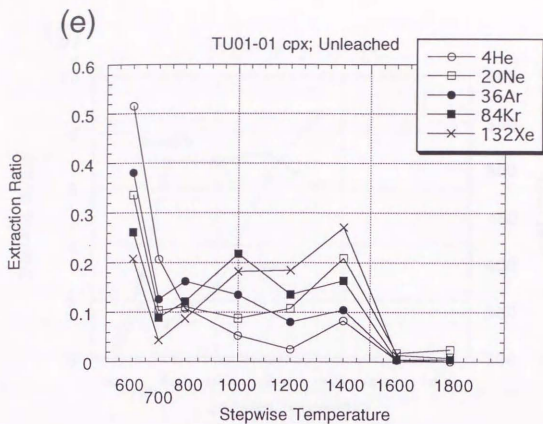
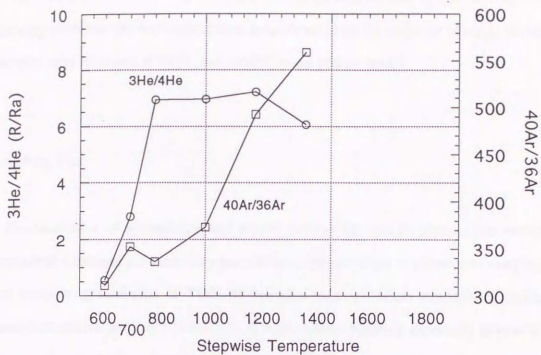


Fig. 3-10. (Continued)

(g)

TU01-01 cpx; Unleached



(h)

TU01-01 cpx; Leached

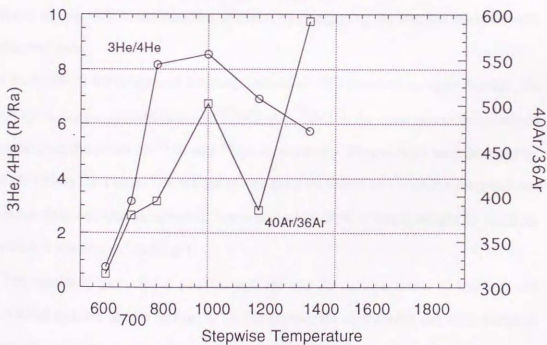


Fig. 3-10. (Continued)

release pattern for olivine is rather complicated. Gases with high $^3\text{He}/^4\text{He}$ and $^{40}\text{Ar}/^{36}\text{Ar}$ were released at higher temperature steps than the case of cpx. Though it is not easy to choose the most appropriate temperature steps for stepwise heating, olivine samples were degassed at 700°C and 1850°C in the present study.

Leaching Test

Contamination of groundmass and altered parts to the sample phenocrysts would dramatically increase the secondary gases of atmospheric origin in phenocryst samples. For instance, groundmass of TU01-01 contains more abundant atmospheric noble gases than olivine and cpx (Table D-4). It is sometimes difficult, especially in case of cpx samples, to check under a binocular whether small amounts of groundmass and/or altered parts stick on samples or not because both thick Ti-augite grains and groundmass seem black. The aim of the test is to evaluate the efficiency of leaching to remove the possible contamination of them, by comparing the leached samples with unleached ones.

I used HNO_3 for reagent of leaching instead of HCl because it might damage the mass spectrometer; contamination of ^{35}HCl and ^{37}HCl to the mass spectrometer would superimpose the peaks of ^{36}Ar and ^{38}Ar , respectively. Phenocrysts were leached by hot 2N- HNO_3 for 1 hour. The weight of cpx samples before and after leaching was not so much different. Olivine samples, however, lost 10-20% of initial weight by leaching (, which is referred as "etching").

The results of gas release patterns and He and Ar isotope ratios of leached and unleached cpx are shown in Fig. 3-10. No significant differences are seen between them. Comparing the leached and unleached olivine samples of RU09-01, no systematic difference was detected (Table D-4). Consequently, samples were not contaminated by the phase(s) which could be leached away by HNO_3 .

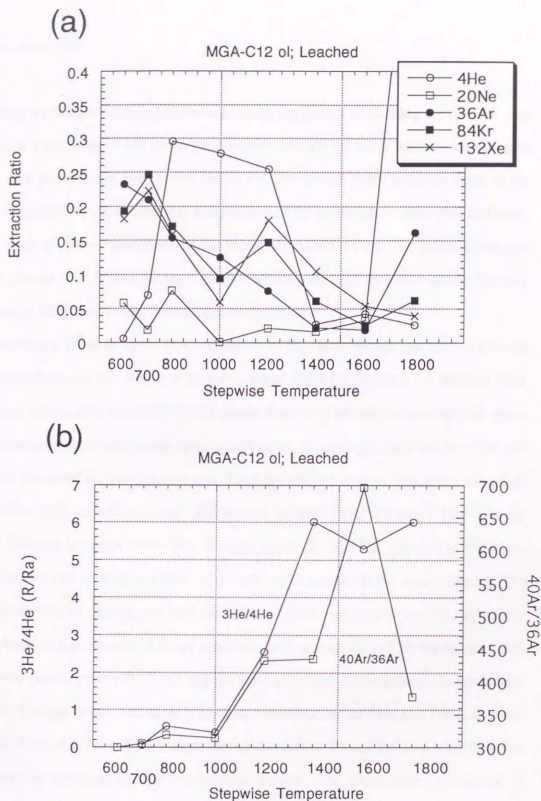


Fig. 3-11. Stepwise test for olivine samples of MGA-C12. (a) Gas release pattern and, (b) change for $^3\text{He}/^4\text{He}$ and $^{40}\text{Ar}/^{36}\text{Ar}$ in each temperature step. See the caption of Fig. 3-10.

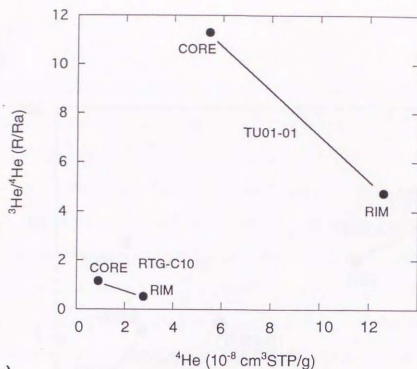
Rim - Core Test

Since we have not detailed knowledge about the history of forming the rim and core parts, it is not assured that noble gas compositions are the same between the rim part and core part. As has been tested for Sr and Nd isotope ratios between them in the previous section, the similar test was performed for noble gases. Rim-rich and core-rich parts of cpx were prepared in the way as described before. The selected samples were the cpx from RTG-C10 and TU01-01 which were used for rim-core test for trace elements, REEs and Sr and Nd isotopic compositions.

Results are listed in Table D-8 and shown in Fig. 3-12. Noble gas abundances are different between rim-rich and core-rich parts. Because samples for the test were crushed into small pieces (#80-#100), contamination of adsorptive atmospheric gases might have affected heavy noble gas compositions. Accordingly, only results of He and Ne are discussed for the rim-core test. The rim-rich part is more concentrated in ^4He and ^{20}Ne than the core-rich part. The isotope ratios of $^3\text{He}/^4\text{He}$ and $^{21}\text{Ne}/^{22}\text{Ne}$ are also different between them. The elevated ratios of $^3\text{He}/^4\text{He}$ and $^{21}\text{Ne}/^{22}\text{Ne}$ are ascribed to the spallation effect by cosmic rays (cosmogenic components). The production rate of cosmogenic ^3He and ^{21}Ne would be similar between the rim and the core because the contents of target materials, such as Mg, Al and Si, are not so much different (see Appendix-B). Then, apparent isotopic effect from cosmogenic production becomes larger in the core, since it has less concentrations of ^4He and ^{20}Ne , than the rim. Difference of He and Ne isotope ratios between the rim and the core is attributed to radiogenic, nucleogenic and cosmogenic effects. The quantitative estimates of cosmogenic components are discussed in the Appendix-B. Difference in noble gas abundances between them, like concentrations of trace elements and REEs discussed above, may reflect the magmatic processes during crystallization.

(a)

41



(b)

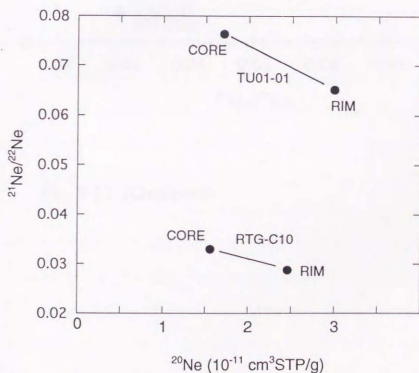


Fig. 3-12. Results of rim-core test for noble gases. (a) Relation of ^4He content and $^3\text{He}/^4\text{He}$, (b) relation of ^{20}Ne content and $^{21}\text{Ne}/^{22}\text{Ne}$, and (c) relation of $^3\text{He}/^4\text{He}$ and $^{21}\text{Ne}/^{22}\text{Ne}$ for the rim-rich part and core-rich part. Crushing data of TU01-01(cpx) and heating data of TU01-01 Groundmass (700°C and 1800°C fraction) are plotted in (c).

(c)

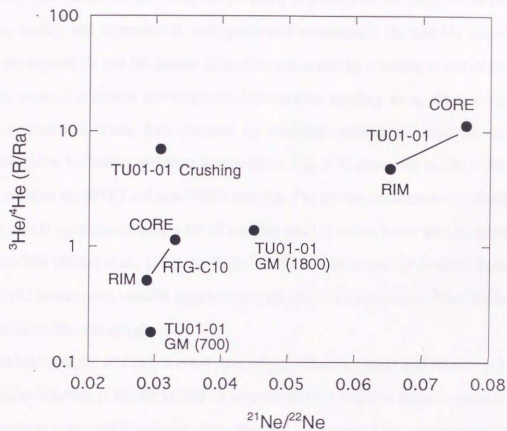


Fig. 3-12. (Continued)

Light Noble Gas Isotopes

All noble gas data in the main analyses are listed in Table D-4. As described in the previous section and Appendix-B, radiogenic and cosmogenic He and Ne would disturb the trapped He and Ne isotope ratios. Gas extraction by crushing is one of the effective method to obtain the magmatic information keeping away from those secondary products. Thus, data obtained by crushing method are used for the discussion below for helium and neon isotope ratios. Fig. 3-13 shows the results of He isotope analyses for HIMU and non-HIMU samples. The prominent features of HIMU samples are (1) quite similar values for all samples and (2) values lower than those of Pacific MORB (Hilton et al., 1993). Uniform $^3\text{He}/^4\text{He}$ is observed for samples from three HIMU islands with variable ages between 10-18Ma. Uniformity of $^3\text{He}/^4\text{He}$ is independent of ^4He concentration.

Non-HIMU samples of Cook-Austral Archipelago (Rurutu recent and Rarotonga) show similar $^3\text{He}/^4\text{He}$ to Pacific MORB. It suggests that the origin of these magmas is not the same as older HIMU magmas and/or they are contaminated by other materials. The large contribution of MORB-like helium to them is one of the possibilities. Samples from the Society Archipelago (Moorea and Tahiti) show higher $^3\text{He}/^4\text{He}$ than HIMU and non-HIMU samples from the Cook-Austral Archipelago.

Fig. 3-14 shows the comparison of $^3\text{He}/^4\text{He}$ of HIMU and EM-OIB in the world, which includes both data from this study and previous studies. Only data obtained by crushing method are compiled in Fig. 3-14. St. Helena, the other HIMU island, has similar (but slightly lower) $^3\text{He}/^4\text{He}$ values (Graham et al., 1992) than Polynesian HIMU samples.

EM samples show rather variable $^3\text{He}/^4\text{He}$ values. EM-OIBs in Atlantic and Indian Oceans, except for Heard Island, show lower $^3\text{He}/^4\text{He}$ than MORB, which are so-called "low- ^3He hotspot". On the other hand, "high- ^3He hotspot" feature is found in

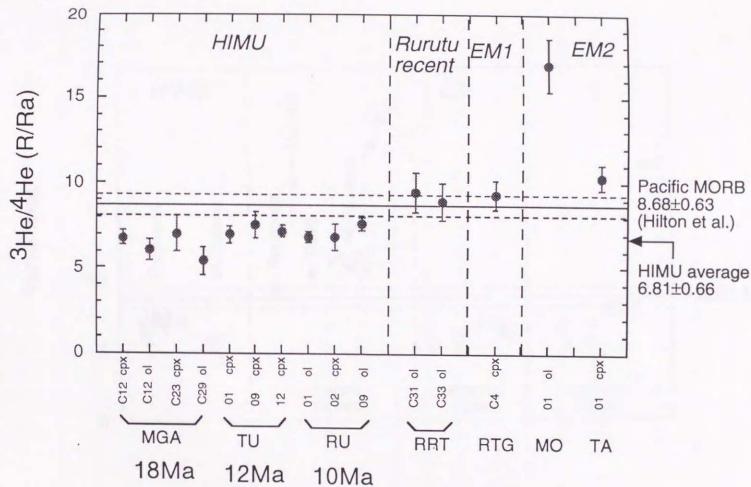


Fig. 3-13. $^3\text{He}/^4\text{He}$ data obtained by the crushing method. The range of $^3\text{He}/^4\text{He}$ of Pacific MORBs ($8.68 \pm 0.63(2\sigma)$) is from Hilton et al. (1993). Sample names are attached on the lateral axis. Abbreviations; MGA, Mangaia; TU, Tubuai; RU and RRT, Rurutu; RTG, Rarotonga; MO, Moorea; TA, Tahiti.

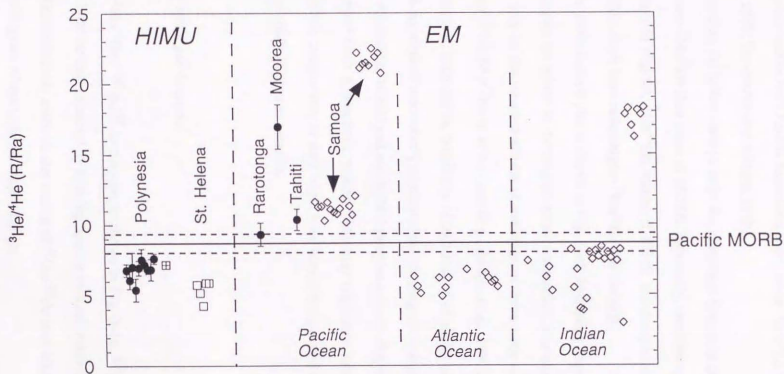


Fig. 3-14. $^3\text{He}/^4\text{He}$ for HIMU and EM samples from the Pacific, Atlantic and Indian Oceans. Only data obtained by crushing method are shown. Solid symbols are data from this study. Data for open symbols are from Kurz et al. (1982), Vance et al. (1989); Graham et al. (1992), Poreda and Farley (1992); Hilton et al. (1995).

Pacific EM-OIBs. The latter feature may have not been convinced because some data of abyssal basalts from Pacific seamounts show lower $^3\text{He}/^4\text{He}$ than MORB (Graham et al., 1988; Staudacher and Allègre, 1989).

Regarding the helium isotope ratio, the prominent feature of HIMU is its uniformity and lower $^3\text{He}/^4\text{He}$ than those of MORB. Especially, considering only the Polynesian and Samoan regions, $^3\text{He}/^4\text{He}$ values of HIMU are conspicuous compared to most EM-OIBs which have rather higher $^3\text{He}/^4\text{He}$ than MORB.

Neon three-isotope plot is shown in Fig. 3-15. In heating experiments, cosmogenic components are added to the trapped neon components. The anomalous neon isotope ratios may be the coupled effects of nucleogenic neon such as $^{18}\text{O}(\alpha, n)^{21}\text{Ne}$ and $^{19}\text{F}(\alpha, n)^{22}\text{Ne}(\beta^+)^{22}\text{Ne}$ in some cases (e.g., Azuma et al., 1993). The rim-core test of cpx, however, excludes the possibility of contribution of nucleogenic components.

Crushing method successively eliminated the nucleogenic components from extracted gases. All data for HIMU and non-HIMU samples indicate that neon isotope ratios are not distinct from atmospheric values. They may originally have trapped gases with atmospheric composition or they might have been contaminated by atmospheric gases due to scarcity of neon in samples.

Heavy noble gas isotopes

The $^3\text{He}/^4\text{He}$ - $^{40}\text{Ar}/^{36}\text{Ar}$ diagram is shown in Fig. 3-16. $^{40}\text{Ar}/^{36}\text{Ar}$ varies from 300 to 1400 for data obtained by both the heating method and crushing method. While $^3\text{He}/^4\text{He}$ is relatively uniform, the variety of $^{40}\text{Ar}/^{36}\text{Ar}$ may have been caused due to different degrees of atmospheric contamination.

Kr and Xe isotopes were measured for all samples, but meaningful data were not obtained for crushing experiments due to less amounts of Kr and Xe in extracted gases.

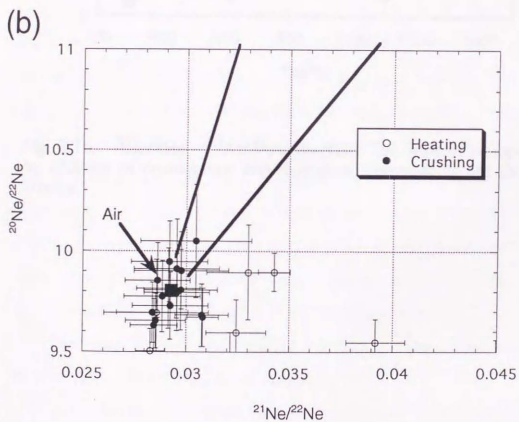
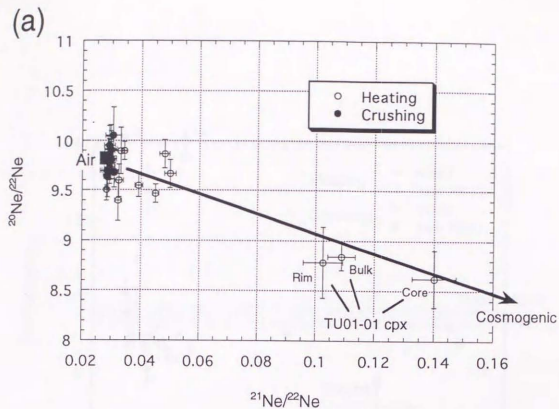


Fig. 3-15. (a) Ne three-isotope plot. A part of samples analyzed by the heating method suffer cosmogenic effects. (b) Magnified figure from figure (a).

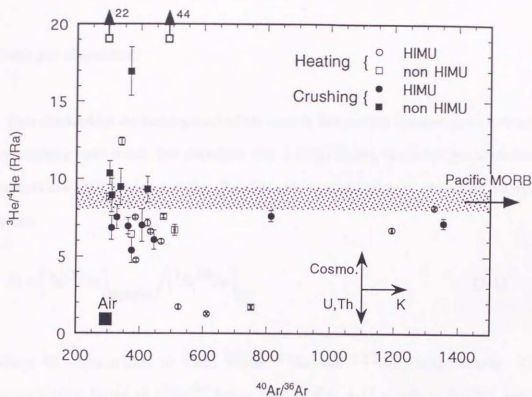


Fig. 3-16. $^3\text{He}/^4\text{He}$ - $^{40}\text{Ar}/^{36}\text{Ar}$ diagram. The shift of isotope ratios by addition of cosmogenic and radiogenic components are shown by arrows.

Kr and Xe isotope ratios were indistinguishable from atmospheric values within analytical uncertainties.

Noble gas abundances

Data obtained by the heating method are used in this section because gases extracted by crushing were much less abundant. Fig. 3-17(a) shows the noble gas abundance patterns of HIMU olivine samples. Relative noble gas abundances are expressed by F-values;

$$F_i = \left(i_X/^{36}\text{Ar} \right)_{\text{sample}} / \left(i_X/^{36}\text{Ar} \right)_{\text{air}} \quad (3-1)$$

where i_X corresponds to ^3He , ^{20}Ne , ^{84}Kr and ^{132}Xe , respectively. The normalization factor of $(^3\text{He}/^{36}\text{Ar})_{\text{air}}$ used in Fig. 3-17 equals to 0.0285, which corresponds to the so-called closed atmosphere (Staudacher and Allègre, 1989).

It is noteworthy that all HIMU samples are depleted in light noble gases and enriched in heavy noble gases. ^3He abundance is the upper limit because of possible addition of cosmogenic ^3He . This feature is distinct from abundance patterns of MORB and Loihi samples. It suggests that either noble gases of HIMU do not originate from normal upper mantle material and Hawaii-type plume sources or some processes to transport and extrude HIMU magmas might have caused such differences. The abundance patterns of HIMU are similar to the pattern of old oceanic crusts and sediments (e.g., Matsuda and Nagao, 1986; Staudacher and Allègre, 1988).

Abundance patterns of non-HIMU samples also show depletion of light noble gases and enrichment of heavy noble gases (Fig. 3-17(b)). However, degrees of Ne depletion and Xe enrichment are not so large as HIMU samples. While F-values are variable for

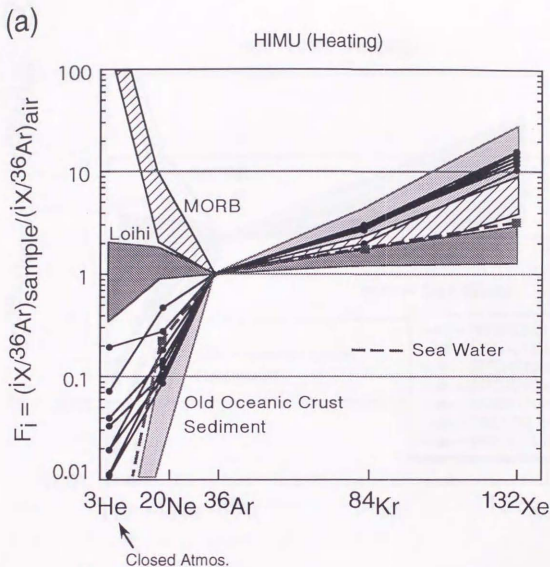


Fig. 3-17. Noble gas abundance patterns for (a) HIMU olivine samples, and (b) non-HIMU samples. Normalizing values of $(^{20}\text{Ne}/^{36}\text{Ar})_{\text{air}}$, $(^{84}\text{Kr}/^{36}\text{Ar})_{\text{air}}$ and $(^{132}\text{Xe}/^{36}\text{Ar})_{\text{air}}$ are 0.524, 0.0207 and 0.000747, respectively (Ozima and Podosek, 1983). $(^3\text{He}/^{36}\text{Ar})_{\text{air}}$ used for normalization is 0.0285 which corresponds the ratio of so-called closed atmosphere (Staudacher and Allègre, 1989). The abundance pattern of air-saturated seawater is indicated by a dotted line. Typical abundance patterns of "MORB", "Loihi" and "old oceanic crust and sediment" are shown by hatches.

(b)

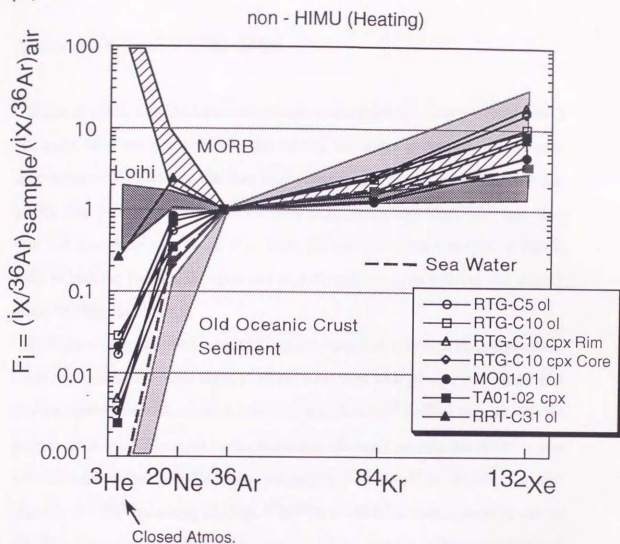


Fig. 3-17. (Continued)

4. Discussion

Constraints to the origin of HIMU and EM

Origin of HIMU and EM magma sources are constrained by newly provided data in this study. They are summarized in this section. EM rocks in the Polynesian region show different He tendency that they have variable and rather higher $^3\text{He}/^4\text{He}$ than MORB (Fig. 3-13). Considering all EM-OIBs in the world, both "high- ^3He " and "low- ^3He " hot spots have been found (Fig. 3-14). On the other hand, $^3\text{He}/^4\text{He}$ of HIMU rocks in both the Polynesian region and St. Helena show quite uniform and slightly lower $^3\text{He}/^4\text{He}$ than MORB.

HIMU have been identified to be the distinct end-member with high Pb isotope ratios. However, Sr and Nd isotope ratios of HIMU have been ambiguously understood that they are plotted below the so-called mantle array in the $\epsilon_{\text{Nd}}\text{-}^{87}\text{Sr}/^{86}\text{Sr}$ diagram. Precise analyses of Sr and Nd isotopes by cpx samples in this study provide that HIMU is also a distinct end-member in Sr-Nd isotope spaces (Fig. 3-9). HIMU has the most depleted character in $^{87}\text{Sr}/^{86}\text{Sr}$ among all OIBs. $^{87}\text{Sr}/^{86}\text{Sr}$ of HIMU is quite uniform as well as $^3\text{He}/^4\text{He}$. Data plots of $^{87}\text{Sr}/^{86}\text{Sr}$ and ϵ_{Nd} of HIMU samples make a straight trend which would be the result of mixing of the upper mantle material and the HIMU end-member. ϵ_{Nd} of HIMU end-member is constrained to be less than +3.3. ϵ_{Nd} seems to shift gradually according to the ages of islands.

Although discussion on trace elements needs much caution due to complicated melting and crystallization processes, some trace element pairs, like Pb/Ta, would give additional constraints. Anomalous patterns of noble gas abundances of HIMU samples should be also taken into consideration.

He isotopic signature of HIMU is characterized by its uniformity and the value which is slightly less than $^3\text{He}/^4\text{He}$ of MORB. Because $^3\text{He}/^4\text{He}$ of the upper mantle and typical plume material is around 8Ra and more than 30Ra, respectively, HIMU source requires some additional components which would have lower $^3\text{He}/^4\text{He}$ than 8Ra. Recycled materials are raised as such component(s) with high $(\text{U}+\text{Th})/^3\text{He}$ ratio. The hypothesis of reaction with the core is not a plausible process for the cause of low $^3\text{He}/^4\text{He}$ for HIMU source, because no process is known to raise $(\text{U}+\text{Th})/^3\text{He}$ by the interaction of core and silicate portion.

EM rocks show variable $^3\text{He}/^4\text{He}$ ratios. Most EM rocks in the Atlantic Ocean show lower $^3\text{He}/^4\text{He}$ than those of MORB, which has been considered to be the evidence of recycled material contribution to the magma sources (Kurz et al., 1982). Most EM lavas in the Pacific Ocean, however, show higher $^3\text{He}/^4\text{He}$ than MORB. It does not conflict with the assumption that EM magmas are originated from recycled materials because Loihi-type less degassed mantle material may be added to them in the southern Pacific area. Considering the Polynesian and the Samoan regions, what seems to be mysterious is that the low $^3\text{He}/^4\text{He}$ is observed only in HIMU rocks while most EM rocks show higher $^3\text{He}/^4\text{He}$. Further, HIMU signature seems to be appeared in the limited situation where quite uniform He isotope ratios should be kept. This problem is further discussed later.

Sr and Nd isotopes show that the HIMU source is quite uniform concerning them. $^{87}\text{Sr}/^{86}\text{Sr}$ of HIMU is the least among OIBs, and similar to MORB. It excludes the possibility that HIMU is recycled sediments because sediments have high Rb/Sr and initial $^{87}\text{Sr}/^{86}\text{Sr}$. The value of $^{87}\text{Sr}/^{86}\text{Sr}$ and its uniformity of HIMU rocks suggest that the origin of HIMU is related to the upper mantle material or MORB. However, this assumption is not consistent with Nd and Pb isotope ratios of HIMU.

Most of the previous studies for the origin of HIMU deal only Pb isotope ratios. Several processes have been proposed to produce high U/Pb ratio in the recycled MORB. One of them is the dehydration of altered MORB during subduction, which has been considered to be coupled with the arc magmatism. Recent dehydration experiments (Kogiso, 1995; Brenan et al., 1995; Keppler, 1996) have shown that Pb is very soluble in fluids. It is a possible process to explain the character of arc magmas including Pb enrichments (Keppler, 1996). The residue remained after dehydration would have been elevated in U/Pb and Th/Pb and subducted into the deep mantle.

However, this model can not explain following points. One is the value of $^{87}\text{Sr}/^{86}\text{Sr}$ of HIMU. As Rb is highly soluble in fluids while Sr is not soluble during dehydration (Keppler, 1996), Rb/Sr would become very low in the dehydrated material. Then, dehydrated and subducted material should show much lower $^{87}\text{Sr}/^{86}\text{Sr}$ due to lower time-integrated Rb/Sr than present MORB. If dehydration occurs in various degrees, it is difficult to explain the constancy of $^{87}\text{Sr}/^{86}\text{Sr}$ of HIMU. Regarding Pb isotope ratios, it is expected from this model that all subducted materials, both altered oceanic crusts and sediments, would have HIMU character with elevated U/Pb. However, it may contradict to the fact that HIMU magmas are limitedly observed among OIBs.

Another possibility for the origin of HIMU is the relatively fresh MORB. The observations of ophiolite provide that the lower part of oceanic crusts suffers only high temperature hydrothermal circulation and it remains relatively fresh (e.g., McCulloch et al., 1981). A hypothesis that the HIMU source is produced by subduction of less-altered MORB affected only by high temperature hydrothermal alteration is examined below based on the investigations of chemical composition of hydrothermal fluids emitted at mid oceanic ridges and field observations of ophiolite.

Extremely concentrated Pb in high temperature hydrothermal fluids suggests that Pb would be highly leached from oceanic crusts (Chauvel et al. (1995)). Though alteration of low temperature fluids raises $^{87}\text{Sr}/^{86}\text{Sr}$ of rocks up to the value of seawater (~ 0.709), high temperature hydrothermal water does not increase $^{87}\text{Sr}/^{86}\text{Sr}$ of oceanic

crusts so much (Staudigel et al., 1981). The change of trace element concentrations in rocks during high temperature hydrothermal circulation is not clear. Hydrothermal vent fluids have been found to be rich in alkali elements including Rb (Michard et al., 1984). It suggests that Rb might be leached from oceanic crusts. Since Sr is not mobile during alteration by seawater (Staudigel et al., 1981), Rb/Sr of oceanic crusts would decrease through the process of high temperature hydrothermal circulation. However, the degree of Rb loss from the oceanic crust in the deeper part is not known.

From studies of Samail ophiolite in Oman, $\delta^{18}\text{O}$ values in the section of ancient oceanic crusts suggest that hydrothermal circulation extends the base of oceanic crusts (Gregory and Taylor, 1981; McCulloch et al., 1981). The lower part (gabbroic layer) and upper part (pillow lavas and sheeted dike layers) of the oceanic crust are characterized by lower and higher $\delta^{18}\text{O}$ than typical oceanic crusts (5.8 per mil), respectively (Gregory and Taylor, 1981; McCulloch et al., 1981). It provides that alteration processes are different between the lower and upper oceanic crust that the former is affected by high temperature hydrothermal circulation with low water/rock ratio, while the latter is further altered by low temperature fluids with high water/rock ratio (McCulloch et al., 1981). High temperature hydrothermal fluids do not change $^{87}\text{Sr}/^{86}\text{Sr}$ so much (McCulloch et al., 1981; Stakes et al., 1984). Chen and Pallister (1981) have indicated that Pb is concentrated in the upper part and depleted in the lower part of Samail ophiolite. As Pb isotope ratios of both upper and lower parts show the similar values, Pb enriched in the upper part might have been derived from the lower part (Chen and Pallister, 1981). It indicates a possibility that Pb is leached from the lower part to mobilize upward.

Dostal et al. (1996) reported the element behavior during several kinds of alteration at Mururoa and Fangataufa atolls in French Polynesia. Compared with submarine low temperature alteration, change of elemental concentration during high temperature hydrothermal alteration is rather limited. Lanphere et al. (1981) investigated the vertical variation of Rb, Sr and $^{87}\text{Sr}/^{86}\text{Sr}$ of Ibra Cross Section of the Samail ophiolite.

$^{87}\text{Sr}/^{86}\text{Sr}$ shows almost constant values around 0.703 in the lower part of the section (gabbroic layer). Although Rb/Sr is variable in the lower part, $^{87}\text{Rb}/^{86}\text{Sr}$ of gabbroes is around 0.05 (Lanphere et al., 1981) which is close to the value of MORB (0.054, Chauvel et al., 1992).

Summarizing above discussion, Pb (and some chalcophile elements like Cu and Zn which are concentrated in hydrothermal deposits of sulfides and Mn-nodules) may behave in a different way from U, Th, Rb and Sr (Chauvel et al., 1995). Accordingly, the lower part of oceanic crusts would lose Pb extensively by high temperature hydrothermal fluids, while $^{87}\text{Sr}/^{86}\text{Sr}$ and Rb/Sr would not change so much.

Since alteration by low temperature fluids occurs only in the upper parts of the oceanic crusts (Hart and Staudigel, 1981; McCulloch et al., 1981), U/Pb and Rb/Sr of the lower part would not change further. Such less-altered MORB with the limited content of H_2O would be exempted from dehydration effects and it would preserve the elemental compositions during subduction.

The Pb/Ta signature is also compatible with the above model. The correlation between Pb/Ta and ϵ_{Nd} indicates that the HIMU end-member has a lower Pb/Ta than MORB. It coincides with a hypothesis that HIMU source originates from hydrothermally altered MORB with Pb depletion.

Relation between HIMU and EM

Accompanying less-altered MORB material, sediments and altered MORB would be also subducted into the deep mantle, though some parts would be prevented from subducting and added under the continental crusts. Zindler and Hart (1986) have suggested that subducted sediments are a candidate for the EM source, because sediments have high and variable Sr and Nd isotope ratios. In addition to them, altered MORB in the upper part of the oceanic crust might become a candidate for recycled

materials. Because MORB altered by low temperature fluids has elevated Rb/Sr and $^{87}\text{Sr}/^{86}\text{Sr}$, it would also become another enriched component.

Hotspot magmas originating from such recycled materials would have the isotopic signature between HIMU and EM. This idea explains the binary mixing trends of HIMU and EM1 for Polynesian basalts (Albarède and Dupuy, 1993) and so-called LoNd trend (Hart et al., 1986). Since sediments have much higher concentration of Sr, Nd and Pb, small contribution of recycled sediments to the HIMU source would dramatically change the isotopic signature from HIMU to EM. Thus, generation of pure HIMU is very limited in an area where there is not any contribution of other recycled materials to the HIMU source (Fig. 4-1). The problem that only HIMU magmas have the "low- ^3He " signature in the Polynesian and the Samoan regions is explained in the same way. Ascending recycled materials would contain less-degassed and degassed mantle material at the initiation and/or during upwelling. This process would strongly affect both solid and He isotopes. Conversely, HIMU signature would be observed only when the HIMU source material is purely melted without any significant effect from exotic components like EM source, less-degassed mantle and degassed mantle.

Nd isotope problem for HIMU

Although decoupling of Sr and Nd isotopes of HIMU has been recognized, the reason has not been discussed so far. The present study has made the isotopic characters of the HIMU end-member much clearer than before. ϵ_{Nd} of HIMU is constrained to be less than +3.3 and it is distinct from ϵ_{Nd} of MORB, while HIMU has similar $^{87}\text{Sr}/^{86}\text{Sr}$ to MORB. Such features provide further constraints for the generation of the HIMU source.

It is required that time-integrated Sm/Nd of the HIMU source should be less than that of the present upper mantle (MORB). First, I examine the processes to change Sm/Nd

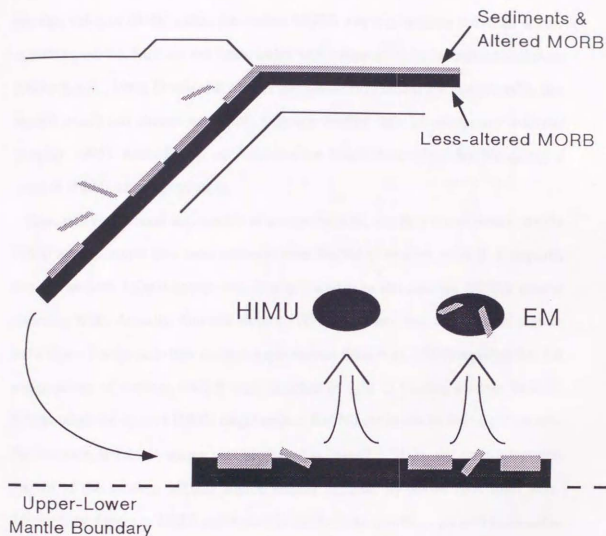


Fig. 4-1. Model showing recycling of subducted materials. Part of subducted sediments and altered MORB materials might have been stripped from slabs during subduction. When subducted materials upwell, mantle plumes with HIMU character are generated in the limited situation that subducted sediments and altered MORB materials do not contribute to the formation of mantle plumes. Mantle plumes including small amounts of sediments and altered MORB materials have the EM character.

of the ancient subducted MORB. During MORB formation, Sm/Nd of melt would become lower than that of the ancient upper mantle material. As shown in Fig. 4-2, however, the change of Sm/Nd is so limited during melting processes to explain the low ϵ_{Nd} value of HIMU unless the ancient MORB was produced by the small degree of melting (<7%). REE are not labile under high temperature hydrothermal alteration (Michard et al., 1983; Dostal et al., 1996). Dehydration (which is not considered in this model) would not change or slightly increase Sm/Nd ratio of subducting material (Kogiso, 1995). Accordingly, no processes are found to decrease Sm/Nd during a series of HIMU source generation.

Thus, it is conjectured that Sm/Nd of ancient MORB, which is considered to be the HIMU source, might have been different from Sm/Nd of modern MORB. It requires that the ancient MORB source was less-depleted than the modern MORB source regarding REE. Actually, Sun and Nesbitt (1978) suggested that the Archean mantle had a higher La/Sm ratio than modern upper mantle. Ohta et al. (1996) reported that the compositions of Archean MORB were enriched in light REEs than modern MORB. Hence, observed ϵ_{Nd} of HIMU might reflect Sm/Nd evolution in the upper mantle. For instance, if HIMU source was produced at 2Ga (Fig. 4-2), the time-integrated Sm/Nd of the modern MORB source should increase by about 10% after 2Ga. Although the degree of LREE enrichment in the Archean mantle is not well known, the recycling time would be in the order of billion years to produce the difference of $^{143}Nd/^{144}Nd$ between HIMU and modern MORB.

I examine the two stage mantle evolution model to explain the Sr and Nd isotope signatures of HIMU and modern MORB. The upper mantle depletion might have been coupled with the growth of continental crusts. Chase and Patchett (1988) discussed the two stage continental growth model; the rather rapid continental growth between 3.0 and 2.5Ga., following gradual progressive growth until present (Fig. 4-3). Then, secular changes of Sr and Nd isotope ratios in the upper mantle and HIMU are

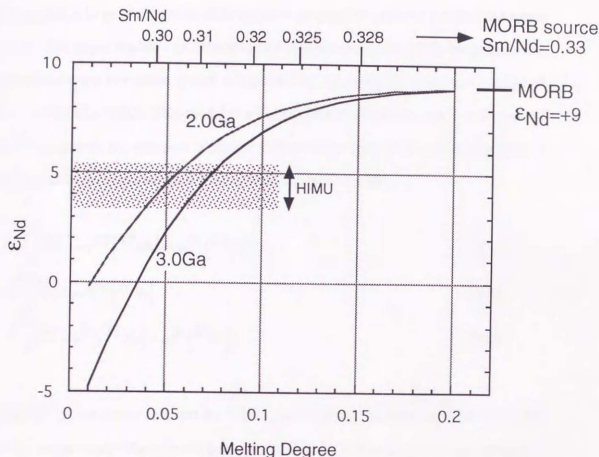


Fig. 4-2. ϵ_{Nd} of HIMU at present is simulated. HIMU source is assumed to be formed by melting of upper mantle material at 2.0Ga and 3.0Ga. Sm/Nd of the upper mantle at 2.0Ga or 3.0Ga is assumed to be similar to that at present (0.33; Hofmann, 1988). Change of Sm/Nd by melting is calculated using partition coefficients of spinel peridotite (McKenzie and O'Nions, 1991).

calculated by applying the first-order continuous transport model (Hart and Brooks, 1968).

It is assumed that the silicate portion of the earth had been homogeneous until 3.0Ga. At that time, a large scale mantle differentiation occurred to generate the depleted upper mantle. The upper mantle has suffered gradual depletion since 3.0Ga by progressive continental crust formation, which is modeled by the continuous transport model of Hart and Brooks (1968). This model is schematically illustrated in Fig. 4-4. In case of the Rb-Sr system, the transport of Rb and Sr from the mantle to the continental crust is assumed to be proportional to their concentrations in the mantle.

$$\frac{d(^{87}\text{Rb})}{dt} = -\lambda^{87}(^{87}\text{Rb}) - \gamma^{\text{Rb}}(^{87}\text{Rb}) \quad (4-1)$$

$$\frac{d(^{86}\text{Sr})}{dt} = -\alpha^{\text{Sr}}(^{86}\text{Sr}) \quad (4-2)$$

$$\frac{d(^{87}\text{Sr})}{dt} = \lambda^{87}(^{87}\text{Rb}) - \alpha^{\text{Sr}}(^{87}\text{Sr}) \quad (4-3)$$

where λ^{87} is the decay constant for ^{87}Rb . γ and α is the transport coefficient for Rb and Sr, respectively. The start of t is set at 3.0Ga in the following calculations (namely, $t=3.0\text{Gy}$ at present).

The solutions have following forms (Hart and Brooks, 1968);

$$\left(\frac{^{87}\text{Sr}}{^{86}\text{Sr}}\right)_t^{\text{UM}} = \left(\frac{^{87}\text{Sr}}{^{86}\text{Sr}}\right)_{3.0\text{Ga}} + \frac{\lambda^{87}(^{87}\text{Rb}/^{86}\text{Sr})_{3.0\text{Ga}} [1 - \exp\{-\lambda^{87} + k^{\text{Sr}}t\}]}{\lambda^{87} + k^{\text{Sr}}} \quad (4-4)$$

$$\left(\frac{^{87}\text{Rb}}{^{86}\text{Sr}}\right)_t^{\text{UM}} = \left(\frac{^{87}\text{Rb}}{^{86}\text{Sr}}\right)_{3.0\text{Ga}} \cdot \exp\{-\lambda^{87} + k^{\text{Sr}}t\} \quad (4-5)$$

where k^{Sr} equals $\gamma \cdot \alpha$. The abbreviation of UM means upper mantle. Rb is assumed to be transported faster than Sr; namely $k^{\text{Sr}} > 0$.

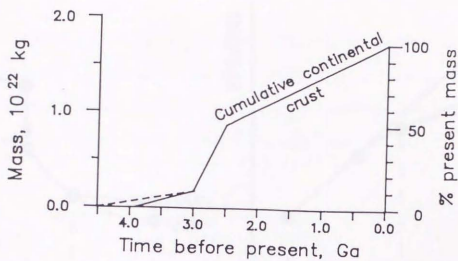


Fig. 4-3. Growth curve of continental crust after Chase and Patchett (1988).

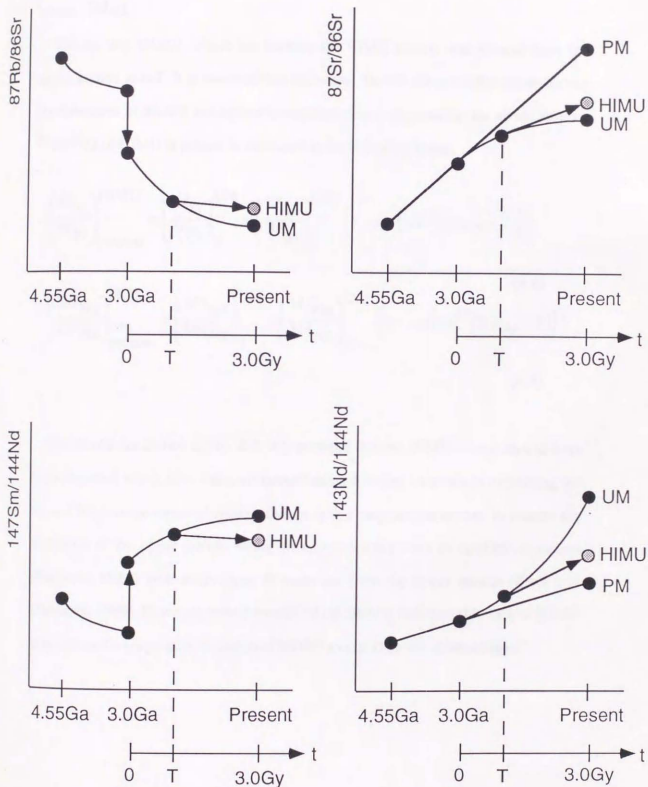


Fig. 4-4. Schematic figures of the first-order continuous transport model. The depleted upper mantle was formed at 3.0Ga and it has gradually depleted until present. The start of t is set at 3.0Ga. HIMU source was formed at T in the model.

$(^{87}\text{Sr}/^{86}\text{Sr})_{\text{present}}$, $(^{87}\text{Rb}/^{86}\text{Sr})_{\text{present}}$ and $(^{87}\text{Sr}/^{86}\text{Sr})_{3.0\text{Ga}}$ are fixed using values listed in Table 4-1. Then, unknown parameters of $(^{87}\text{Rb}/^{86}\text{Sr})_{3.0\text{Ga}}$ and k_{Sr} are uniquely determined. It is also applied to the Sm-Nd system for the upper mantle, where $k_{\text{Nd}} < 0$.

The ancient MORB, which has become the HIMU source, was formed from the upper mantle at $t=T$. It is assumed that Rb/Sr and Sm/Nd did not differentiate during the formation of MORB and hydrothermal alteration as discussed in the above section. $^{87}\text{Sr}/^{86}\text{Sr}$ of HIMU at present is simulated in the following forms;

$$\left(\frac{^{87}\text{Sr}}{^{86}\text{Sr}}\right)_{\text{present}}^{\text{HIMU}} = \left(\frac{^{87}\text{Sr}}{^{86}\text{Sr}}\right)_{\text{T}}^{\text{UM}} + \left(\frac{^{87}\text{Rb}}{^{86}\text{Sr}}\right)_{\text{T}}^{\text{UM}} \cdot \left[1 - \exp\{-\lambda^{87}(3.0\text{Gy} - T)\}\right] \quad (4-6)$$

$$\left(\frac{^{143}\text{Nd}}{^{144}\text{Nd}}\right)_{\text{present}}^{\text{HIMU}} = \left(\frac{^{143}\text{Nd}}{^{144}\text{Nd}}\right)_{\text{T}}^{\text{UM}} + \left(\frac{^{147}\text{Sm}}{^{144}\text{Nd}}\right)_{\text{T}}^{\text{UM}} \cdot \left[1 - \exp\{-\lambda^{87}(3.0\text{Gy} - T)\}\right] \quad (4-7)$$

The results are shown in Fig. 4-5. It is required that the HIMU source should have been recycled at 2-2.5Ga. The continuous transport model succeeds in explaining the Sr and Nd isotope ratios of HIMU, though it is a very simple model. In reality, the depletion of the upper mantle would be more complex such as episodic depletion (DePaolo, 1980) with some input of materials from the lower mantle (Stein and Hofmann, 1994). However, even a simplified calculation indicates that ϵ_{Nd} of HIMU may reflect the progressive depletion of MORB source since the Archean time.

Table 4-1. Parameters used for first-order continuous transport model.

	PM 4.55Ga (initial)	PM 3.0Ga (before diff.)	UM 3.0Ga (after diff.)	UM present
$^{87}\text{Sr}/^{86}\text{Sr}$	0.6990(*)	0.7010(\$)	0.7010(\$)	0.7024(¶)
$^{87}\text{Rb}/^{86}\text{Rb}$	0.093(*)	0.091(\$)	0.045(‡)	0.024(¶)
$^{143}\text{Nd}/^{144}\text{Nd}$	0.50682(*)	0.50882(\$)	0.50882(\$)	0.513310 ($\epsilon=+9.2$)(¶)
$^{147}\text{Sm}/^{144}\text{Nd}$	0.19845(*)	0.19645(\$)	0.19845(‡)	0.2400(¶)

Radioactive decay constant

$$\lambda_{87} = 1.42 \times 10^{-11} \text{ yr}^{-1}$$

$$\lambda_{147} = 6.54 \times 10^{-12} \text{ yr}^{-1}$$

Calculated transport coefficient

$$k_{\text{Sr}} = 2.0 \times 10^{-10} \text{ yr}^{-1}$$

$$k_{\text{Nd}} = -7.0 \times 10^{-11} \text{ yr}^{-1}$$

The primitive mantle (PM) was differentiated at 3.0Ga to produce depleted upper mantle (UM).

(*) Initial values of the bulk silicate earth.

(\$) Simulated values of the bulk silicate earth at 3.0Ga.

(¶) Values of the modern depleted mantle (MORB source).

(‡) Calculated to fit the 1-st order model.

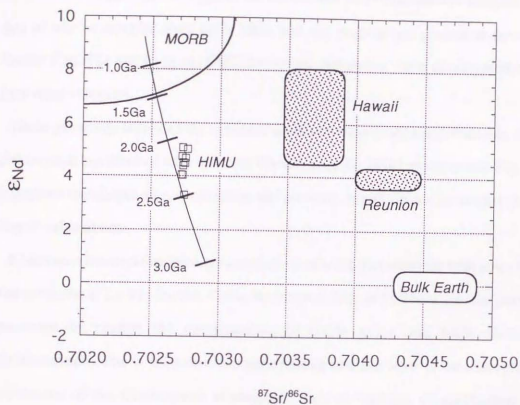


Fig. 4-5. Calculated Sr and Nd isotope ratios of HIMU source by the first-order continuous transport model. The time of formation of HIMU source (T) is shown at tick marks.

It is characteristic that HIMU samples show depletion of light noble gases and enrichment of heavy noble gases compared to those of the atmosphere. Fig. 4-6 shows the relation of F_{20} , F_{84} and F_{132} in the HIMU and Rarotonga olivine samples. The data of olivine samples from other OIBs and arc magmas are plotted in the same figures. F_{20} , F_{84} and F_{132} of HIMU are unique comparing those of olivine samples from other volcanics.

Noble gas compositions of air, saturated air in seawater (Ozima and Podosek, 1983) and magmas equilibrated with seawater (Patterson et al., 1994) are shown in Fig. 4-6. It suggests that simple air contamination and seawater dissolution to the magma do not form F-value trends.

It has been observed that there are correlations of noble gas elements with some trace elemental ratios; La/Yb, Sm/Nd, Ti/Eu, for instance (Fig. 4-7). There are two possible processes to change the compositions of noble gases and trace elements simultaneously. One is the two-component mixing and the other is the coincidental occurrence of the fractionation of magmas, such as melting, crystallization and degassing.

The former requires two components; especially, the one component is characterized by very low F_{20} (<0.1) and very high F_{84} (>3.0) and F_{132} (>16), which is shown by hatches in Figs. 4-6 and 4-7. Such noble gas pattern is classified in "Type 1" by Ozima and Alexander (1976). It has been found in old oceanic crusts and oceanic sediments (Matsuda and Nagao, 1986; Staudacher and Allègre, 1988). Whether highly fractionated noble gas pattern found in HIMU is originated from the source character of recycled oceanic crusts and sediments or their secondary contamination into the magma is not distinguished by the present data alone.

The latter possibility requires that melting, crystallization and degassing processes cause the change of noble gas and trace elemental abundances in a parallel way. It is

examined in Figs. 4-6 and 4-7. Since lighter noble gases are more incompatible than heavier noble gases in silicate minerals (Hiyagon and Ozima, 1986; Broadhurst et al., 1992; Shibata et al., 1994), F_{20} and La/Yb would increase and F_{84} and F_{132} would decrease as crystallization proceeds in a magma. Concerning melting effects, F_{20} and La/Yb would be higher and F_{84} and F_{132} would be lower in magmas than those of their source rocks. There are two types of degassing; one is disequilibrium degassing which follows after the mass fractionation law (Kaneoka, 1980) and the other is equilibrium degassing controlled by solubility. Here, the former is not available because no mass fractionation is observed in $^{38}Ar/^{36}Ar$, Ne, Kr and Xe isotope ratios (and constant $^3He/^4He$). In the equilibrium degassing, F_{20} would increase as degassing proceeds due to the higher solubility of Ne than Ar, and vice versa for F_{84} and F_{132} . La/Yb would not change during degassing. It is concluded that the source rock before suffering such processes as melting, crystallization and degassing should have very low F_{20} (<0.1) and very high F_{84} (>3.0) and F_{132} (>16) as shown by hatches in Figs. 4-6 and 4-7. Accordingly, the component with such indigenous noble gas abundance pattern is also required to produce HIMU magmas.

From the present data alone, it is difficult to identify whether such feature was originated from the recycled material or secondary contaminated oceanic crusts and/or sediments. However, the latter possibility can not explain why such feature is found more prominent in HIMU than in MORB and other OIBs. The former possibility does not contradict with the model for the HIMU source proposed above. Less-altered MORB which suffered only high temperature hydrothermal circulation would have the feature with Ne depletion and Kr and Xe enrichment. It would preserve the feature due to limited dehydration during subduction. Altered MORB and sediments, on the other hand, would have the same feature, but they may lose noble gases by dehydration during subduction (Hilton et al., 1992; Hiyagon, 1994).

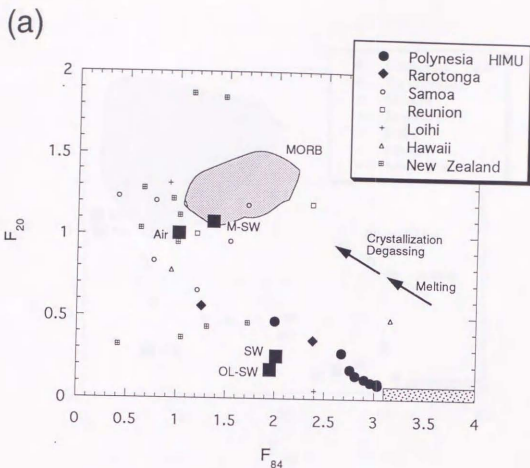


Fig. 4-6. (a) F_{84} versus F_{20} plot and (b) F_{132} versus F_{20} plot for HIMU and Rarotonga samples. The marks of "Air" and "SW" show the compositions of air and air-saturated seawater, respectively. The mark of "M-SW" indicates composition of magma equilibrated with seawater calculated as Patterson et al. (1990) using solubility data of alkali olivine basalt (Lux, 1987). The mark of "OL-SW" indicates the composition of olivine equilibrated with "M-SW" using noble gas solubility data of olivine (Shibata et al., 1994). Olivine data for other OIBs and arc magmas (New Zealand) are shown by small marks. The range of data of MORB glasses is also indicated. Changes of F -values by melting, crystallization and degassing are schematically illustrated by arrows. Required end-member component for HIMU samples is shown by the hatch. Data from Kaneoka and Takaoka (1978), Kaneoka and Takaoka (1980), Kaneoka et al. (1983), Staudacher et al. (1989), Staudacher et al. (1990), Hiyagon et al. (1992), Poreda and Farley (1992) and Patterson et al. (1994).

(b)

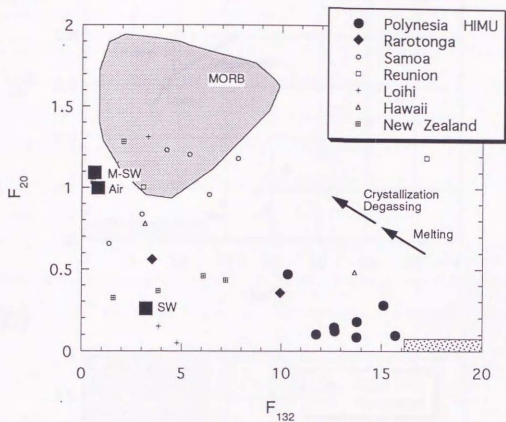
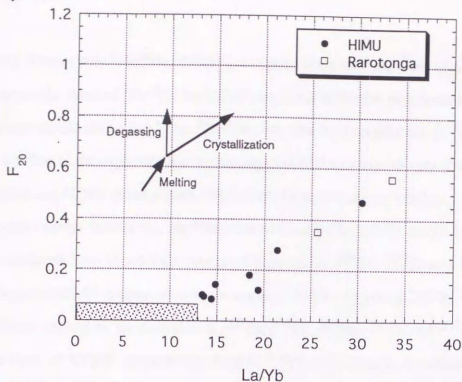


Fig. 4-6. (Continued)

(a)



(b)

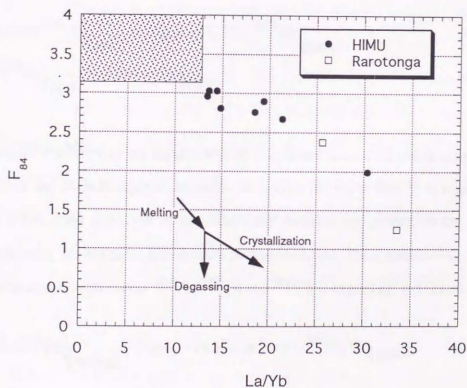


Fig. 4-7. La/Yb (whole rock) versus F_{20} and F_{84} (olivine) plots for HIMU and Rarotonga samples. Changes of F -values by melting, crystallization and degassing are schematically illustrated by arrows. Required end-member component for HIMU samples is shown by the hatch.

I will discuss why $^3\text{He}/^4\text{He}$ of HIMU samples shows uniform value of 6.8 ± 0.7 Ra. However, the value of $^3\text{He}/^4\text{He}$ for HIMU samples is rather too high because recycled materials should have much lower $^3\text{He}/^4\text{He}$ than 1Ra due to production of ^4He from U and Th. One of the explanation is the mixing of HIMU source with very low $^3\text{He}/^4\text{He}$ ($R < 1\text{Ra}$) and MORB-Source ($R = 8.68\text{Ra}$). First, I examine this possibility.

For the mixing calculation, the ^4He concentration in the HIMU source is required. ^4He produced from U and Th is estimated from excess ^{206}Pb , ^{207}Pb and ^{208}Pb . As the origin of HIMU is assumed to be the ancient MORB, the excess ^{206}Pb , ^{207}Pb and ^{208}Pb are defined by the deviation of $^{206}\text{Pb}/^{204}\text{Pb}$, $^{207}\text{Pb}/^{204}\text{Pb}$ and $^{208}\text{Pb}/^{204}\text{Pb}$ from those of MORB, respectively. Excess ^{206}Pb , for instance, is calculated if the value of $^{206}\text{Pb}/^{204}\text{Pb}$ of HIMU end-member (which is expressed by Z_{206}) is known;

$$\left(\text{excess}^{206}\text{Pb}\right)_{[\text{ppm}]} = (Z_{206} - 18.2) \times \left(^{204}\text{Pb}\right)_{[\text{ppm}]} \quad (4-8)$$

$$\left(^{204}\text{Pb}\right)_{[\text{ppm}]} = 0.014 \times (\text{Pb})_{[\text{ppm}]} \quad (4-9)$$

where $^{206}\text{Pb}/^{204}\text{Pb}$ of the present MORB is assumed to be 18.2 which is the average value of the MORB. Z_{206} is, actually, not known but more than 21.6. It is assumed that Z_{206} , Z_{207} and Z_{208} of the HIMU end-member are plotted on the so-called mantle array (or Northern Hemisphere Reference Line). Then, excess ^4He produced simultaneously with excess ^{206}Pb , ^{207}Pb and ^{208}Pb is expressed as follows;

$$\left(\text{excess}^4\text{He}\right)_{[\text{mol/g}]} = (Z_{206} - 18.2) \times (8.7 \times 10^{-10}) \times (\text{Pb})_{[\text{ppm}]} \quad (4-10)$$

Note that it is the minimum estimate because Pb isotope ratios of the ancient MORB would be lower than those of present MORB. The estimated values of $^{206}\text{Pb}/^{204}\text{Pb}$,

$^{207}\text{Pb}/^{204}\text{Pb}$ and $^{208}\text{Pb}/^{204}\text{Pb}$ of the 2Ga MORB are 14.67, 15.06 and 34.05, respectively (Chauvel et al., 1992).

The $^4\text{He}/\text{Pb}$ of HIMU end-member is expressed by the function of Z_{206} ($Z_{206} > 21.6$). On the other hand, ^4He concentration of MORB source is 4.7×10^{-11} mol/g (Porcelli & Wasserburg, 1995) and 7.5×10^{-11} mol/g (O'Nions and Tolstikhin, 1996). Pb concentration of MORB source is 0.0576ppm (Chauvel et al., 1992).

The mixing line is simulated in Fig. 4-8 (^4He concentration of MORB source from Porcelli and Wasserburg (1995)). Calculation is carried out in the case that Z_{206} is 22.0, 30.0 and 40.0. Fig. 4-8 indicates that simple mixing is not valid to explain the $^3\text{He}/^4\text{He}$ and $^{206}\text{Pb}/^{204}\text{Pb}$ values of Polynesian HIMU samples. As suggested above, $^4\text{He}/\text{Pb}$ of HIMU end-member used in the mixing calculation is the minimum estimate. Larger $^4\text{He}/\text{Pb}$ of the HIMU end-member for the mixing calculation results in getting an inappropriate trend from explaining them.

Another explanation of $^3\text{He}/^4\text{He}$ of HIMU samples (6.81Ra) is the He open system model. In the above discussion, it is supposed that ^4He produced from U and Th have been trapped in HIMU source rocks with ^{206}Pb , ^{207}Pb and ^{208}Pb . Helium would be lost from the HIMU source material to the surrounding mantle due to the high diffusivity of helium. We assume here that the HIMU source has a sheet-like shape and resides around the upper-lower mantle boundary (Fig. 4-1), where the situation is analogous to the image proposed by Ringwood (1990). Then the diffusion time of helium in the HIMU source is estimated (Fig. 4-9).

Diffusivity of helium used for the calculation of Fig. 4-9 is assumed to be 1×10^{-8} m^2/sec . It corresponds to the He diffusivity in the melt at 1600°C which is extrapolated using the compiled data of Ozima and Podosek (1983). Temperature of 1600°C is equivalent to the temperature at the upper-lower mantle boundary (Brown and Shankland, 1981; Ito and Katsura, 1989). Volume diffusion of He in olivines at 1600°C is estimated to be 2.3×10^{-10} m^2/sec (extrapolated of the diffusion data of Hart (1984)). However, grain boundary diffusion is the controlling process rather than

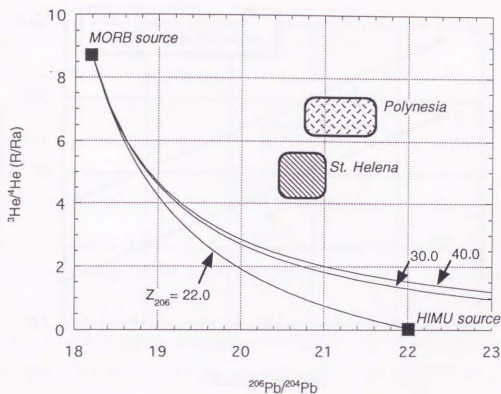


Fig. 4-8. He-Pb isotope mixing trends between MORB source and HIMU source. The end-member compositions of MORB source are as follows; $^3\text{He}/^4\text{He}$, 8.7 Ra; $^{206}\text{Pb}/^{204}\text{Pb}$, 18.2; (^4He), 4.7×10^{-11} mol/g (Porcelli and Wasserburg, 1995); (Pb), 0.0576 ppm (Chauvel et al., 1992). The end-member compositions of the HIMU source are; $^3\text{He}/^4\text{He}$, 0.05 Ra. $^{206}\text{Pb}/^{204}\text{Pb}$ (Z_{206}) of HIMU is variable (22.0, 30.0 and 40.0). $^4\text{He}/\text{Pb}$ ratio of the HIMU source is calculated by eq.(4-10). The hatched area corresponds to the range for data of Polynesian HIMU samples.

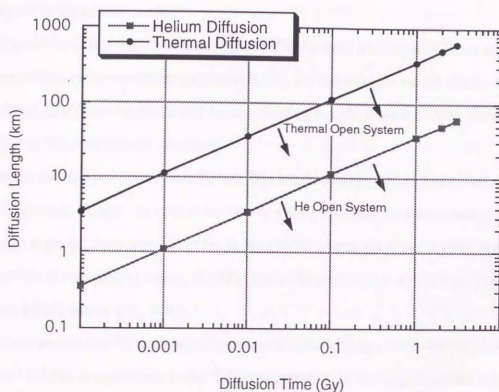


Fig. 4-9. Diffusion length as a function of diffusion time. The assumed thermal diffusivity and helium diffusivity are 1×10^{-6} and 1×10^{-8} m^2/sec , respectively. Diffusion length corresponds to $2\sqrt{Dt}$, where D is diffusivity and t is time, respectively.

volume diffusion. Although grain boundary diffusion is not well known, Trull and Kurz (1993) have discussed that grain boundary diffusion of He would not exceed the diffusivity in melts and fluids. Accordingly, $1 \times 10^{-8} \text{ m}^2/\text{sec}$ for He diffusivity is adopted in the present model.

Fig. 4-9 indicates that if the thickness of HIMU source rock layer is 10km and they have resided in the mantle for more than 0.1Gy, for instance, He would wholly diffuse between HIMU source rocks and the surrounding mantle materials. This situation is called as "He open system" hereafter.

When the He open system is achieved, ^3He would entirely diffuse and concentration of ^3He would be uniform in both the HIMU source rock and the surrounding MORB source material. However, $^3\text{He}/^4\text{He}$ in the HIMU source becomes slightly less than $^3\text{He}/^4\text{He}$ of surrounding mantle (8.68Ra) due to the production of ^4He from U and Th in the HIMU source (Fig. 4-10).

It is assumed that ^4He concentration was uniform (C_{DM}^4) in the initial condition, where C_{DM}^4 is equivalent to the ^4He concentration in the upper mantle. For $t > 0$, concentration of ^4He equals to C_{DM}^4 at $x = \infty$. The excess ^4He is defined as the average of the excess ^4He in the HIMU source rocks.

$$\text{excess } ^4\text{He} = \int_0^{L/2} (C^4 - C_{\text{DM}}^4) dx / \int_0^{L/2} dx \quad (4-11)$$

where $C^4(t, x)$ is the concentration of ^4He and L is the thickness of the HIMU source rocks. $^3\text{He}/^4\text{He}$ in the HIMU source is a function of time after subduction.

$$^3\text{He}/^4\text{He} = \frac{C_{\text{DM}}^3}{C_{\text{DM}}^4 + \text{excess } ^4\text{He}} \quad (4-12)$$

The parameters are the concentration of U and the diffusivity of He.

The process of calculation is shown in the Appendix-C. Relation between time and thickness is simulated to satisfy the $^3\text{He}/^4\text{He}$ of HIMU samples. The solution is shown in Fig. 4-11 as a function of U concentration. There are two constraints for the calculation. One is that t should be less than 4.55Gy. The other is that total produced ^4He in the HIMU source rock should be more than 4.9×10^{-10} mol/g (see Appendix-C). The latter constraint corresponds to that $^{206}\text{Pb}/^{204}\text{Pb}$ should be more than 21.6 for the HIMU source. If the HIMU source is composed of fresh or slightly altered MORB (Line 2 in Fig. 4-11), the solution of thickness and age of the HIMU source is highly constrained; thickness and age should be between 0.8–6km and more than 0.6Gy, respectively.

The most important result in this calculation is that the thickness of HIMU source rock should be less than 6km and probably in the order of 1km as long as the present model is valid. The estimated thickness of HIMU source rock layer would be consistent to that of subducted lower oceanic crusts related to HIMU origin. This result suggests that extensive delamination of subducted oceanic crust does not occur in the source region. Piling and thickening of subducted oceanic crusts would be also rejected as the HIMU source.

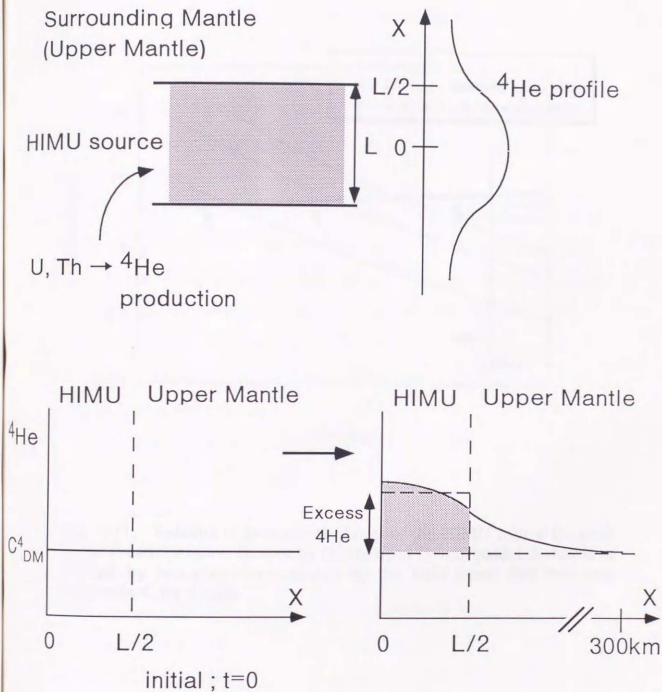


Fig. 4-10. Schematic illustration of the He open system model. Radiogenic 4He is produced from U and Th in the HIMU source layer with the thickness of L . The diffusive profile of radiogenic 4He is calculated as described in the Appendix-C. Excess 4He is defined by eq.(4-11).

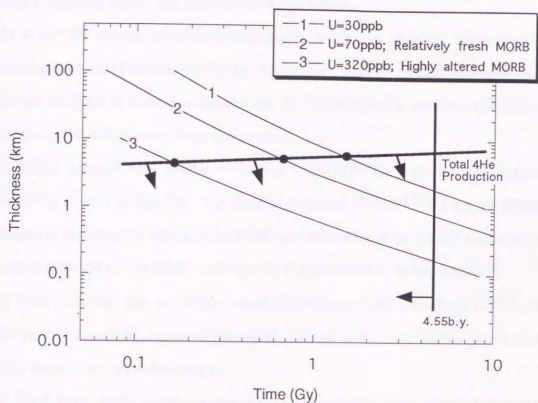


Fig. 4-11. Relation of time and thickness of the HIMU source for each given U concentration derived by the He open system model. Solution is limited by two constraints shown by the bold lines. See text and Appendix-C for details.

5. Summary

To investigate the origin of HIMU and EM sources, I carried out analyses of Sr and Nd isotopes, trace and rare earth elements and noble gas isotopes for hotspot magmas in the Polynesian region. The main results are as follows.

- (1) Sr and Nd isotope ratios were measured by using cpx samples, which enables complete removal of secondary effects to the magmas, such as seawater contamination. Further, analyses of noble gas isotopes and Sr, Nd isotopes for the same phenocryst samples provide clear comparison one another.
- (2) HIMU samples have similar $^{87}\text{Sr}/^{86}\text{Sr}$ to MORB. They show quite uniform $^{87}\text{Sr}/^{86}\text{Sr}$ as well as $^3\text{He}/^4\text{He}$. The small variation of $^{143}\text{Nd}/^{144}\text{Nd}$ among HIMU samples is explained by mixing of the HIMU end-member and the MORB source in the upper mantle. ϵ_{Nd} of the HIMU end-member is constrained to be less than +3.3.
- (3) Trace elemental data would give another information for the origin of HIMU and EM sources. Especially, elemental pairs of Pb-Ta and Ce-Pb have been proposed to be better tracers to examine their origin.
- (4) $^3\text{He}/^4\text{He}$ of HIMU samples is quite uniform and slightly lower values than that of MORB. On the other hand, EM samples in the Polynesian region show variable and higher $^3\text{He}/^4\text{He}$ than those of MORB.
- (5) Noble gas abundance patterns of HIMU are noteworthy by Ne (and possibly He) depletion and Kr and Xe enrichment relative to those of the atmosphere.

The origin of the HIMU and EM sources have been inferred on the basis of constraints obtained in this study.

- (1) Low $^3\text{He}/^4\text{He}$ of HIMU requires high time-integrated $(\text{U}+\text{Th})/^3\text{He}$, which favors a model that the HIMU source was related to recycled materials which were once located near the Earth's surface.
- (2) Along with the He isotope constraint, uniform and relatively low $^{87}\text{Sr}/^{86}\text{Sr}$ is required for the HIMU source. These constraints, considering Pb isotopes together,

favor the model that the HIMU source was the subducted less-altered MORB-like material which suffered only high temperature hydrothermal circulation.

(3) $^{143}\text{Nd}/^{144}\text{Nd}$ evidence of HIMU suggests that the ancient MORB source in the upper mantle at the time of the HIMU source formation was more enriched than the present one regarding Sm/Nd. Based on the first-order transport model to express the depletion history of the upper mantle, the age of HIMU source formation has been estimated to be around 2Ga.

(4) The value of $^3\text{He}/^4\text{He}$ for the HIMU source is explained by a He open system model which includes the effects of ^4He production and diffusion between the HIMU source and the surrounding mantle materials. Applying this model, the thickness of the HIMU source is estimated to be in the order of 1km.

Acknowledgments

I am grateful to Prof. I. Kaneoka for his continuous supports and many insightful suggestions. I am also grateful to Prof. E. Nakamura and Prof. K. Nagao for giving me the chance for Sr, Nd isotopes, noble gases and trace element analyses with helpful suggestions. Prof. K. Aoki kindly gave me suggestions on sample description and preparation. I would like to thank members in ISEI, Okayama University, especially Prof. A. Makishima, Dr. T. Shibata, Dr. M. Yoshikawa, Dr. T. Moriguti, Dr. Y. Iizuka, Mr. T. Nakano, Mr. K. Kobayashi and Mr. Akiyoshi for their help on chemical analyses. I wish to thank Prof. K. Notsu, Prof. T. Fujii and Prof. Y. Hamano for valuable comments and criticisms. Prof. Y. Tatsumi and Dr. T. Kogiso kindly provided me with samples from some Polynesian islands. Dr. Y. N. Miura and Mr. H. Kumagai gave me great help for setting up the MS at ERI. Suggestions from Dr. H. Hiyagon, Dr. T. Sasada, Dr. K. Kaneko, Mr. T. Sano and Mr. N. Iwata were helpful for improving this thesis.

References

- Albarède, F., and C. Dupuy, Relationship between geochemical components in Polynesian hot spots, *Abstract International Workshop on Intraplate Volcanism: The Polynesian Plume Province*, 1, 1993.
- Allègre, C. J., B. Dupré, and O. Brévar, Chemical aspects of the formation of the core, *Philos. Trans. R. Soc. Lond.*, A306, 49-59, 1982.
- Azuma, S.-I., M. Ozima, and H. Hiyagon, Anomalous neon and xenon in an Archean anorthosite from West Greenland, *Earth Planet. Sci. Lett.*, 114, 341-352, 1993.
- Ben Othman, D., W. M. White, and J. Patchett, The geochemistry of marine sediments, island arc magma genesis, and crust-mantle recycling, *Earth Planet. Sci. Lett.*, 94, 1-21, 1989.
- Brenan, J. M., H. F. Shaw, F. J. Ryerson, and D. L. Phinney, Mineral-aqueous fluid partitioning of trace elements at 900°C and 2.0GPa: Constraints on the trace element chemistry of mantle and deep crustal fluids, *Geochim. Cosmochim. Acta*, 59, 3331-3350, 1995.
- Broadhurst, C. L., M. J. Drake, B. E., Hagee, and T. J. Bernatowicz, Solubility and partitioning of Ne, Ar, Kr and Xe in minerals and synthetic basaltic melts, *Geochim. Cosmochim. Acta*, 56, 709-723, 1992.
- Brown, J. M., and T. J. Shankland, Thermodynamic parameters in the Earth as determined from seismic profiles, *Geophys. J. R. Astr. Soc.*, 66, 579-596, 1981.
- Cazenave, A., and C. Thoraval, Mantle dynamics constrained by degree 6 surface topography, seismic tomography and geoid: Inference on the origin of the South Pacific Superswell, *Earth Planet. Sci. Lett.*, 122, 207-219, 1994.
- Chase, C. G., and P. J. Patchett, Stored mafic/ultramafic crust and early Archean mantle depletion, *Earth Planet. Sci. Lett.*, 91, 66-72, 1988.
- Chauvel, C., S. L. Goldstein, and A. W. Hofmann, Hydration and dehydration of oceanic crust controls Pb evolution in the mantle, *Chem. Geol.*, 126, 65-75, 1995.
- Chauvel, C., A. W. Hofmann, and P. Vidal, HIMU-EM: The French Polynesian connection, *Earth Planet. Sci. Lett.*, 110, 99-119, 1992.
- Chen, J. M., and J. S. Pallister, Lead isotopic studies of the Samail ophiolite, Oman, *J. Geophys. Res.*, 86, 2699-2708, 1981.

- DePaolo, D. J., Crustal growth and mantle evolution: inferences from models of element transport and Nd and Sr isotopes, *Geochim. Cosmochim. Acta*, 44, 1185-1196, 1980.
- Dostal, J., C. Dupuy, and P. Dudoignon, Distribution of boron, lithium and beryllium in ocean island basalts from French Polynesia: implications for the B/Be and Li/Be ratios as tracers of subducted components, *Mineral. Magazine*, 60, 563-580, 1996.
- Dziewonski, A. M., Mapping the lower mantle: Determination of lateral heterogeneity in P velocity up to degree and order 6, *J. Geophys. Res.*, 89, 5929-5952, 1984.
- Duncan, R. A., and I. McDougall, Linear volcanism in French Polynesia, *J. Volcanol. Geotherm. Res.*, 1, 197-227, 1976.
- Dupuy, C., H. G. Barszczus, J. Dostal, P. Vidal, and J.-M. Liotard, Subducted and recycled lithosphere as the mantle source of ocean island basalts from southern Polynesia, central Pacific, *Chem. Geol.*, 77, 1-18, 1989.
- Dupuy, C., H. G. Barszczus, J. M. Liotard, and J. Dostal, Trace element evidence for the origin of oceanic island basalts: an example from the Austral Islands (French Polynesia), *Contrib. Mineral. Petrol.*, 98, 293-302, 1988.
- Fisk, M. R., B. G. J. Upton, C. E. Ford, and W. M. White, Geochemical and experimental study of the genesis of magmas of Réunion Island, Indian Ocean, *J. Geophys. Res.*, 93, 4933-4950, 1988.
- Fukao, Y., Seismic tomogram of the Earth's mantle: geodynamic implications, *Nature*, 258, 625-630, 1992.
- Graham, D., J. Lupton, F. Albarède, and M. Condomines, Extreme temporal homogeneity of helium isotopes at Piton de la Fournaise, Réunion Island, *Nature*, 347, 545-548, 1990.
- Graham, D. W., S. E. Humphris, W. J. Jenkins, and M. D. Kurz, Helium isotope geochemistry of some volcanic rocks from Saint Helena, *Earth Planet. Sci. Lett.*, 110, 121-131, 1992.
- Graham, D. W., A. Zindler, M. D. Kurz, W. J. Jenkins, R. Batiza, and H. Staudigel, He, Pb, Sr and Nd isotope constraints on magma genesis and mantle heterogeneity beneath young Pacific seamounts, *Contrib. Mineral. Petrol.*, 99, 446-463, 1988.
- Green, T. H., Experimental studies of trace-element partitioning applicable to igneous petrogenesis - Sedona 16 years later, *Chem. Geol.*, 117, 1-36, 1994.

- Green, T. H., and N. J. Pearson, Rare earth element partitioning between clinopyroxene and silicate liquid at moderate to high pressure, *Contrib. Mineral. Petrol.*, 91, 24-36, 1985.
- Gregory, R. T., and H. P. Taylor, Jr., An oxygen isotope profile in a section of cretaceous oceanic crust, Samail ophiolite, Oman: evidence for $\delta^{18}\text{O}$ buffering of the oceans by deep (>5km) seawater-hydrothermal circulation at mid-ocean ridges, *J. Geophys. Res.*, 86, 2737-2755, 1981.
- Hart, S. R., He diffusion in olivine, *Earth Planet. Sci. Lett.*, 70, 297-302, 1984.
- Hart, S. R., and C. Brooks, Rb-Sr mantle models, *Carnegie Institution Washington, Year Book*, 426-429, 1968-1969.
- Hart, S. R., D. C. Gerlach, and W. M. White, A possible new Sr-Nd-Pb mantle array and consequences for mantle mixing, *Geochim. Cosmochim. Acta*, 50, 1551-1557, 1986.
- Hart, S. R., and H. Staudigel, The control of alkalis and uranium in seawater by ocean crust alteration, *Earth Planet. Sci. Lett.*, 58, 202-212, 1982.
- Hawkesworth, C. J., J. M. Hergt, R. M. Ellam, and F. McDermott, Element fluxes associated with subduction related magmatism, *Phil. Trans. R. Soc. Lond.*, A335, 393-405, 1991.
- Hémond, C., C. W. Devey, and C. Chauvel, Source compositions and melting processes in the Society and Austral plumes (South Pacific Ocean): Element and isotope (Sr, Nd, Pb, Th) geochemistry, *Chem. Geol.*, 115, 7-45, 1994.
- Hilton, D. R., J. Barling and G. E. Wheller, Effect of shallow-level contamination on the helium isotope systematics of ocean-island lavas, *Nature*, 373, 330-333, 1995.
- Hilton, D. R., K. Hammerschmidt, G. Loock, and H. Friedrichsen, Helium and argon isotope systematics of the central Lau Basin and Valu Fa Ridge: Evidence of crust/mantle interactions in a back-arc basin, *Geochim. Cosmochim. Acta*, 57, 2819-2841, 1993.
- Hilton, D. R., J. A. Hoogewerff, M. J. Van Bergen, and K. Hammerschmidt, Mapping magma sources in the east Sunda-Banda arcs, Indonesia: Constraints from helium isotopes, *Geochim. Cosmochim. Acta*, 56, 851-859, 1992.
- Hiyagon, H., Retention of solar helium and neon in IDPs in deep sea sediment, *Science*, 263, 1257-1259, 1994.
- Hiyagon, H., and M. Ozima, Partition of noble gases between olivine and basalt melt, *Geochim. Cosmochim. Acta*, 50, 2045-2057, 1986.

Hiyagon, H., M. Ozima, B. Marty, S. Zashu, and H. Sakai, Noble gases in submarine glasses from mid-oceanic ridges and Loihi seamount: Constraints on the early history of the Earth, *Geochim. Cosmochim. Acta*, **56**, 1301-1316, 1992.

Hofmann, A. W., Chemical differentiation of the Earth: the relationship between mantle, continental crust, and oceanic crust, *Earth Planet. Sci. Lett.*, **90**, 297-314, 1988.

Hofmann, A. W., K. P. Jochum, M. Seufert, and W. M. White, Nb and Pb in oceanic basalts: new constraints on mantle evolution, *Earth Planet. Sci. Lett.*, **79**, 33-45, 1986.

Hofmann, A. W., and W. M. White, Mantle plumes from ancient oceanic crust, *Earth Planet. Sci. Lett.*, **57**, 421-436, 1982.

Honda, M., I. McDougall, D. B. Patterson, A. Doulgeris, and D. A. Clague, Noble gases in submarine pillow basalt glasses from Loihi and Kilauea, Hawaii: a solar component in the Earth, *Geochim. Cosmochim. Acta*, **57**, 859-874, 1993.

Ito, E., and T. Katsura, A temperature profile of the mantle transition zone, *Geophys. Res. Lett.*, **16**, 425-428, 1989.

Kaneoka, I., Rare gas isotopes and mass fractionation: an indicator of gas transport into of from a magma, *Earth Planet. Sci. Lett.*, **48**, 284-292, 1980.

Kaneoka, I., and N. Takaoka, Excess ^{129}Xe and high $^3\text{He}/^4\text{He}$ ratios in olivine phenocrysts of Kapuho lava and xenolithic dunites from Hawaii, *Earth Planet. Sci. Lett.*, **39**, 382-386, 1978.

Kaneoka, I., and N. Takaoka, Rare gas isotopes in Hawaiian ultramafic nodules and volcanic rocks: constraint on genetic relationships, *Science*, **208**, 1366-1368, 1980.

Kaneoka, I., and N. Takaoka, Noble-gas state in the Earth's interior - some constraints on the present state, *Chem. Geol. (Isot. Geosci. Sect.)*, **52**, 75-95, 1985.

Kaneoka, I., N. Takaoka, and D. A. Clague, Noble gas systematics for coexisting and dunite xenoliths from Loihi Seamount, *Earth Planet. Sci. Lett.*, **66**, 427-437, 1983.

Keppeler, H., Constraints from partitioning experiments on the composition of subduction-zone fluids, *Nature*, **380**, 237-240, 1996.

Kogiso, T., Role of the subducted oceanic crusts in the origin of HIMU ocean island basalts: evidence from dehydration experiments and geochemistry of Polynesian basalts, Ph.D. Thesis, Kyoto University, 1995.

- Kurz, M. D., D. Colodner, T. W. Trull, R. B. Moore, and K. O'Brien, Cosmic ray exposure dating with in situ produced cosmogenic ^3He : results from young Hawaiian lava flows, *Earth Planet. Sci. Lett.*, 97, 177-189, 1990.
- Kurz, M. D., W. J. Jenkins, and S. R. Hart, Helium isotopic systematics of oceanic islands and mantle heterogeneity, *Nature*, 297, 43-47, 1982.
- Kurz, M. D., W. J. Jenkins, S. R. Hart, and D. Clague, Helium isotopic variations in volcanic rocks from Loihi Seamount and the Island of Hawaii, *Earth Planet. Sci. Lett.*, 66, 388-406, 1983.
- Kurz, M. D., P. S. Meyer, and H. Sigurdsson, Helium isotopic systematics within the neovolcanic zones of Iceland, *Earth Planet. Sci. Lett.*, 74, 291-305, 1985.
- Lanphere, M. A., R. G. Coleman, and C. A. Hopson, Sr isotopic tracer study of the Samail ophiolite, Oman, *J. Geophys. Res.*, 86, 2709-2720, 1981.
- Lux, G., The behavior of noble gases in silicate liquids: Solution, diffusion, bubbles and surface effects, with applications to natural samples, *Geochim. Cosmochim. Acta*, 51, 1549-1560, 1987.
- Makishima, A., T. Nakano, T. Moriguti, and E. Nakamura, Quantitative analysis of incompatible elements with ICP-MS, 1995 Japan Earth and Planetary Science Joint Meeting, 315, 1995 (in Japanese).
- Matsuda, J.-I., and K. Nagao, Noble gas abundances in a deep-sea sediment core from eastern equatorial Pacific, *Geochem. Jour.*, 20, 71-80, 1986.
- McCulloch, M. T., R. T. Gregory, G. J. Wasserburg, and H. P. Taylor, Jr., Sm-Nd, Rb-Sr, and $^{18}\text{O}/^{16}\text{O}$ isotopic systematics in an oceanic crustal section: evidence from the Samail ophiolite, *J. Geophys. Res.*, 86, 2721-2735, 1981.
- McDonough, W. F., and S.-S. Sun, The composition of the Earth, *Chem. Geol.*, 120, 223-253, 1995.
- McKenzie, D., and R. K. O'Nions, Mantle reservoirs and ocean island basalts, *Nature*, 301, 229-231, 1983.
- McKenzie, D., and R. K. O'Nions, Partial melt distributions from inversion of rare earth element concentrations, *Jour. Petrol.*, 32, 1021-1091, 1991.
- McNutt, M. K., and A. V. Judge, The superswell and mantle dynamics beneath the South Pacific, *Science*, 248, 969-975, 1990.

- Michard, A., F. Albarède, G. Michard, J. F. Minster and J. L. Charlou, Rare-earth elements and uranium in high-temperature solutions from East Pacific Rise hydrothermal vent field (13°N), *Nature*, 303, 795-797, 1983.
- Michard, G., F. Albarède, F. Michard, J.-F. Minster, J.-L. Charlou, and N. Tan, Chemistry of solutions from the 13°N East Pacific Rise hydrothermal site, *Earth Planet. Sci. Lett.*, 67, 297-307, 1984.
- Miura, Y., and K. Nagao, Noble gases in six GSJ igneous rock samples, *Geochem. Jour.*, 25, 163-171, 1991.
- Morgan, W. J., Convection plumes in the lower mantle, *Nature*, 230, 42-43, 1971.
- Nakamura, Y., and M. Tatsumoto, Pb, Nd, and Sr isotopic evidence for a multicomponent source for rocks of Cook-Austral Islands and heterogeneities of mantle plumes, *Geochim. Cosmochim. Acta*, 52, 2909-2924, 1988.
- Nagao, K., A. Ogata, Y. N. Miura, and K. Yamaguchi, Ar isotope analysis for K-Ar dating using two modified-VG5400 mass spectrometers-I: isotope dilution method, *J. Mass Spectrom. Soc. Jpn.*, 44, 39-61, 1996.
- Newsom, H. E., W. M. White, K. P. Jochum, and A. W. Hofmann, Siderophile and chalcophile element abundances in oceanic basalts, Pb isotope evolution and growth of the Earth's core, *Earth Planet. Sci. Lett.*, 80, 299-313, 1986.
- Nimis, P., A clinopyroxene geobarometer for basaltic systems based on crystal-structure modeling, *Contrib. Mineral. Petrol.*, 121, 115-125, 1995.
- Ohta, H., S. Maruyama, E. Takahashi, Y. Watanabe, and Y. Kato, Field occurrence, geochemistry and petrogenesis of the Archean mid-ocean ridge basalts (AMORBs) of the Cleaverville area, Pilbara craton, Western Australia, *Lithos*, 37, 199-221, 1996.
- O'Nions, R. K., and I. N. Tolstikhin, Limits on the mass flux between lower and upper mantle and stability of layering, *Earth Planet. Sci. Lett.*, 139, 213-222, 1996.
- Ozima, M., and C. Alexander, Jr., Rare gas fractionation patterns in terrestrial samples and the Earth-atmosphere evolution model, *Rev. Geophys. Space Phys.*, 14, 385-390, 1976.
- Ozima, M., and F. A. Podosek, *Noble Gas Geochemistry*, Cambridge University Press, Cambridge, 1983.
- Palacz, Z. A., and D. Saunders, Coupled trace element and isotope enrichment in the Cook-Austral-Samoa islands, southwest Pacific, *Earth Planet. Sci. Lett.*, 79, 270-280, 1986.

- Patterson, D. B., M. Honda, and I. McDougall, Atmospheric contamination: a possible source for heavy noble gases in basalts from Loihi Seamount, Hawaii, *Geophys. Res. Lett.*, 17, 705-708, 1990.
- Patterson, D. B., M. Honda, and I. McDougall, Noble gases in mafic phenocrysts and xenoliths from New Zealand, *Geochim. Cosmochim. Acta*, 58, 4411-4427, 1994.
- Porcelli, D., and G. J. Wasserburg, Mass transfer of helium, neon, argon, and xenon through a steady-state upper mantle, *Geochim. Cosmochim. Acta*, 59, 4921-4937, 1995.
- Poreda, R. J., and K. A. Farley, Rare gases in Samoan xenoliths, *Earth Planet. Sci. Lett.*, 113, 129-144, 1992.
- Poreda, R., J.-G. Schilling, and H. Craig, Helium and hydrogen isotopes in ocean-ridge basalts north and south of Iceland, *Earth Planet. Sci. Lett.*, 78, 1-17, 1986.
- Ringwood, A. E., Slab-mantle interactions, 3. Petrogenesis of intraplate magmas and structure of the upper mantle, *Chem. Geol.*, 82, 187-207, 1990.
- Roy-Barman, M., and C. J. Allègre, $^{187}\text{Os}/^{186}\text{Os}$ in oceanic island basalts: tracing oceanic crust recycling in the mantle, *Earth Planet. Sci. Lett.*, 129, 145-161, 1995.
- Shea, M. A., D. F. Smart, and L. C. Gentile, Estimating cosmic ray vertical cut-off rigidities as a function of the McIlwain L-parameter for different epochs of the geomagnetic field, *Phys. Earth Planet. Inter.* 48, 200-205, 1987.
- Shibata, T., A. Makishima, and E. Nakamura, Trace neodymium isotope analysis and its application to geological problems, *Abstract for the 1989 Annual Meeting of the Geochemical Society of Japan*, 73, 1989 (in Japanese).
- Shibata, T., E. Takahashi, and M. Ozima, Noble gas partitioning between basaltic melt and olivine crystals at high pressures, in *Noble Gas Geochemistry and Cosmochemistry* (eds. J. Matsuda), Terra Scientific Publishing Company, Tokyo, 343-354, 1994.
- Stakes, D. S., H. P. Taylor, Jr., and R. L. Fisher, Oxygen-isotope and geochemical characterization of hydrothermal alteration in ophiolite complexes and modern oceanic crust, in *Ophiolites and Oceanic Lithosphere* (eds. I. G. Gass, S. J. Lippard, and A. W. Shelton), Geol. Soc. Space Publ., No. 13, 199-215, 1984.
- Staudacher, T., and C. J. Allègre, Recycling of oceanic crust and sediments: the noble gas subduction barrier, *Earth Planet. Sci. Lett.*, 89, 173-183, 1988.
- Staudacher, T., and C. J. Allègre, Noble gases in glass samples from Tahiti: Teahitia, Rocard and Mehétia, *Earth Planet. Sci. Lett.*, 93, 210-222, 1989.

Staudacher, T., and C. J. Allègre, Cosmogenic neon in ultramafic nodules from Asia and in quartzite from Antarctica, *Earth Planet. Sci. Lett.*, 106, 87-102, 1991.

Staudacher, T., and C. J. Allègre, Ages of the second caldera of Piton de la Fournaise volcano (Réunion) determined by cosmogenic ray produced ^3He and ^{21}Ne , *Earth Planet. Sci. Lett.*, 119, 395-404, 1993.

Staudacher, T., P. Sarda, and C. J. Allègre, Noble gas systematics of Réunion Island, Indian Ocean, *Chem. Geol.*, 89, 1-17, 1990.

Staudacher, T., Ph. Sarda, S. H. Richardson, C. J. Allègre, I. Sagna, and L. V. Dmitriev, Noble gases in basalt glasses from a Mid-Atlantic Ridge topographic high at 14°N : geodynamic consequences, *Earth Planet. Sci. Lett.*, 96, 119-133, 1989.

Staudigel, H., S. R. Hart, and S. H. Richardson, Alteration of the oceanic crust: processes and timing, *Earth Planet. Sci. Lett.*, 52, 311-327, 1981.

Stein, M., and A. W. Hofmann, Mantle plumes and episodic crustal growth, *Nature*, 372, 63-68, 1994.

Stille, P., D. M. Unruh, and M. Tatsumoto, Pb, Sr, Nd, and Hf isotopic constraints on the origin of Hawaiian basalts and evidence for a unique mantle source, *Geochim. Cosmochim. Acta*, 50, 2303-2319.

Sun, S.-S., and W. F. McDonough, Chemical and isotopic systematics of oceanic basalts: implications for mantle composition and processes, in *Magmatism in the Ocean Basins* (eds. A. D. Saunders, and M. J. Norry), Geol. Soc. Spec. Pub. No 42, 313-345, 1989.

Sun, S.-S., and R. W. Nesbitt, Petrogenesis of Archean ultrabasic and basic volcanics: evidence from rare earth elements, *Contrib. Mineral. Petrol.*, 65, 301-325, 1978.

Tatsumi, Y., and S. Eggins, *Subduction Zone Magmatism*, Blackwell, Cambridge, 1995.

Tatsumoto, M., Isotopic composition of lead in oceanic basalt and its implication to mantle evolution, *Earth Planet. Sci. Lett.*, 38, 63-87, 1978.

Trull, T. W., and M. D. Kurz, Experimental measurements of ^3He and ^4He mobility in olivine and clinopyroxene at magmatic temperatures, *Geochim. Cosmochim. Acta*, 57, 1313-1324, 1993.

Turner, D. L., and R. D. Jarrard, K-Ar dating of the Cook-Austral island chain: a test of the hot-spot hypothesis, *J. Volcanol. Geotherm. Res.*, 12, 187-220, 1982.

Vance, D., J. O. H. Stone, and R. K. O'Nions, He, Sr and Nd isotopes in xenoliths from Hawaii and other oceanic islands, *Earth Planet. Sci. Lett.*, 96, 147-160, 1989.

Weaver, B. L., The origin of ocean island basalt end-member compositions: trace element and isotopic constraints, *Earth Planet. Sci. Lett.*, 104, 381-397, 1991.

White, W. M., and A. W. Hofmann, Sr and Nd isotope geochemistry of oceanic basalts and mantle evolution, *Nature*, 296, 821-825, 1982.

Wilson, J. T., Convection currents and continental drift, *Phil. Trans. R. Soc.*, A258, 145-167, 1971.

Woodhead, J. D., P. Greenwood, R. S. Harmon and P. Stoffers, Oxygen isotope evidence for recycled crust in the source of EM-type ocean island basalts, *Nature*, 362, 809-813, 1993.

Yoshikawa, M., and E. Nakamura, Precise isotope determination of trace amounts of Sr in magnesium-rich samples, *J. Min. Petr. Econ. Geol.*, 88, 548-561, 1993.

Zindler, A., and S. Hart, Chemical geodynamics, *Ann. Rev. Earth Planet. Sci.*, 14, 493-571, 1986.

Appendix - A; Setting up of the noble gas mass spectrometry system at Earthquake Research Institute, University of Tokyo

Mass Spectrometer

The sector-type mass spectrometer installed in ERI is VG-5400 (Slot No. V9) produced by VG Isotech. Installation was carried out by install engineers from May, 1994. Once MS was ready for use, however, terrible chlorine contamination from the gas extraction line (produced by the Ayumi Kogyo Co.) delayed the use of the machine. Chlorine contamination in the mass spectrometer was eliminated by baking at 320°C for several times with chlorine free gas purification line and the machine was re-tuned and checked from January, 1996.

Nier-type ion source is equipped in the MS. The condition of the ion source is fixed as follows (June, 1996); trap current, 420 μ A; filament current, 2.7A; emission current, 1.5mA; repeller voltage, -4.2V; acceleration voltage of electron, 78V; acceleration voltage of ion, 4.05kV. The mass resolution is more than 600(M/ Δ M).

Three kinds of collectors are equipped for detection of an ion beam. Faraday cup is a collector with the lowest sensitivity and is used for detecting a strong beam such as ^4He and ^{40}Ar . Daly multiplier is consisted of Daly knob and photon multiplier. The voltage of Daly knob and photon multiplier is fixed at 7.5kV and 0.82kV, respectively. Effective multiplying rate of the Daly system is about 10^5 . Feedback resistors for the Faraday system and the Daly system are $10^{11}\Omega$ and $10^8\Omega$, respectively. EM(Electron Multiplier)-ion counting system is used for weak ion beams, especially, ^3He , Ne, Kr and Xe. The voltage of EM is set at 2.1kV.

The ion pump (Varian, StarCell pump, 45l/s), turbo molecular pump (Balzers, TPU 060) and rotary pump (Shimadzu, GDH-160) are equipped for getting a good vacuum condition in the mass spectrometer. The mass spectrometer is usually pumped by an ion pump and the pressure is kept at $2\text{--}3\times 10^{-10}$ torr. Pressure in the MS is monitored by a

metal ionization gauge (ULVAC, M-13). Rotary pump is used for pumping the vessels of the High Faraday electronic system and photon multiplier. Turbo molecular pump is used in baking the mass spectrometer but is not used in a usual operation. Hydrogen is absorbed by two Sorb-Ac getters (SAES, NP-10) at room temperature and they are degassed only when the mass spectrometer is baked.

Baking of MS is performed by covering baking boxes on MS. Baking temperature is kept constant by automatic switching of heaters. MS is heated at 250-320°C over night for normal baking procedures.

Full tuning of the mass spectrometer was carried on April, 1996. Full tuning includes repositioning the magnet and the flight tube and setting the voltage of Daly knob and discriminator level of the counting system. Normal tuning includes changing source parameters as EV's (acceleration voltage of electron), repeller voltage, beam focus and beam centre. Full tuning would not be required further, but normal tuning should be carried out when the intensity of the beam is decreased and peak shape is changed.

The mass spectrometer is controlled by a HP computer with the operation software developed by Professor K. Nagao (Institute for Study of Earth's Interior, Okayama University). The software has been kindly offered by him. It was slightly modified for the system of the mass spectrometer at ERI.

Gas Extraction and Purification Line

The gas extraction and purification line was produced by the Ayumi Kogyo Co. However, it was terribly contaminated by chlorine and hydrocarbon, which caused large blanks and contaminated the mass spectrometer. Then, all parts were washed and cleaned by nitric acid, acetone, ethanol and distilled water on October, 1995 and much good vacuum was realized; the pressure in the line before and after cleaning is in the order of 10^{-8} and 10^{-9} torr, respectively. In the system, six metal valves produced

by the Ayumi Kogyo Co. had been used, but they were so often out of order that they were changed to the products of the Ulvac Corporation. Now, more than 70% of the parts of the line originally made by the Ayumi Kogyo Co. have been replaced by the parts made by the Ulvac Co.

The outline of the gas extraction and purification line is shown in Fig. A-1. The ultra high vacuum in the line is kept by two turbo molecular pumps (Shimadzu, TMP-150) and one ion pump (ANELVA, 912-7160, 60 l/s). The pressure is less than 5×10^{-9} torr if titanium-zirconium getters are not heated. Three rotary pumps (Shimadzu, GDH-160; Shinku kiko, GVD-165A) are equipped with it. Two of them are used for TMPs and one for a diffusion pump (Ayumi Kogyo, DU-3, 600 l/s). Three titanium-zirconium getters, two charcoal traps, one stainless sieve trap and a cryogenic pump (Sumitomo, SRT204) are used for purifying and separating noble gases. The pressure in the line is monitored by three vacuum gauges (nude gauge - ANELVA, NIG-2F; metal ionization gauge - ULVAC, M-13; Pirani gauge - ULVAC, WPB-10).

We have two kinds of gas extraction systems; heating and crushing. Heating furnace is consisted of a tantalum tube, a molybdenum crucible and resistive heater around the Ta tube. Diffusion pump(DP) works to evacuate outside of the Ta tube to protect the oxidation of a Ta tube and the heater (at $10^{-6} \sim 10^{-7}$ torr). W-Re thermo-couple is placed just below the Ta tube to monitor the temperature of the crucible. It is possible to heat the crucible at about 2000°C. Samples are loaded in a glass sample holder of a Christmas tree type, which is connected to the heating furnace through a flange. Samples are usually wrapped in aluminium foil.

Crushers were newly developed for extracting noble gases from rock samples by crushing. It is possible to extract noble gases mainly in fluid inclusions. Secondary produced noble gases such as radiogenic, nucleogenic and cosmogenic components are eliminated by the crushing method. It is, in particular, applicable to old samples.

Up to three crushers can be connected to the purification line (Fig. A-1). The metal vacuum valves (Ayumi Industry Co.) were remodelled into the crushers with a piston

(16mm diameter), a sample holder and tablets (Fig. A-2). Up to 1.5g of samples can be loaded. When sample volumes are large and sample grains are piled in more than two layers, they should be separated by inserting tablets to crush effectively. All parts are made of stainless steel (SUS304).

Crushing is performed by the movement of a piston up and down. The power of crushing is controlled by torque of the rotating head. The torque should not exceed 250 kgcm to avoid the leakage. It is possible to crush olivines and clinopyroxenes (solidity 6-7). Crushing should be carried out for several times to make samples into the grain sizes of less than #100 mesh. The extracted gases, especially heavy noble gases, might be trapped on the fresh surface of crushed samples. Two ways are applied to avoid it. The crusher is heated at 120°C and a cold charcoal trap (liquid nitrogen) is worked during crushing.

We have three standard gas tanks for the calibration of isotope ratios and noble gas sensitivity. One tank for helium calibration contains Kaminoyama well gas. One pipette of gas includes about 8×10^{-6} cm³STP of ⁴He (May, 1996). It is diluted for the use of standard helium gas. The diluted atmosphere is in the other two tanks for Ne, Ar, Kr and Xe calibration. One pipette from the tank for Ar calibration includes about 4×10^{-10} cm³STP of ³⁶Ar. The other tank used for Ne, Kr and Xe calibration contains about 80 times denser gases than the tank used for Ar calibration.

Procedure of noble gas measurement

When samples are newly loaded in the sample holder, the purification and extraction line is baked at 150-200°C in vacuum for more than 8 hours. Samples are pre-heated at 160°C during baking by using tape heaters. Pre-heating temperature is kept constant by a thermo-controller. Degassing of heating furnace is carried out for about half hour at

1900°C for several times during baking. Heating furnace is further degassed after baking to reduce the blank level.

Samples in the sample holder are dropped into the heating furnace by an iron piece which are moved by a hand-magnet outside. In case of this study, two stepwise heating method is applied. The furnace is heated at about 400°C before samples are dropped because it takes long time to heat at low temperature. After dropping them, the furnace is heated for 30 or 40 minutes at 700°C or 800°C for the low temperature fraction. For the high temperature fraction, the furnace is kept at 1700°C or 1850°C for 15-20 minutes. Temperature is carefully increased not to burst samples by rapid degassing.

After the gas extraction by heating method, three titanium-zirconium getters are used for purifying noble gases. In case of crushing experiments, two getters are used for gas purification. They are heated at about 700-800°C to react with active gases (except for hydrogen) from extracted gases. Hydrogen is physically adsorbed on the titanium-zirconium foil when it is cooled.

Purified noble gases are separated by cold charcoal traps. Ar, Kr and Xe are trapped in CH1 which is cooled by liquid nitrogen. Separation of He and Ne is performed by a cryogenic pump with charcoal (CHcryo) which is cooled at 60K. After helium analysis, trapped neon at CHcryo is released by heating it. Stainless sieve trap at the inlet of MS is cooled by liquid nitrogen during neon analysis. It effectively reduces double charges of ^{40}Ar and $^{44}\text{CO}_2$ which interfere with ^{20}Ne and ^{22}Ne . After He and Ne analyses, all gases trapped (Ar, Kr and Xe) in CH1 are once removed and purified again by titanium-zirconium getters. Ar is separated by trapping Kr and Xe on the charcoal traps cooled at -70°C. Separation of Kr and Xe is carried out by cooling them at -15°C. Charcoal traps are kept at -70°C and -15°C using ethanol cooled by dryice.

It takes about seven hours for the full measurement of He, Ne, Ar, Kr and Xe.

Blanks were measured in the same way as measuring samples. Hot blanks in the low temperature fraction (700°C or 800°C) were 2.4×10^{-9} , 2.3×10^{-12} , $0.8 \cdot 3 \times 10^{-12}$, $0.2 \cdot 1 \times 10^{-14}$ and $0.8 \cdot 7 \times 10^{-14}$ cm³STP for ⁴He, ²⁰Ne, ³⁶Ar, ⁸⁴Kr and ¹³²Xe, respectively. Hot blanks in the high temperature fraction (1700°C or 1850°C) were $2 \cdot 4 \times 10^{-9}$, $2 \cdot 9 \times 10^{-12}$, $0 \cdot 3 \cdot 1 \times 10^{-11}$, $0 \cdot 3 \cdot 4 \times 10^{-13}$ and $0 \cdot 2 \cdot 1 \times 10^{-13}$ cm³STP for ⁴He, ²⁰Ne, ³⁶Ar, ⁸⁴Kr and ¹³²Xe, respectively. Isotopic ratios of blanks were same as those of air except for helium. Helium blank mostly originates from the penetration of atmospheric helium through the Pyrex glass of the sample holder. Helium isotopic ratio of the hot blank (2.3 Ra) is different from that of the atmosphere due to probable isotopic fractionation. Since samples are wrapped in aluminium foil, the blanks with it were measured using the typical amount of aluminium foil (30-40 mg). They were 5.5×10^{-10} , 2.2×10^{-13} , 1.1×10^{-13} and 7.3×10^{-14} cm³STP for ⁴He, ³⁶Ar, ⁸⁴Kr and ¹³²Xe, respectively. The ²⁰Ne could not be detected in this case.

Blanks of crushing experiment were much smaller than those of hot blank. They were $0.6 \cdot 2 \times 10^{-12}$, $0.5 \cdot 2 \times 10^{-13}$, $2 \cdot 3 \times 10^{-14}$ and $0.4 \cdot 2 \times 10^{-14}$ cm³STP for ²⁰Ne, ³⁶Ar, ⁸⁴Kr and ¹³²Xe, respectively. Blank for ⁴He during crushing was not detected. Isotopic ratios of Ne, Ar, Kr and Xe were atmospheric.

Isotope analyses on MS

All noble gases are separated in the purification line before isotope analyses. Isotope ratios are measured by the peak jump method. For helium analysis, intensity of ³He and ⁴He are measured with the electron multiplier-counting system and a Faraday cup, respectively. The resolution power (600 M/ΔM) of MS is enough to separate the ³He⁺ peak from HD⁺ and ³H⁺ peaks. Helium isotope ratio is calibrated by measuring the

standard gases from Kaminoyama well, Yamagata, Japan, during the series of experiment. $^3\text{He}/^4\text{He}$ of the standard gas was determined to be 6.04 ± 0.29 R/Ra by comparing the atmospheric helium isotope ratio. It is nearly the same as the reported value of 5.95 ± 0.30 R/Ra (Hiyagon et al., 1992). The accuracy of helium isotope analysis has been guaranteed by measuring $^3\text{He}/^4\text{He}$ of rock samples which have been reported from other laboratories (Table A-1). Nodule samples from Réunion Island, which shows a quite constant $^3\text{He}/^4\text{He}$ (e.g., Graham et al., 1990; Staudacher et al., 1990), were also used for checking helium analysis.

Although Ar and CO₂ are trapped by the stainless sieve trap which is cooled by liquid nitrogen, interferences of $^{40}\text{Ar}^{++}$ and $^{44}\text{CO}_2^{++}$ on $^{20}\text{Ne}^+$ and $^{22}\text{Ne}^+$ can not be removed during neon analysis. The production ratios of doubly charged ions of Ar and CO₂ were often checked during the series of experiment. $^{40}\text{Ar}^{++}/^{40}\text{Ar}^+$ and $^{44}\text{CO}_2^{++}/^{44}\text{CO}_2^+$ were 0.25 and 0.008, respectively. The amounts of $^{40}\text{Ar}^+$ and $^{44}\text{CO}_2^+$ are measured at the start and the end of each run. Calculated $^{40}\text{Ar}^{++}$ and $^{44}\text{CO}_2^{++}$ are reduced from the apparent peak heights of $^{20}\text{Ne}^+$ and $^{22}\text{Ne}^+$ to obtain their true peak heights. Neon analyses are usually carried out with the electron multiplier-counting system.

Both High Faraday and Daly multiplier are applied for argon analysis. $^{38}\text{Ar}/^{36}\text{Ar}$ is usually determined by using a Daly multiplier. Two ways are available for $^{40}\text{Ar}/^{36}\text{Ar}$ measurement. One is that ^{40}Ar peak height detected by High Faraday is divided by ^{36}Ar peak height detected by also High Faraday. The other way is using the ^{36}Ar peak height determined by the Daly multiplier. Both ways provide the same results if $^{40}\text{Ar}/^{36}\text{Ar}$ is less than about 3000. However, the former way is not applicable when $^{40}\text{Ar}/^{36}\text{Ar}$ exceeds 3000 due to the small peak height of ^{36}Ar detected by High Faraday.

Kr and Xe analyses are usually performed using the electron multiplier-counting system. The interferences of hydrocarbons on Kr and Xe peaks were negligible in most

cases. The isotopic fractionation in the MS was calibrated by the repeated measurements of standard atmospheric gases for Ne, Ar, Kr and Xe.

The constant sensitivity of MS for each kind of noble gas is checked by repeated analyses of different amount of gases. The absolute sensitivity of Ar was determined by measuring standard samples of MMhb-1 and JG-1 (biotite). The relative sensitivities of He/Ar, Ne/Ar, Kr/Ar and Xe/Ar were determined by measuring standard gases of diluted air. The error for the noble gas abundance is about 5% for all noble gases. The dependence of fractionation factors on gas pressure is found for He, but for other isotopes. When the intensity of ^4He exceeds 0.4V on Daly multiplier, which corresponds to about 1×10^{-7} torr for ^4He partial pressure, the apparent $^3\text{He}/^4\text{He}$ shifts higher from the normal value. (The shifts of $^3\text{He}/^4\text{He}$ fractionation on the helium partial pressure is reverse of those reported by Honda et al. (1993).) Hence, a part of helium sample gas is expanded into the MS to check its amount before the main analysis. The helium sample gas is diluted if the intensity of ^4He exceeds the criteria (0.4V on Daly multiplier) for the helium isotope analyses.

Table A-1. Comparison of noble gas measurement between ERI-MS and MS in other laboratories (ISEI, Okayama Univ. and Geophysical Dept., Univ. Tokyo (Chibutsu)).

	Weight		4He (cm3STP/g)	20Ne	36Ar	84Kr	132Xe		R/Ra	error
JP-1 (Horoman, Peridotite)										
ERI, Tokyo	0.96753	Heating	7.73E-07	8.61E-11	2.43E-10	1.11E-11	1.75E-12		8.99	0.34
Misasa (Miura & Nagao, 1991)	?	Heating	6.60E-07	3.60E-10	3.40E-10	1.80E-11	3.90E-12		9.00	0.14
GLP86W (MORB, glass)										
ERI, Tokyo	0.06642	Heating	1.17E-05	2.21E-10	4.36E-10	1.31E-11	3.86E-12		8.24	0.30
Chibutsu (Hiyagon et al., 1992)	3.4303	Heating	1.19E-05	1.18E-10	1.84E-10	4.75E-12	6.88E-13		8.02	0.29
Reunion Nodule										
ERI, Tokyo	0.8782	Heating	2.46E-07	3.20E-10	2.45E-10	9.09E-12	5.23E-13		12.46	0.59
ERI, Tokyo	0.7419	Crushing	5.01E-08	3.09E-11	2.82E-11	1.07E-12	1.58E-13		12.63	0.58

	Weight		20Ne/22Ne	error	21Ne/22Ne	error	38Ar/36Ar	error	40Ar/36Ar	error
JP-1 (Horoman, Peridotite)										
ERI, Tokyo	0.96753	Heating	9.92	0.16	0.0290	0.0015	0.1873	0.0005	365.2	1.5
Misasa (Miura & Nagao, 1991)	?	Heating	9.55	0.76	0.0301	0.0007	0.1898	0.0004	384	47
GLP86W (MORB, glass)										
ERI, Tokyo	0.06642	Heating	11.57	0.43	0.0415	0.0045	0.1863	0.0008	2865	12
Chibutsu (Hiyagon et al., 1992)	3.4303	Heating	11.68	0.27	0.0468	0.0027	0.1857	0.0177	4606	68
Reunion Nodule										
ERI, Tokyo	0.8782	Heating	11.75	0.14	0.0359	0.0010	0.1874	0.0006	4386	20
ERI, Tokyo	0.7419	Crushing	12.04	0.28	0.0375	0.0023	0.1885	0.0019	6330	37

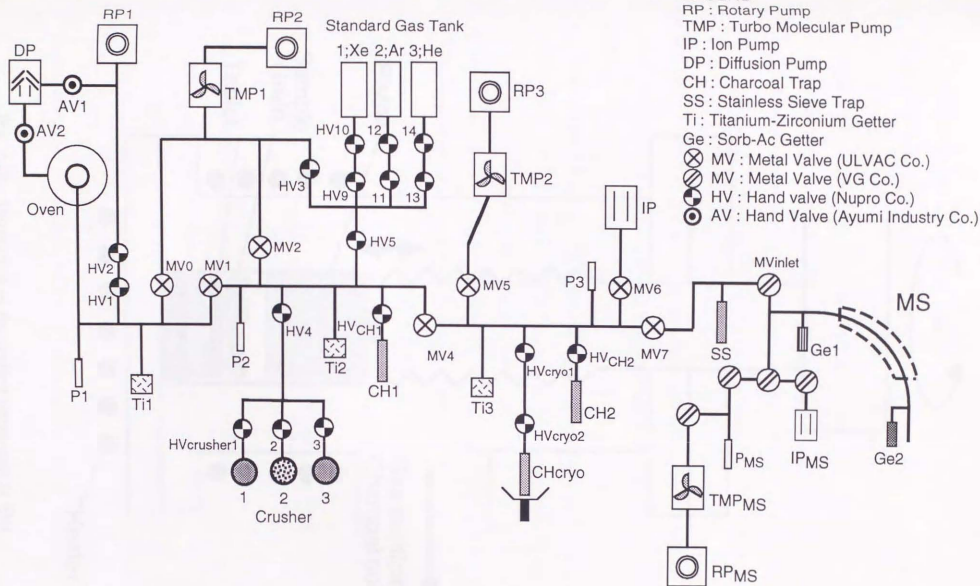


Fig. A-1. Illustration of the noble gas mass spectrometry system at ERI, Univ. of Tokyo.

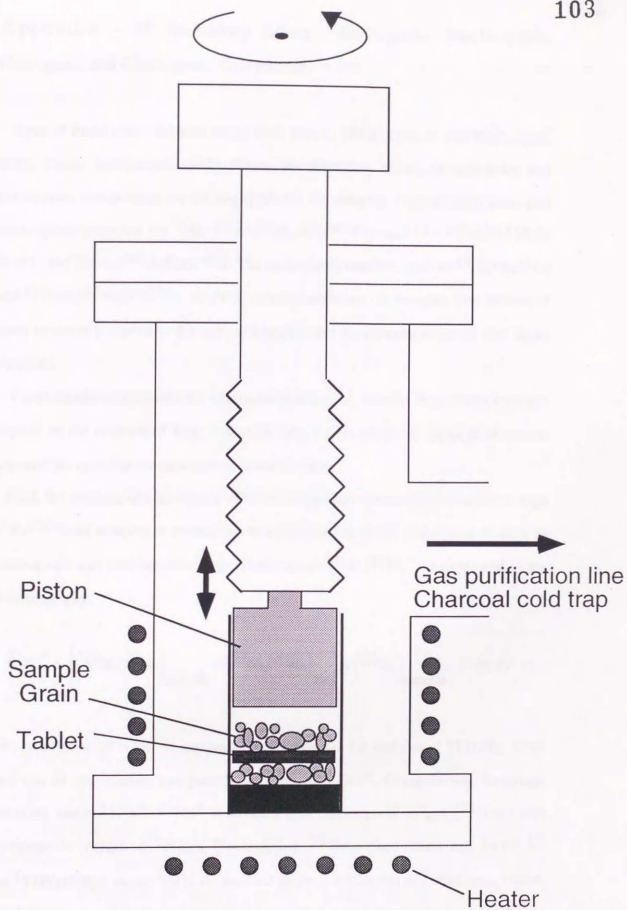


Fig. A-2. Illustration of the crusher developed at ERI.

Appendix - B; Secondary Effect - Radiogenic, Nucleogenic, Fissiogenic and Cosmogenic Components

Ages of rocks measured here range from 1Ma to 18Ma (Duncan and McDougall, 1976; Turner and Jarrard, 1982). Hence, the secondary effects of radiogenic and nucleogenic components are not negligible for old samples. Possible radiogenic and nucleogenic products are ^4He , $^{20,21,22}\text{Ne}$, $^{83,84,86}\text{Kr}$ and $^{131,132,134,136}\text{Xe}$ from U and Th, and ^{40}Ar from ^{40}K . The nucleogenic reaction, such as $^{18}\text{O}(\alpha,n)^{21}\text{Ne}$ and $^{19}\text{F}(\alpha,n)^{22}\text{Na}(\beta^+)^{22}\text{Ne}$, would also contribute to the old samples. The amount of them is directly related to the ages of samples and the content of parent and target elements.

Cosmogenic components are spallation products by cosmic rays. Their amounts depend on the contents of target materials (Mg, Al, Si, etc.), the intensity of cosmic rays and the ages that samples were exposed by them.

First, the amounts of cosmogenic ^{21}Ne in samples are examined. I assume that high $^{21}\text{Ne}/^{20}\text{Ne}$ of samples is caused due to addition of secondary components such as cosmogenic and nucleogenic origin. Then excess ^{21}Ne ($^{21}\text{Ne}^*$) is expressed in the following way.

$$^{21}\text{Ne}^* = \left\{ \left(^{21}\text{Ne}/^{20}\text{Ne} \right)_{\text{sample}} - \left(^{21}\text{Ne}/^{20}\text{Ne} \right)_{\text{air}} \right\} \times \left(^{20}\text{Ne} \right)_{\text{sample}} \quad (\text{B-1})$$

The calculation of $^{21}\text{Ne}^*$ is summarized in Table B-1 for samples of TU01-01. Core and rim of cpx contain comparable amounts of $^{21}\text{Ne}^*$. Groundmass, however, contains more $^{21}\text{Ne}^*$. $^{21}\text{Ne}^*$ is divided into nucleogenic origin ($^{21}\text{Ne}_n$) and cosmogenic origin ($^{21}\text{Ne}_c$). Nucleogenic $^{21}\text{Ne}_n$ production are $8 \times 10^{-15} \text{ cm}^3 \text{STP/g(U)}/\text{yr}$ where Th/U is assumed to be 3.3 (Ozima and Podosek, 1983). Typical amount of U is 0.01ppm and 1ppm in cpx and groundmass, respectively

(Tables D-1 and D-2). The calculated $^{21}\text{Ne}_n$ in cpx and groundmass is 8×10^{-16} and $8 \times 10^{-14} \text{ cm}^3\text{STP/g}$ for 10m.y., respectively. Accordingly, $^{21}\text{Ne}_n$ in cpx is negligible compared to trapped ^{21}Ne .

Most of $^{21}\text{Ne}^*$ in cpx is attributed to $^{21}\text{Ne}_c$ rather than $^{21}\text{Ne}_n$. Because cutoff rigidity at Tahiti is similar to that at Hawaii (Shea et al., 1987), Production rate of $^{21}\text{Ne}^*$ at the sea level around Tahiti is assumed to be $1.2 \times 10^{-18} \text{ cm}^3\text{STP/g/yr}$ which is the similar value estimated at Hawaii (Kurz et al., 1990; Staudacher and Allègre, 1993). $^{21}\text{Ne}^*$ in cpx can be produced with the exposure for about 0.1m.y.; the exposure age is much smaller than the age of the island.

Amounts of $^{21}\text{Ne}^*$ in groundmass and cpx are different (Table B-1). One of the possibility is the different contents of target materials. The dependency on chemical composition for $^{21}\text{Ne}_c$ production is expressed as follows (Staudacher and Allègre, 1991);

$$^{21}\text{Ne}_c = C \times (1 \times \text{Mg} + 0.36 \times \text{Al} + 0.19 \times \text{Si} + 0.04 \times \text{Ca} + 0.01 \times (\text{Fe} + \text{Ni}))$$

(B-2)

where C is a normalization factor and element concentrations are expressed by weight percent. Calculated $^{21}\text{Ne}_c/C$ values for groundmass, cpx-rim and cpx-core are listed in Table B-2, which suggests that $^{21}\text{Ne}_c$ production rate would not be so much different among them.

Another possibility for the difference in $^{21}\text{Ne}^*$ between groundmass and cpx is the contribution of $^{21}\text{Ne}_n$ to the groundmass. $^{21}\text{Ne}_n$ produced from 1ppm U for 10m.y. is estimated to be $8 \times 10^{-14} \text{ cm}^3\text{STP/g}$ as discussed begore.

If $^{21}\text{Ne}_c$ in cpx is $1.3 \times 10^{-13} \text{ cm}^3\text{STP/g}$, which is the average of $^{21}\text{Ne}_c$ in the rim and the core, cosmogenic ^3He ($^3\text{He}_c$) is calculated to be $4.6 \times 10^{-13} \text{ cm}^3\text{STP/g}$ using $^{21}\text{Ne}_c/^3\text{He}_c = 3.5$ (Staudacher and Allègre, 1993). Accordingly, $^3\text{He}_c$ dominates total ^3He in cpx and groundmass (Table B-3).

Finally, radiogenic ^4He and ^{40}Ar have been estimated. 0.01 ppm of U in cpx produces ^4He with the amount of $2 \times 10^{-8} \text{ cm}^3\text{STP/g}$ for 10m.y., which is not negligible compared to the total amount of ^4He in samples. If K content in cpx is 0.01% (K/U=10000), cpx would gain $3.9 \times 10^{-9} \text{ cm}^3\text{STP/g}$ of radiogenic ^{40}Ar for 10m.y. Radiogenic ^{40}Ar contributes less than 10% of total ^{40}Ar for most samples.

Table B-1. Estimate of $^{21}\text{Ne}^*$ for cpx and groundmass samples of TU01-01.

Ne (1700°C)

	^{20}Ne	$^{21}\text{Ne}/^{20}\text{Ne}$	$^{21}\text{Ne}^*$
Groundmass	1.13×10^{-10}	4.75×10^{-3}	2.02×10^{-13}
Cpx - Core	1.29×10^{-11}	12.1×10^{-3}	1.18×10^{-13}
Cpx - Rim	2.12×10^{-11}	9.74×10^{-3}	1.44×10^{-13} ($\text{cm}^3\text{STP/g}$)

Table B-2. List of $^{21}\text{Ne}_C/\text{C}$ values of cpx and whole rock samples of TU01-01. The values are calculated from eq.(B-2).

$^{21}\text{Ne}_C/\text{C}$

Weight (%)	Whole Rock	Cpx - Rim	Cpx - Core
Mg	7.94	6.83	8.78
Al	2.75	2.26	1.24
Si	21.19	21.09	23.38
Ca	9.20	16.16	16.37
Fe	9.77	6.50	4.09
Ni	-	-	-
$^{21}\text{Ne}_C/\text{C}$	13.42	12.36	14.36

Table B-3. Summary for He abundance in cpx and groundmass samples of TU01-01.

He		^4He	$^3\text{He}/^4\text{He}$	^3He
Groundmass	800°C	1.60×10^{-6}	0.18 Ra	4.03×10^{-13}
	1700°C	1.21×10^{-7}	1.37 Ra	2.32×10^{-13}
	total	1.72×10^{-6}	0.26 Ra	6.26×10^{-13}
Cpx - Core	800°C	2.88×10^{-8}	8.18 Ra	3.30×10^{-13}
	1700°C	2.58×10^{-8}	12.28 Ra	4.44×10^{-13}
	total	5.46×10^{-8}	10.12 Ra	7.74×10^{-13}
Cpx - Rim	800°C	8.36×10^{-8}	3.22 Ra	3.77×10^{-13}
	1700°C	4.23×10^{-8}	7.08 Ra	4.19×10^{-13}
	total	1.26×10^{-7}	4.52 Ra	7.97×10^{-13}

($\text{cm}^3\text{STP/g}$)

Appendix - C; He open system model

The problem to be solved is the distribution of ^4He ($C^4(t,x)$) with the production of ^4He in HIMU source rocks (Fig. 4-10). The situation is expressed by the diffusion equation;

$$\frac{\partial C^4}{\partial t} - \frac{\partial^2 C^4}{\partial x^2} = Q \quad (\text{C-1})$$

where Q is the production rate of ^4He in HIMU source rocks.

$$Q = 2.83 \times 10^{-28} \times C(U) \text{ mol/g/sec} \quad \text{for } 0 < x < L/2 \quad (\text{C-2})$$

$$Q = 0 \quad \text{for } L/2 < x \quad (\text{C-3})$$

where $C(U)$ is the concentration of U in HIMU source rocks in ppb.

The boundary conditions are;

$$C^4 = C_{DM}^4 \quad \text{at } t=0 \quad (\text{C-4})$$

$$C^4 = 0 \quad \text{at } x=a \quad (\text{C-5})$$

The latter boundary condition is adopted to make the calculation simpler, instead of the boundary condition; $C^4=0$ at $x=\infty$. a is fixed at 300km which corresponds to half of the upper mantle thickness.

The diffusion equation (C-1) is solved by the Fourier transformation.

$$C^4 = \frac{2Q}{aD} \sum_n \frac{\sin(\lambda_n L/2) \cos(\lambda_n x)}{\lambda_n^3} \cdot \{1 - \exp(-D\lambda_n^2 t)\} + C_{DM}^4 \quad (\text{C-6})$$

$$\text{excess } ^4\text{He} = \frac{4Q}{aDL} \sum_n \frac{\{\sin(\lambda_n L / 2)\}^2}{\lambda_n^4} \cdot \{1 - \exp(-D\lambda_n^2 t)\} \quad (\text{C-7})$$

$$\lambda_n = \frac{(2n+1)\pi}{2a} \quad (\text{C-8})$$

Using $D=10^{-8} \text{ m}^2/\text{sec}$ and $t=0.1\text{Gy}$, $D\lambda_n^2 t$ equals 0.008 for $n=1$. Accordingly, $(1 - \exp(-D\lambda_n^2 t))$ is approximated to be $D\lambda_n^2 t$ for small values of n , which indicates that eq.(C-7) is insensitive to the change of D .

Fig. C-1 shows the evolution of excess ^4He in case that the thickness(L) is fixed at 1km, for instance. The evolution lines are dependent on the U content. It has been reported that relatively fresh MORBs typically contains 50-150ppb of U (Tatsumoto, 1978). The lateral dotted lines in Fig. C-1 indicate the amount of excess ^4He required to explain the $^3\text{He}/^4\text{He}$ of HIMU samples(6.81Ra); required excess ^4He was estimated from C_{DM}^4 of Porcelli and Wasserburg (1995) ("P & W") and O'Nions and Tolstikhin (1996) ("O & T"). The solution is obtained as the crossing point of the solid line and the dotted line at a given U content. The relation between time and thickness is shown with the U content as a parameter (Fig. 4-11).

The minimum amount of ^4He produced in the HIMU source is estimated from the eq.(4-10). The least value of Z_{206} is 21.6. The estimated value for least Pb concentration is 0.14ppm for less altered MORBs or gabbros (Chen and Pallister, 1981; Hawkesworth et al., 1991). Then, the minimum amount of ^4He produced is simulated to be $4.1 \times 10^{-10} \text{ mol/g}$, which provides the constraint for the age of HIMU source. When U is 15ppb for instance, it takes more than 2.4Gy to produce $4.1 \times 10^{-10} \text{ mol/g}$ of ^4He . In Figs. C-1 and 4-11, the dots on the line indicate this constraint on the evolution of excess ^4He .

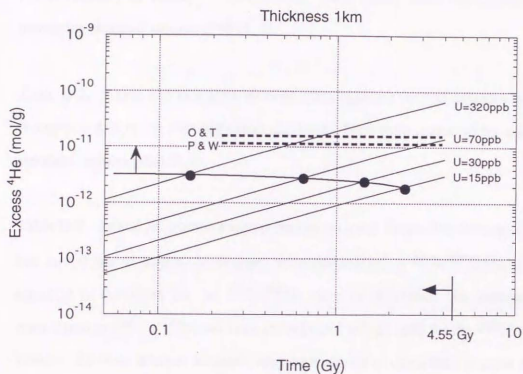


Fig. C-1. Time dependent evolution of excess ^4He in HIMU source rock for each given U concentration in case that L equals to 1 km. The lateral dotted lines indicate the amount of excess ^4He required to explain $^3\text{He}/^4\text{He}$ of HIMU samples; excess ^4He estimated from C^4_{DM} values of Porcelli and Wasserburg (1995) (4.7×10^{-11} mol/g; "P & W") and O'Nions and Tolstikhin (1996) (7.5×10^{-11} mol/g; "O & T"). The dots on the line show the constraint that HIMU source rock should produce more than 4.1×10^{-10} mol/g (see Appendix-C).

Appendix - D; Data Table

Table D-1. Trace and rare earth element concentrations for whole rock samples (in ppm). Accuracy is within 7% (Makishima et al., 1995). Data were corrected by measuring standard samples (PMLB_3).

Table D-2. Trace and rare earth element concentrations for cpx samples (in ppm). Accuracy is within 7% (Makishima et al., 1995). Data were corrected by measuring standard samples (PMLB_3).

Table D-3. Sr and Nd isotope analyses for cpx samples. Errors (2σ) correspond to the last two digits of values. Sr isotopes were normalized to $^{86}\text{Sr}/^{88}\text{Sr}=0.1194$ and adjusted to 0.710238 for the $^{87}\text{Sr}/^{86}\text{Sr}$ value of NIST981. Nd isotopes were normalized to $^{146}\text{Nd}/^{144}\text{Nd}=0.7219$ and adjusted to 0.511838 for the $^{143}\text{Nd}/^{144}\text{Nd}$ value of La Jolla isotopic standard. ϵ_{Nd} corresponds to deviations in parts per 10^4 from the present day bulk Earth values; $^{143}\text{Nd}/^{144}\text{Nd}=0.512638$.

Table D-4. Noble gas abundances and isotope ratios for samples degassed by the heating method. Errors correspond to 1σ . All data were corrected for blanks listed in Table D-9. Heating time for low temperature fraction (700°C or 800°C) and high temperature fraction (1700°C or 1850°C) were 40-60 minutes and 20 minutes, respectively. Samples attached "(M)" were measured at ISEI, Okayama University (Misasa). The other samples were measured at ERI, University of Tokyo. Excess ^{40}Ar is defined as follows;

$$\text{Excess } ^{40}\text{Ar} = \left\{ \left(^{40}\text{Ar}/^{36}\text{Ar} \right)_{\text{sample}} - \left(^{40}\text{Ar}/^{36}\text{Ar} \right)_{\text{air}} \right\} \times \left(^{36}\text{Ar} \right)_{\text{sample}}$$

Kr and Xe isotope ratios were normalized by those of air as follows;

$$F_i = \left(i_{\text{Kr}}/^{84}\text{Kr} \right)_{\text{sample}} / \left(i_{\text{Kr}}/^{84}\text{Kr} \right)_{\text{air}} \quad \text{for Kr isotope ratios}$$

$$F_i = \left(i_{\text{Xe}}/^{132}\text{Xe} \right)_{\text{sample}} / \left(i_{\text{Xe}}/^{132}\text{Xe} \right)_{\text{air}} \quad \text{for Xe isotope ratios.}$$

Table D-5. Noble gas abundances and isotope ratios for samples degassed by the crushing method. Errors correspond to 1σ . Crushing was carried out for 10 times. All data were corrected for blanks listed in Table D-9. Kr and Xe ratios could not be obtained due to their small abundances. ^4He for some samples were not detected (indicated as "N.D.).

Table D-6. Noble gas abundances and He and Ar isotope ratios for cpx samples (MGA-C12, TU01-01) degassed by the stepwise heating for comparison between unleached and leached cpx.

Table D-7. Noble gas abundances and He and Ar isotope ratios for a leached olivine sample (MGA-C12) degassed by the stepwise heating.

Table D-8. Noble gas abundances and He, Ne and Ar isotope ratios obtained by rim-core tests for cpx samples of TU01-01 and RTG-C10.

Table D-9. Blanks for noble gas analyses at ERI, Univ. of Tokyo and ISEI, Okayama Univ. Heating time for low temperature fraction (700°C or 800°C) and high temperature fraction (1700°C or 1850°C) were 40 minutes and 15-20 minutes, respectively. Isotope ratios of blanks were atmospheric for Ne, Ar, Kr and Xe. ^3He peak was not detected for crushing blanks. $^3\text{He}/^4\text{He}$ of heating blanks is 2-3Ra. ^4He , ^{84}Kr and ^{132}Xe for some samples were not detected (indicated as "N.D.).

Table D-1. Trace and rare earth element concentrations for whole rock samples.

Sample	RTG-C4	RTG-C5	RTG-C8	RTG-C10	MGA-C8	MGA-C12
La	32.0	60.2	66.3	48.7	20.1	29.8
Ce	68.1	117	134	101	44.9	63.2
Pr	8.5	13.9	16.1	11.7	5.7	7.6
Nd	37.2	56.0	66.8	48.8	24.3	32.9
Sm	7.5	10.3	12.7	9.7	5.1	6.4
Eu	2.4	3.3	4.0	3.1	1.7	2.0
Gd	6.8	9.1	11.2	8.4	4.8	6.0
Tb	0.9	1.2	1.5	1.2	0.7	0.8
Dy	4.8	6.1	7.7	5.9	3.7	4.6
Ho	0.8	1.0	1.4	1.1	0.7	0.8
Er	1.8	2.4	3.0	2.3	1.6	2.0
Tm	0.2	0.3	0.4	0.3	0.2	0.3
Yb	1.4	1.8	2.4	1.9	1.4	1.6
Lu	0.2	0.2	0.3	0.2	0.2	0.2
Rb	22.4	142	48.3	95.3	10.0	14.1
Sr	589	892	1054	850	279	381
Y	21.3	29.5	36.1	27.4	19.0	21.5
Cs	0.2	1.1	0.5	0.4	0.1	0.1
Ba	346	748	752	474	124	174
Pb	2.8	4.5	5.3	3.9	1.4	1.7
Th	3.7	7.6	7.9	6.1	2.2	3.3
U	0.9	1.5	1.9	1.5	0.7	1.0
Be	0.7	0.9	2.6	1.4	0.4	0.9
Zr	164	193	344	207	76.6	117
Nb	33.9	63.4	75.0	57.8	26.3	38.0
Hf	4.7	5.8	8.0	5.5	2.4	3.4
Ta	2.5	4.7	5.0	4.0	2.0	2.7

Table D-1. (Continued)

Sample MGA-C23 MGA-C29 TU01-01 TU04-01 TU09-01 TU12-01

La	28.8	31.2	42.6	158	63.8	37.5
Ce	61.4	67.8	84.3	321	126	77.0
Pr	7.4	8.5	9.7	34.4	14.2	9.1
Nd	31.2	35.4	38.8	128	54.7	36.8
Sm	6.1	7.3	7.3	19.7	9.7	7.1
Eu	1.9	2.4	2.3	5.4	3.0	2.3
Gd	5.8	7.0	6.6	17.9	8.8	6.7
Tb	0.8	1.0	0.9	2.3	1.2	1.0
Dy	4.3	5.6	5.0	12.1	6.2	5.1
Ho	0.8	1.0	0.9	2.3	1.1	0.9
Er	1.9	2.5	2.3	5.7	2.5	2.2
Tm	0.3	0.3	0.3	0.8	0.3	0.3
Yb	1.6	2.1	2.0	5.5	2.1	1.9
Lu	0.2	0.3	0.3	0.8	0.3	0.3
Rb	14.2	14.4	18.3	111	19.7	16.9
Sr	370	427	524	1518	701	484
Y	21.0	26.1	25.9	65.2	29.2	23.3
Cs	0.1	0.1	0.1	1.1	0.5	0.2
Ba	170	177	253	411	360	240
Pb	1.6	1.7	2.7	9.0	3.6	2.0
Th	3.3	3.3	4.7	23.7	7.8	3.8
U	1.0	1.0	1.2	6.9	2.2	1.0
Be	1.5	2.1	0.6	6.0	2.4	1.0
Zr	114	150	131	808	162	96.5
Nb	32.9	41.8	51.8	249	78.0	47.2
Hf	3.0	4.0	3.8	18.2	4.3	2.7
Ta	2.3	2.9	3.8	17.8	5.0	3.2

Table D-1. (Continued)

Sample TBA-C25 RU01-01 RU02-01 RU08-01 RU09-01 RRT-C31 RRT-C33

La	101	23.1	27.5	75.0	19.5	49.0	49.8
Ce	191	51.0	60.2	157	41.0	107	111
Pr	20.4	6.3	7.5	18.1	4.9	13.4	13.7
Nd	76.6	26.4	31.7	73.2	21.6	56.9	57.4
Sm	13.0	5.6	6.6	13.9	4.6	11.2	11.1
Eu	4.0	1.8	2.2	4.6	1.5	3.6	3.5
Gd	11.6	5.5	6.3	13.1	4.5	10.3	10.2
Tb	1.5	0.8	0.9	1.8	0.7	1.5	1.4
Dy	7.6	4.4	5.1	9.4	3.7	7.6	7.3
Ho	1.4	0.9	0.9	1.8	0.7	1.4	1.3
Er	3.0	2.0	2.2	4.2	1.6	3.1	3.1
Tm	0.4	0.3	0.3	0.6	0.2	0.4	0.4
Yb	2.4	1.7	1.9	3.4	1.4	2.6	2.6
Lu	0.3	0.2	0.3	0.5	0.2	0.3	0.3
Rb	48.8	6.6	7.2	33.3	8.4	22.7	23.7
Sr	1115	364	431	1038	297	870	897
Y	38.1	20.7	24.8	60.5	18.2	36.5	36.2
Cs	0.6	0.1	0.1	0.3	0.2	0.2	0.2
Ba	554	114	166	375	116	284	300
Pb	6.5	1.3	2.0	2.7	1.1	2.4	2.4
Th	13.9	2.4	3.0	6.3	2.0	4.7	4.9
U	3.6	0.7	0.9	1.7	0.6	1.4	1.5
Be	2.5	1.3	1.0	1.5	0.7	1.3	2.7
Zr	223	102	138	337	103	216	260
Nb	116	25.7	37.9	81.3	24.3	53.3	63.5
Hf	5.4	2.7	4.0	8.7	3.0	5.2	6.0
Ta	7.1	1.7	3.0	5.9	1.7	3.6	3.9

Table D-2. Trace and rare earth element concentrations for cpx samples.

Sample	RTG-C4	RTG-C5	RTG-C8	RTG-C10	RTG-C10		MGA-C8
					Core	Rim	
La	4.0	4.1	7.9	3.2	7.5	2.1	
Ce	15.0	15.1	28.5	11.1	25.7	7.7	
Pr	2.8	2.8	5.3	2.0	4.7	1.4	
Nd	16.6	14.9	29.5	10.9	24.8	7.8	
Sm	5.0	4.2	8.4	3.1	6.8	2.3	
Eu	1.7	1.5	2.7	1.1	2.2	0.8	
Gd	4.9	4.3	8.1	3.0	6.5	2.4	
Tb	0.7	0.6	1.1	0.4	0.9	0.4	
Dy	3.8	3.2	5.8	2.4	5.1	2.1	
Ho	0.6	0.5	0.9	0.4	0.8	0.4	
Er	1.3	1.1	1.9	0.8	1.8	0.8	
Tm	0.2	0.1	0.2	0.1	0.2	0.1	
Yb	0.8	0.7	1.3	0.6	1.3	0.6	
Lu	0.1	0.1	0.2	0.1	0.2	0.1	
Rb	0.05	0.1	0.1	0.1	0.1	0.03	
Sr	93.5	113	133	88.6	126	54.4	
Y	16.0	14.8	25.0	10.6	24.1	9.3	
Cs							
Ba	1.3	0.8	1.6	1.6	1.4	0.3	
Pb	0.1	0.1	0.1	0.1	0.1	0.1	
Th	0.1	0.1	0.1	0.1	0.1	0.03	
U	0.01	0.01	0.01	0.01	0.02		
Be	0.2	0.2	0.3	0.1		0.1	
Zr	37.0	25.7	56.2	14.0		6.9	
Nb	1.1	0.6	1.4	0.4		0.4	
Hf	1.9	1.3	2.7	0.7		0.4	
Ta	0.1	0.1	0.2	0.04		0.04	

Table D-2. (Continued)

Sample	MGA-C12	MGA-C23	MGA-C29	TU01-01 Core	TU01-01 Rim	TU09-01
La	3.1	3.2	2.6	2.9	6.0	5.3
Ce	11.2	11.8	9.8	10.0	20.8	18.4
Pr	2.1	2.2	1.9	1.8	3.6	3.2
Nd	11.6	12.1	10.7	9.8	19.4	16.8
Sm	3.4	3.5	3.3	2.7	5.3	4.4
Eu	1.2	1.2	1.1	0.9	1.7	1.5
Gd	3.6	3.6	3.5	2.9	5.3	4.4
Tb	0.5	0.5	0.5	0.4	0.8	0.6
Dy	3.0	2.9	2.9	2.4	4.6	3.3
Ho	0.5	0.5	0.5	0.4	0.8	0.5
Er	1.1	1.1	1.2	0.9	1.8	1.1
Tm	0.1	0.1	0.1	0.1	0.2	0.1
Yb	0.8	0.8	0.9	0.7	1.4	0.8
Lu	0.1	0.1	0.1	0.1	0.2	0.1
Rb	0.1	0.1	0.1	0.1	0.2	0.04
Sr	60.5	63.5	55.7	60.6	75.4	105
Y	13.3	14.0	14.0	11.6	21.4	15.2
Cs						
Ba	0.7	1.1	1.0	0.2	1.2	0.5
Pb	0.1	0.05	0.04	0.1	0.1	0.1
Th	0.05	0.05	0.04	0.04	0.1	0.1
U	0.01	0.01	0.01	0.01	0.02	0.01
Be	0.1	0.1	0.2	0.1	0.2	0.3
Zr	11.4	17.7	22.2	14.9	41.3	31.3
Nb	0.7	0.9	0.8	0.4	1.0	0.9
Hf	0.6	0.9	1.0	0.8	2.2	1.7
Ta	0.1	0.1	0.1	0.05	0.2	0.1

Table D-2. (Continued)

Sample TU12-01 RU01-01 RU02-01 RU09-01

La	2.8	1.9	2.1	1.9
Ce	9.6	7.1	7.5	6.9
Pr	1.7	1.3	1.4	1.2
Nd	9.2	7.7	7.9	7.1
Sm	2.6	2.5	2.5	2.3
Eu	0.9	0.9	0.8	0.8
Gd	2.7	2.7	2.6	2.5
Tb	0.4	0.4	0.4	0.4
Dy	2.3	2.5	2.3	2.3
Ho	0.4	0.4	0.4	0.4
Er	0.9	1.0	0.9	0.9
Tm	0.1	0.1	0.1	0.1
Yb	0.7	0.7	0.7	0.7
Lu	0.1	0.1	0.1	0.1
Rb	0.1	0.03	0.1	0.4
Sr	57.4	45.9	49.8	48.1
Y	10.6	10.7	11.2	10.7
Cs				
Ba	0.5	1.6	0.4	5.7
Pb	0.1	0.02	0.02	0.04
Th	0.1	0.02	0.03	0.1
U	0.01			0.02
Be	0.1	0.1	0.1	0.1
Zr	7.3	16.0	12.0	15.4
Nb	0.5	0.7	0.6	1.3
Hf	0.4	0.9	0.7	0.8
Ta	0.1	0.1	0.1	0.1

Table D-3. Sr and Nd isotope analyses for cpx samples.

Sample	$^{87}\text{Sr}/^{86}\text{Sr}$	error (2σ)	$^{143}\text{Nd}/^{144}\text{Nd}$	error (2σ)	ϵ_{Nd}
RTG-C4	0.704067	10	0.512696	10	1.1
RTG-C5	0.704403	8	0.512692	12	1.1
RTG-C8	0.704128	9	0.512717	13	1.5
RTG-C10 core	0.704034	10	0.512716	15	1.5
RTG-C10 rim	0.704061	10	0.512729	11	1.8
MGA-C8	0.702733	8	0.512863	10	4.4
MGA-C12	0.702731	9	0.512845	16	4.0
MGA-C23	0.702746	12	0.512868	12	4.5
MGA-C29	0.702742	8	0.512807	17	3.3
TU01-01 core	0.702731	9	0.512898	12	5.1
TU01-01 rim	0.702713	9	0.512920	11	5.5
TU09-01	0.702766	10	0.512895	12	5.0
TU12-01	0.702734	10	0.512869	12	4.5
RU01-01	0.702751	9	0.512878	12	4.7
RU02-01	0.702720	9	0.512846	14	4.1
RU09-01	0.702725	9	0.512881	15	4.7

Table D-4. Noble gas abundances and isotope ratios obtained by heating method.

	weight(g)		Temp.	4He (E-9cc/g)	20Ne (E-12cc/g)	36Ar (E-12cc/g)	84Kr (E-12cc/g)	132Xe (E-12cc/g)	40Ar excess (E-9cc/g)
RTG-C5 ol (M)	2.096	Unleached	700deg	6.29	3.60	41.0	0.901	0.0699	1.56
			1850deg	1.03	51.2	146	3.92	0.422	
			total	7.32	54.8	187	4.82	0.492	
RTG-C10 ol (M)	1.926	Unleached	700deg	5.21	5.75	395	18.4	2.22	55.4
			1850deg	62.1	127	325	17.0	3.12	
			total	67.3	133	720	35.4	5.34	
MGA-C8 ol (M)	2.392	Unleached	700deg	22.5	4.93	505	21.1	1.43	21.6
			1850deg	67.9	49.8	225	21.3	5.47	
			total	90.3	54.7	730	42.4	6.90	
MGA-C12 ol (M)	3.032	Unleached	700deg	103	7.10	542	22.9	3.16	23.7
			1850deg	52.6	66.0	232	21.2	4.81	
			total	156	73.1	774	44.2	7.97	
MGA-C12 cpx	1.500	Unleached	700deg	154	36.2	60.8	2.17	0.319	3.67
			1800deg	78.8	44.8	169	9.38	1.73	38.2
			total	233	81.0	230	11.6	2.05	41.9
MGA-C12 cpx	1.508	Leached	700deg	143	10.5	37.6	1.60	0.211	6.58
			1800deg	85.0	24.4	61.9	3.35	0.670	28.3
			total	228	34.9	99.5	4.95	0.881	34.8
MGA-C29 cpx	2.979	Leached	800deg	137	13.6	32.5	1.88	0.586	4.93
			1700deg	53.2	47.0	99.9	5.05	0.930	31.6
			total	191	60.5	132	6.93	1.52	36.5
TU01-01 ol (M)	1.609	Unleached	700deg	55.3	7.54	361	16.6	2.39	207
			1850deg	246	73.2	190	13.8	3.82	
			total	301	80.7	551	30.5	6.22	
TU09-01 ol (M)	2.068	Unleached	700deg	98.3	6.57	146	5.82	0.929	11.5
			1850deg	25.1	75.8	189	7.96	1.65	
			total	123	82.3	334	13.8	2.58	

Table D-4. (Continued)

weight(g)			Temp.	4He (E-9cc/g)	20Ne (E-12cc/g)	36Ar (E-12cc/g)	84Kr (E-12cc/g)	132Xe (E-12cc/g)	40Ar excess (E-9cc/g)
TU12-01 ol (M)	1.512	Unleached	700deg	23.5	7.22	758	37.6	4.56	
			1850deg	34.7	54.0	190	19.3	4.42	
			total	58.2	61.2	948	56.9	8.99	25.6
RU01-01 ol (M)	2.091	Unleached	700deg	13.2	21.7	1116	51.9	5.43	
			1850deg	124	48.2	180	27.6	5.96	
			total	137	69.9	1296	79.5	11.4	326
RU02-01 ol (M)	2.041	Unleached	700deg	5.06	10.7	1105	57.0	7.27	
			1850deg	33.9	47.0	165	22.7	5.79	
			total	39.0	57.7	1269	79.7	13.1	28.4
RU09-01 ol (M)	2.409	Unleached	700deg	24.0	9.56	1020	47.2	5.91	
			1850deg	70.4	55.9	278	34.2	9.29	
			total	94.3	65.5	1298	81.3	15.2	42.1
RU09-01 ol	0.728	Leached	700deg	9.15	20.1	542	34.3	10.7	7.02
			1850deg	161	46.7	447	44.6	22.3	95.3
			total	170	66.8	990	78.9	32.9	102
RRT-C31 ol	1.672	Leached	800deg	1.13	1.54	14.3	0.529	0.0584	0.109
			1850deg	5.38	57.7	33.2	0.967	0.199	6.43
			total	6.51	59.3	47.5	1.50	0.257	6.54
TA01-02 cpx	1.522	Leached	800deg	6.79	34.2	82.6	3.57	0.467	0.99
			1700deg	7.78	262	696	23.8	4.36	10.8
			total	14.6	296	778	27.4	4.82	11.8
MO01-01 ol	1.856	Leached	800deg	1.34	10.7	28.3	0.718	0.135	1.03
			1850deg	3.78	39.6	84.5	2.38	0.248	8.39
			total	5.12	50.2	113	3.10	0.382	9.42
TU01-01 GM (Ground mass)	1.109	Unleached	700deg	1598	418	208	23.7	16.3	56.9
			1800deg	121	113	217	19.9	11.6	216
			total	1718	530	425	43.5	27.8	273

Table D-4. (Continued)

	R/Ra	error (R/Ra)	20Ne/22Ne	error 21Ne/22Ne (20/22)		error (21/22)	38Ar/36Ar	error (38/36)	40Ar/36Ar	error (40/36)
RTG-C5 ol (M)	4.84	1.27					0.1864	0.0009	300.3	0.2
	22.4	3.5					0.1855	0.0022	304.8	0.7
	8.82						0.1857		303.8	
RTG-C10 ol (M)	9.57	0.97					0.1870	0.0006	297.0	0.1
	5.97	0.11					0.1858	0.0011	466.4	0.5
	6.43						0.1864		372.5	
MGA-C8 ol (M)	2.76	0.22					0.1864	0.0002	299.5	0.1
	7.51	0.07					0.1858	0.0016	384.2	0.7
	6.43						0.1862		325.1	
MGA-C12 ol (M)	0.420	0.037					0.1862	0.0003	299.8	0.1
	4.75	0.09					0.1868	0.0012	387.9	0.5
	1.93						0.1863		326.1	
MGA-C12 cpx	0.341	0.033	9.98	0.13	0.0300	0.0010	0.1870	0.0006	355.8	1.5
	1.72	0.15	9.55	0.11	0.0392	0.0014	0.1877	0.0004	521.8	1.9
	0.807		9.74		0.0351		0.1875		477.8	
MGA-C12 cpx	0.389	0.055	10.02	0.23	0.0317	0.0016	0.1874	0.0006	470.7	1.7
	1.70	0.13	9.87	0.14	0.0480	0.0018	0.1880	0.0006	751.8	3.2
	0.880		9.91		0.0431		0.1878		645.6	
MGA-C29 cpx	0.125	0.013	9.75	0.15	0.0287	0.0012	0.1877	0.0004	447.3	1.7
	1.27	0.08	9.90	0.09	0.0343	0.0008	0.1877	0.0004	611.9	2.2
	0.445		9.87		0.0330		0.1877		571.5	
TU01-01 ol (M)	3.07	0.18					0.1864	0.0007	303.2	0.2
	8.16	0.13					0.1885	0.0026	1325	3
	7.27						0.1872		670.8	
TU09-01 ol (M)	1.73	0.08					0.1874	0.0009	316.0	0.2
	12.4	0.3					0.1854	0.0017	340.4	0.6
	3.99						0.1863		330.0	

Table D-4. (Continued)

	R/Ra	error (R/Ra)	$^{20}\text{Ne}/^{22}\text{Ne}$	error $^{21}\text{Ne}/^{22}\text{Ne}$ (20/22)		error (21/22)	$^{38}\text{Ar}/^{36}\text{Ar}$	error (38/36)	$^{40}\text{Ar}/^{36}\text{Ar}$	error (40/36)
TU12-01 ol (M)	1.55	0.26					0.1871	0.0004	296.9	0.1
	7.15	0.24					0.1858	0.0022	422.7	0.9
	3.70						0.1868		322.5	
RU01-01 ol (M)	2.02	0.37					0.1872	0.0004	296.0	0.1
	6.72	0.14					0.1887	0.0024	1193	3
	6.35						0.1876		546.9	
RU02-01 ol (M)	2.96	0.77					0.1863	0.0007	294.6	0.2
	7.56	0.12					0.1861	0.0019	473.5	0.8
	7.26						0.1863		317.9	
RU09-01 ol (M)	1.36	0.15					0.1871	0.0004	297.3	0.1
	6.61	0.08					0.1870	0.0015	432.6	0.6
	5.38						0.1871		328.0	
RU09-01 ol	2.09	0.19					0.1875	0.0002	308.4	2.0
	6.69	0.35	9.40	0.20	0.0322	0.0012	0.1881	0.0006	508.7	3.5
	6.44		9.40		0.0322		0.1878		398.9	
RRT-C31 ol	20.2	3.4					0.1861	0.0013	303.1	2.4
	43.6	2.8	9.67	0.14	0.0499	0.0020	0.1863	0.0006	489.0	3.8
	39.6		9.67		0.0499		0.1863		433.1	
TA01-02 cpx	0.360	0.033	9.95	0.20	0.0287	0.0019	0.1873	0.0005	307.4	2.0
	4.93	0.26	9.51	0.11	0.0283	0.0007	0.1882	0.0002	311.0	2.0
	2.80		9.56		0.0283		0.1881		310.6	
MO01-01 ol	6.06	1.02	10.04	0.20	0.0313	0.0017	0.1858	0.0007	332.0	2.3
	10.7	0.7	9.60	0.17	0.0324	0.0015	0.1867	0.0006	394.8	2.7
	9.49		9.69		0.0322		0.1864		379.1	
TU01-01 GM (Ground mass)	0.184	0.015	9.82	0.08	0.0294	0.0006	0.1875	0.0004	569.2	2.2
	1.39	0.08	9.47	0.09	0.0450	0.0011	0.1884	0.0005	1293	5
	0.269		9.74		0.0327		0.1879		938.4	

Table D-4. (Continued)

	F78	F80	F82	F83	F86	error (F78)	error (F80)	error (F82)	error (F83)	error (F86)
RTG-C5 ol (M)	1.089 0.963 0.986	1.059 0.990 1.002	0.981 1.011 1.006	0.984 1.008 1.004	0.994 0.989 0.990	0.047 0.031	0.038 0.037	0.023 0.018	0.034 0.027	0.012 0.013
RTG-C10 ol (M)	1.014 1.015 1.014	1.043 1.033 1.038	1.028 1.017 1.022	1.024 1.015 1.019	1.003 0.999 1.001	0.014 0.018	0.005 0.011	0.004 0.007	0.003 0.008	0.003 0.006
MGA-C8 ol (M)	1.028 1.041 1.035	1.054 1.034 1.043	1.033 1.029 1.030	1.018 1.020 1.019	0.998 1.004 1.001	0.015 0.019	0.005 0.007	0.003 0.004	0.004 0.006	0.002 0.005
MGA-C12 ol (M)	1.032 1.017 1.024	1.068 1.039 1.054	1.041 1.031 1.036	1.030 1.024 1.027	1.005 1.006 1.005	0.012 0.011	0.005 0.008	0.003 0.005	0.002 0.006	0.002 0.004
MGA-C12 cpx	0.966 1.017 1.007	1.003 1.003 1.003	0.996 0.998 0.998	0.997 0.999 0.998	0.999 0.997 0.998	0.056 0.031	0.041 0.013	0.013 0.007	0.021 0.007	0.012 0.005
MGA-C12 cpx	0.979 1.013 1.002	0.998 1.010 1.006	1.001 0.996 0.998	1.000 0.997 0.998	0.998 0.998 0.998	0.075 0.043	0.026 0.022	0.013 0.012	0.012 0.007	0.012 0.007
MGA-C29 cpx	1.027 1.003 1.010	0.993 0.995 0.995	0.999 0.991 0.993	0.993 0.998 0.996	1.004 0.995 0.997	0.043 0.036	0.016 0.011	0.013 0.011	0.018 0.005	0.013 0.009
TU01-01 ol (M)	0.988 1.003 0.994	1.060 1.003 1.036	1.025 1.007 1.017	1.009 1.008 1.009	0.995 1.001 0.998	0.019 0.016	0.006 0.013	0.005 0.006	0.009 0.013	0.004 0.008
TU09-01 ol (M)	0.963 1.038 1.006	1.039 0.996 1.014	1.013 1.014 1.013	1.013 1.001 1.006	0.984 1.001 0.994	0.041 0.027	0.014 0.010	0.007 0.009	0.005 0.014	0.003 0.007

Table D-4. (Continued)

	F78	F80	F82	F83	F86	error (F78)	error (F80)	error (F82)	error (F83)	error (F86)
TU12-01 ol (M)	1.031 1.020 1.028	1.049 1.002 1.033	1.030 1.023 1.028	1.021 1.012 1.018	1.005 1.000 1.003	0.010 0.021	0.005 0.012	0.005 0.007	0.003 0.012	0.003 0.005
RU01-01 ol (M)	1.033 0.997 1.027	1.052 1.019 1.046	1.029 1.020 1.027	1.020 1.009 1.018	1.000 0.994 0.999	0.020 0.020	0.009 0.014	0.003 0.007	0.004 0.015	0.002 0.006
RU02-01 ol (M)	1.044 1.035 1.041	1.074 1.026 1.060	1.044 1.029 1.040	1.038 1.020 1.032	1.015 1.004 1.012	0.013 0.022	0.008 0.008	0.002 0.004	0.002 0.005	0.002 0.003
RU09-01 ol (M)	1.057 1.026 1.045	1.083 1.048 1.069	1.049 1.039 1.045	1.040 1.028 1.035	1.015 1.014 1.014	0.014 0.018	0.005 0.008	0.002 0.005	0.003 0.004	0.002 0.003
RU09-01 ol	0.998 0.978 0.987	1.001 0.990 0.995	0.991 0.989 0.990	0.990 0.992 0.991	0.996 0.997 0.996	0.024 0.024	0.009 0.016	0.011 0.013	0.007 0.010	0.006 0.010
RRT-C31 ol	1.039 1.095 1.075	1.002 0.983 0.989	1.007 0.987 0.994	1.007 0.988 0.995	0.994 1.010 1.004	0.207 0.124	0.028 0.030	0.052 0.017	0.030 0.020	0.042 0.010
TA01-02 cpx	1.026 0.973 0.980	1.008 0.972 0.977	0.992 0.979 0.981	0.989 0.987 0.988	0.994 1.002 1.001	0.024 0.021	0.012 0.015	0.013 0.013	0.017 0.010	0.010 0.012
MO01-01 ol	1.064 1.020 1.031	1.012 1.002 1.005	0.973 0.989 0.986	0.991 0.989 0.989	0.994 1.002 1.000	0.085 0.073	0.047 0.019	0.028 0.018	0.025 0.014	0.022 0.009
TU01-01 GM (Ground mass)	1.017 0.986 1.003	0.998 0.995 0.996	0.999 0.998 0.999	0.996 0.999 0.997	1.002 1.002 1.002	0.028 0.027	0.012 0.014	0.006 0.006	0.007 0.008	0.005 0.006

Table D-4. (Continued)

	F124	F126	F128	F129	F130	F131	F134	F136	error (F124)	error (F126)	error (F128)	error (F129)	error (F130)	error (F131)	error (F134)	error (F136)
RTG-C5 ol (M)	0.396 0.839 0.782	0.709 0.989 0.953	0.967 0.949 0.952	1.013 0.986 0.990	1.043 0.961 0.972	1.027 0.969 0.976	0.984 1.001 0.999	1.031 0.982 0.988	0.135 0.172	0.266 0.108	0.110 0.021	0.041 0.023	0.051 0.028	0.055 0.024	0.057 0.015	0.050 0.012
RTG-C10 ol (M)	0.982 1.014 1.001	0.971 0.951 0.959	0.984 0.983 0.984	0.994 0.997 0.996	0.980 0.989 0.986	0.990 0.985 0.987	1.013 1.012 1.013	0.992 0.994 0.993	0.053 0.050	0.062 0.058	0.013 0.014	0.005 0.005	0.009 0.008	0.009 0.004	0.005 0.004	0.008 0.008
MGA-C8 ol (M)	0.931 1.001 0.986	1.022 1.008 1.011	0.981 0.988 0.987	0.992 0.998 0.997	0.985 0.999 0.997	0.979 0.997 0.993	0.995 1.006 1.003	0.985 0.997 0.995	0.048 0.037	0.094 0.045	0.021 0.010	0.006 0.005	0.014 0.008	0.008 0.004	0.013 0.005	0.013 0.006
MGA-C12 ol (M)	0.964 1.023 1.000	0.997 1.001 1.000	1.001 0.990 0.994	0.985 0.993 0.990	0.985 0.994 0.990	0.987 0.993 0.991	1.007 1.014 1.012	0.992 0.997 0.995	0.040 0.046	0.046 0.049	0.012 0.008	0.004 0.004	0.008 0.005	0.003 0.004	0.007 0.004	0.008 0.006
MGA-C12 cpx	0.959 0.987 0.983	0.986 1.008 1.005	1.033 0.999 1.005	0.989 0.998 0.996	0.984 1.010 1.006	0.994 0.997 0.996	1.026 1.001 1.005	1.007 0.997 0.999	0.338 0.120	0.266 0.158	0.059 0.021	0.021 0.011	0.028 0.021	0.026 0.015	0.034 0.014	0.038 0.014
MGA-C12 cpx	1.125 0.902 0.955	1.059 0.878 0.921	0.998 1.014 1.010	0.982 1.012 1.005	0.997 1.001 1.000	0.981 0.993 0.990	0.984 0.990 0.989	0.993 0.986 0.987	0.542 0.148	0.262 0.164	0.077 0.050	0.033 0.023	0.059 0.042	0.040 0.031	0.037 0.025	0.041 0.033
MGA-C29 cpx	1.020 1.091 1.064	0.952 1.046 1.010	1.034 1.010 1.019	1.001 1.002 1.002	1.009 1.003 1.005	0.998 0.997 0.997	0.988 1.001 0.996	1.000 0.996 0.997	0.060 0.127	0.104 0.155	0.038 0.024	0.023 0.008	0.021 0.017	0.018 0.013	0.017 0.015	0.019 0.012
TU01-01 ol (M)	0.993 0.995 0.994	0.973 1.096 1.046	0.988 0.989 0.989	0.998 1.001 1.000	0.988 1.008 1.000	0.996 0.996 0.996	1.014 1.021 1.018	1.001 1.005 1.004	0.058 0.041	0.053 0.073	0.020 0.018	0.007 0.006	0.016 0.017	0.013 0.006	0.007 0.006	0.009 0.007
TU09-01 ol (M)	0.963 1.014 0.995	1.024 0.959 0.982	1.006 0.990 0.996	1.001 0.989 0.993	0.984 0.971 0.976	0.990 0.990 0.990	0.989 1.006 1.000	1.005 0.997 1.000	0.085 0.063	0.103 0.061	0.015 0.024	0.007 0.006	0.013 0.020	0.011 0.007	0.007 0.006	0.010 0.010

Table D-4. (Continued)

	F124	F126	F128	F129	F130	F131	F134	F136	error (F124)	error (F126)	error (F128)	error (F129)	error (F130)	error (F131)	error (F134)	error (F136)
TU12-01 ol (M)	1.095 0.971 1.028	1.026 0.971 0.997	0.996 0.987 0.991	0.995 0.989 0.992	1.001 0.976 0.988	0.999 0.999 0.999	1.006 1.004 1.005	0.999 0.992 0.995	0.041 0.451	0.069 0.308	0.009 0.011	0.006 0.006	0.010 0.013	0.003 0.005	0.011 0.006	0.007 0.007
RU01-01 ol (M)	1.019 1.005 1.012	0.967 0.990 0.979	0.987 0.992 0.990	0.989 0.998 0.994	0.986 0.998 0.992	0.989 0.990 0.989	1.012 1.013 1.012	0.993 1.000 0.997	0.027 0.032	0.051 0.050	0.008 0.011	0.003 0.003	0.005 0.008	0.003 0.004	0.003 0.004	0.006 0.007
RU02-01 ol (M)	1.002 1.019 1.010	0.976 1.021 0.997	0.983 0.985 0.984	0.990 0.993 0.991	0.986 0.992 0.989	0.994 0.990 0.992	1.013 1.015 1.014	1.000 1.005 1.002	0.040 0.026	0.056 0.053	0.008 0.008	0.002 0.003	0.011 0.006	0.004 0.004	0.006 0.004	0.006 0.008
RU09-01 ol (M)	1.003 1.028 1.018	1.020 1.021 1.020	0.999 0.990 0.994	0.993 0.993 0.993	0.999 0.997 0.998	0.993 0.996 0.995	1.008 1.014 1.011	0.999 1.006 1.003	0.027 0.036	0.044 0.047	0.012 0.009	0.003 0.004	0.008 0.005	0.005 0.004	0.005 0.004	0.006 0.005
RU09-01 ol	0.927 0.942 0.937	0.966 1.039 1.016	0.973 0.981 0.979	0.993 0.993 0.993	0.992 0.992 0.992	1.000 0.999 1.000	1.002 1.011 1.008	1.008 1.013 1.011	0.118 0.075	0.096 0.127	0.015 0.020	0.010 0.010	0.007 0.006	0.011 0.008	0.011 0.008	0.013 0.012
RRT-C31 ol	1.699 1.324 1.409	0.972 1.075 1.052	0.975 0.984 0.982	0.963 0.997 0.989	1.025 0.988 0.996	1.004 1.001 1.002	1.008 1.018 1.016	0.992 1.000 0.998	0.528 0.217	0.414 0.400	0.124 0.098	0.051 0.036	0.113 0.048	0.048 0.023	0.051 0.056	0.067 0.055
TA01-02 cpx	1.075 0.947 0.959	0.887 0.973 0.965	0.998 0.985 0.986	1.007 0.993 0.995	0.994 0.998 0.997	0.992 1.001 1.000	1.015 1.007 1.007	0.996 1.009 1.008	0.282 0.113	0.220 0.105	0.067 0.017	0.033 0.008	0.032 0.009	0.022 0.011	0.046 0.010	0.031 0.012
MO01-01 ol	1.500 1.336 1.394	1.199 0.970 1.051	1.021 1.009 1.013	1.003 1.007 1.006	1.043 0.998 1.014	1.007 1.016 1.013	1.042 1.014 1.024	1.011 1.021 1.018	0.336 0.291	0.640 0.330	0.079 0.069	0.035 0.038	0.054 0.034	0.054 0.029	0.047 0.039	0.055 0.020
TU01-01 GM (Ground mass)	0.979 1.029 1.000	0.985 1.024 1.001	1.005 0.995 1.001	1.001 0.997 0.999	1.003 0.999 1.001	0.999 0.999 0.999	0.998 1.002 1.000	1.003 1.005 1.004	0.088 0.066	0.045 0.071	0.014 0.015	0.005 0.006	0.006 0.009	0.004 0.005	0.007 0.007	0.011 0.009

Table D-5. Noble gas abundances and isotope ratios obtained by crushing method.

	weight(g)		⁴ He (E-9cc/g)	²⁰ Ne (E-12cc/g)	³⁶ Ar (E-12cc/g)	⁸⁴ Kr (E-12cc/g)	¹³² Xe (E-12cc/g)	⁴⁰ Ar excess (E-9cc/g)
RTG-C4 cpx	1.303	Leached	3.59	44.6	46.2	1.34	0.148	5.89
RTG-C5 ol	1.248	Leached	N.D.	45.8	187	4.05	0.221	0.958
RTG-C5 cpx	0.797	Leached	N.D.	135	312	7.05	0.404	9.80
RTG-C8 cpx	1.395	Leached	N.D.	22.1	53.1	1.94	0.497	0.387
RTG-C10 cpx	1.383	Leached	N.D.	31.5	122	4.60	0.511	4.06
MGA-C12 cpx	1.067	Unleached	5.57					
MGA-C12 ol	0.564	Unleached	7.97	4.72	47.5	3.28	1.58	7.06
MGA-C23 cpx	1.328	Leached	3.61	25.4	42.2	1.11	0.115	4.65
MGA-C29 ol	0.515	Leached	12.1	39.5	605	12.9	0.580	47.3
TU01-01 cpx	1.490	Leached	13.9	40.6	99.4	3.67	0.595	6.65
TU09-01 cpx	1.303	Leached	2.70	11.5	35.7	1.02	0.161	1.12
TU12-01 cpx	1.300	Leached	189	74.9	136	4.38	0.613	144
RU01-01 ol	0.728	Leached	16.2					
RU02-01 cpx	1.091	Leached	8.56	31.3	166	4.03	0.348	2.46
RU09-01 ol	1.542	Leached	37.8	5.76	29.0	0.945	0.144	15.0
RRT-C31 ol	0.767	Leached	4.25	55.2	72.4	1.71	0.159	3.06
RRT-C33 ol	1.517	Leached	2.20	62.6	196	4.13	0.205	2.92
MO01-01 ol	0.852	Leached	1.33	33.6	64.4	1.64	0.127	4.72
TA01-02 cpx	1.490	Leached	1.59	26.6	65.4	1.60	0.143	0.574

Table D-5. (Continued)

	R/Ra	error(R/Ra)	20Ne/22Ne	error 21Ne/22Ne (20/22)	error (21/22)	38Ar/36Ar	error (38/36)	40Ar/36Ar	error (40/36)	
RTG-C4 cpx	9.30	0.83	9.82	0.20	0.0291	0.0015	0.1866	0.0006	422.9	2.8
RTG-C5 ol			9.70	0.15	0.0284	0.0017	0.1866	0.0003	300.6	1.9
RTG-C5 cpx			9.66	0.14	0.0285	0.0014	0.1872	0.0002	326.9	2.1
RTG-C8 cpx			9.91	0.25	0.0295	0.0021	0.1864	0.0006	302.8	2.0
RTG-C10 cpx			9.80	0.19	0.0295	0.0016	0.1875	0.0004	328.6	2.1
MGA-C12 cpx	6.77	0.45								
MGA-C12 ol	6.06	0.61								
MGA-C23 cpx	6.99	1.04	9.81	0.20	0.0297	0.0018	0.1881	0.0007	444.2	2.4
MGA-C29 ol	5.39	0.80	9.68	0.16	0.0308	0.0013	0.1857	0.0012	405.6	2.8
							0.1869	0.0004	373.7	1.6
TU01-01 cpx	6.94	0.52	9.73	0.17	0.0292	0.0018	0.1870	0.0005	362.4	2.3
TU09-01 cpx	7.52	0.77	10.05	0.28	0.0305	0.0027	0.1873	0.0006	326.8	2.3
TU12-01 cpx	7.16	0.33	9.67	0.15	0.0308	0.0008	0.1877	0.0003	1354	9
RU01-01 ol	6.83	0.33								
RU02-01 cpx	6.83	0.77	9.78	0.18	0.0288	0.0018	0.1869	0.0004	310.3	2.0
RU09-01 ol	7.60	0.36					0.1881	0.0008	812.9	5.9
RRT-C31 ol	9.46	1.17	9.86	0.19	0.0286	0.0016	0.1858	0.0009	337.8	2.3
RRT-C33 ol	8.92	1.08	9.63	0.13	0.0284	0.0011	0.1864	0.0004	310.3	2.0
MO01-01 ol	17.0	1.6	9.90	0.19	0.0298	0.0023	0.1861	0.0007	368.7	2.5
TA01-02 cpx	10.4	0.8	9.95	0.20	0.0292	0.0019	0.1867	0.0004	304.3	2.0

Table D-6. Noble gas abundances and He and Ar isotope ratios obtained by stepwise tests for unleached and leached cpx samples of MGA-C12 and TU01-01.

	Weight(g)	Temp.	4He (E-9cc/g)	20Ne (E-12cc/g)	36Ar (E-12cc/g)	84Kr (E-12cc/g)	132Xe (E-12cc/g)
MGA-C12 cpx (unleached)	1.865	600	88.7	18.6	39.0	1.41	0.0402
		700	55.0	10.6	18.0	0.632	0.0140
		800	28.6	6.70	29.4	0.916	0.0234
		1000	13.2	4.10	28.8	1.68	0.0419
		1200	8.38	2.65	25.1	1.94	0.0723
		1400	12.0	16.2	44.9	3.71	0.206
		1600	0.0177	1.53	1.76	0.067	0.00757
		1800	0.0561	1.56	0.927	0.029	0.00143
		total	206	62.0	188	10.4	0.407
MGA-C12 cpx (leached)	1.787	600	82.1	17.6	42.9	1.44	0.0481
		700	57.6	4.48	11.2	0.545	0.0136
		800	33.8	4.20	18.7	0.619	0.0174
		1000	13.2	6.63	9.86	0.414	0.0131
		1200	9.47	3.86	8.25	0.475	0.0231
		1400	10.8	13.4	42.6	1.78	0.0897
		1600	0.123	1.97	2.44	0.102	0.0082
		1800	0.0162	3.88	3.29	0.107	0.00498
		total	207	56.1	139	5.48	0.218
TU01-01 cpx (unleached)	1.535	600	115	27.9	141	5.38	0.163
		700	46.2	8.59	46.7	1.84	0.0346
		800	24.2	9.24	60.1	2.50	0.0683
		1000	12.0	7.29	50.0	4.49	0.143
		1200	5.81	8.99	30.0	2.80	0.145
		1400	18.7	17.3	38.9	3.36	0.212
		1600	0.820	1.50	1.69	0.0932	0.0112
		1800	0.241	2.07	1.74	0.0974	0.00652
		total	223	82.9	371	20.6	0.783
TU01-01 cpx (leached)	1.523	600	108	51.1	137	5.52	0.135
		700	44.8	7.51	41.5	2.10	0.0412
		800	24.6	5.34	42.9	2.83	0.0669
		1000	9.58	3.10	10.2	1.14	0.0484
		1200	7.37	6.86	20.0	0.898	0.0495
		1400	14.0	12.6	28.2	1.67	0.113
		1600	0.323	0.96	1.42	0.067	0.0102
		1800	0.392	0.88	0.144	0.00806	0.00136
		total	209	88.3	281	14.2	0.466

Table D-6. (Continued)

	3He/4He (R/Ra)	error	38Ar/36Ar	error	40Ar/36Ar	error
MGA-C12 cpx (unleached)	0.20	0.02	0.1871	0.0005	345.6	1.7
	0.53	0.04	0.1866	0.0006	398.7	1.9
	1.21	0.16	0.1872	0.0011	365.5	2.4
	1.38	0.13	0.1880	0.0005	402.8	1.6
	1.51	0.12	0.1873	0.0005	430.5	1.9
	3.28	0.38	0.1882	0.0007	717.9	3.7
			0.1873	0.0033	439.4	3.3
			0.1891	0.0032	326.1	3.0
MGA-C12 cpx (leached)	0.16	0.02	0.1869	0.0005	357.3	1.4
	0.54	0.04	0.1877	0.0011	547.7	2.5
	1.30	0.13	0.1873	0.0006	403.1	1.9
	1.38	0.29	0.1873	0.0016	455.7	2.1
	1.61	0.25	0.1866	0.0016	558.1	2.5
	3.32	0.34	0.1874	0.0005	865.8	4.7
			0.1888	0.0018	648.2	4.6
			0.1867	0.0024	387.3	3.1
TU01-01 cpx (unleached)	0.56	0.05	0.1867	0.0004	310.8	1.3
	2.81	0.15	0.1876	0.0004	352.2	1.4
	6.94	0.45	0.1878	0.0006	336.4	1.2
	6.96	0.46	0.1883	0.0006	373.3	1.4
	7.22	0.59	0.1869	0.0010	492.9	3.0
	6.06	0.38	0.1908	0.0009	559.0	2.1
			0.1925	0.0026	1014.3	9.3
			0.1879	0.0026	445.0	3.6
TU01-01 cpx (leached)	0.75	0.05	0.1872	0.0004	315.0	1.3
	3.16	0.17	0.1878	0.0006	379.4	1.6
	8.17	0.54	0.1883	0.0005	394.6	1.7
	8.55	0.73	0.1878	0.0009	501.8	2.3
	6.92	0.61	0.1867	0.0011	385.0	1.6
	5.74	0.36	0.1919	0.0008	592.4	2.8
			0.1982	0.0027	518.5	4.0
			0.1757	0.0048	815.1	11.7

Table D-7. Noble gas abundances and He and Ar isotope ratios obtained by stepwise tests for leached olivine sample of MGA-C12.

	Weight(g)	Temp.	4He (E-9cc/g)	20Ne (E-12cc/g)	36Ar (E-12cc/g)	84Kr (E-12cc/g)	132Xe (E-12cc/g)
MGA-C12 ol (unleached)	1.808	600	1.00	2.95	177	13.6	3.81
		700	12.2	0.939	159	17.3	4.68
		800	51.4	3.88	117	12.0	3.32
		1000	48.3	0.0462	95.1	6.64	1.25
		1200	44.3	1.06	58.1	10.3	3.76
		1400	4.69	0.83	16.7	4.30	2.20
		1600	7.45	1.65	14.1	1.79	1.14
		1850	4.53	39.1	122.6	4.37	0.830
		total	174	50.5	760	70.2	21.0
MGA-C12 ol (unleached)		Temp. 3He/4He (R/Ra)	error 38Ar/36Ar		error 40Ar/36Ar		error
	600			0.1874	0.0002	300.4	1.9
	700	0.07	0.02	0.1879	0.0002	305.8	2.0
	800	0.57	0.04	0.1866	0.0003	319.2	2.0
	1000	0.40	0.03	0.1878	0.0004	315.0	2.0
	1200	2.56	0.24	0.1886	0.0007	432.9	2.8
	1400	6.01	0.51	0.1871	0.0012	436.0	3.0
	1600	5.30	0.32	0.1864	0.0010	696.6	5.0
	1850	6.01	0.44	0.1879	0.0003	377.1	2.4

Table D-8. Noble gas abundances and He, Ne and Ar isotope ratios obtained by rim-core tests for cpx samples of TU01-01 and RTG-C10.

	weight(g)	⁴ He (E-9cc/g)	²⁰ Ne (E-12cc/g)	³⁶ Ar (E-12cc/g)	⁸⁴ Kr (E-12cc/g)	¹³² Xe (E-12cc/g)	⁴⁰ Ar excess (E-9cc/g)
TU01-01 cpx	0.449 800deg	83.6	8.73	66.3	3.65	0.698	1.17
Rim	1700deg	42.3	21.2	129	7.29	1.75	6.62
	total	126	29.9	195	10.9	2.45	7.78
TU01-01 cpx	0.690 800deg	28.8	4.22	116	6.21	0.838	0.850
Core	1700deg	25.8	12.9	144	9.34	2.18	3.40
	total	54.6	17.1	259	15.6	3.01	4.25
RTG-C10 cpx	0.793 800deg	19.1	6.10	32.5	1.94	0.675	0.421
Rim	1700deg	8.59	18.5	105	5.36	1.17	6.45
	total	27.7	24.6	137	7.30	1.85	6.87
RTG-C10 cpx	1.090 800deg	5.11	0.259	25.9	1.37	0.329	0.292
Core	1700deg	3.96	15.3	114	5.50	1.22	6.54
	total	9.06	15.6	140	6.87	1.55	6.84

Table D-8. (Continued)

	R/Ra	error (R/Ra)	20Ne/22Ne	error (20/22)	21Ne/22Ne	error (21/22)	38Ar/36Ar	error (38/36)	40Ar/36Ar	error (40/36)
TU01-01 cpx	3.28	0.32	9.08	0.59	0.0346	0.0045	0.1882	0.0007	313.1	1.3
Rim	7.68	0.44	8.78	0.35	0.103	0.007	0.1881	0.0006	346.8	1.4
	4.76		8.87		0.0828		0.1882		335.3	
TU01-01 cpx	9.10	0.49	8.51	0.56	0.0319	0.0060	0.1875	0.0005	302.9	1.2
Core	13.8	0.9	8.62	0.29	0.140	0.007	0.1875	0.0005	319.2	1.3
	11.3		8.59		0.1135		0.1875		311.9	
RTG-C10 cpx	0.426	0.069	9.14	0.39	0.0295	0.0040	0.1866	0.0009	308.5	1.2
Rim	0.694	0.099	9.69	0.27	0.0286	0.0025	0.1861	0.0005	357.2	1.4
	0.509		9.56		0.0288		0.1862		345.7	
RTG-C10 cpx	1.11	0.24					0.1872	0.0009	306.8	1.2
Core	1.18	0.30	9.90	0.24	0.0330	0.0020	0.1860	0.0005	352.8	1.3
	1.14		9.90		0.0330		0.1862		344.3	

Table D-9. Hot blanks and crushing blanks.

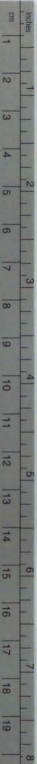
ERI, Tokyo

Date (1996)	Sample	Heating Temp.	Heating Time (minutes)	abundance cm ³ STP/g	4He	20Ne	36Ar	84Kr	132Xe
Low Temp. fraction (700 or 800 deg)									
6-Jun	Hot Blank	700	40	2.319E-09	1.903E-12	1.969E-12	1.128E-13	7.048E-14	
23-Jun	Hot Blank	700	40	3.168E-09	2.234E-12	1.108E-12	2.416E-14	1.674E-14	
9-Jul	Hot Blank	800	40	2.351E-09	2.425E-12	3.087E-12	7.218E-14	5.525E-14	
15-Jul	Hot Blank	800	40	2.877E-09	2.227E-12	1.411E-12	3.034E-14	1.332E-14	
25-Aug	Hot Blank	700	40	4.227E-09	3.498E-12	2.172E-12	2.968E-14	1.225E-14	
1-Sep	Hot Blank	800	40	4.17E-09	2.088E-12	9.002E-13	2.167E-14	8.214E-15	
20-Sep	Hot Blank	700	40	2.855E-09	3.368E-12	1.848E-12	5.628E-14	3.99E-14	
25-Sep	Hot Blank	700	40	3.202E-09	3.341E-12	8.038E-13	N.D.	9.425E-15	
High Temp. fraction (1700 or 1850 deg)									
6-Jun	Hot Blank	1800	20	1.838E-09	2.314E-12	3.212E-12	1.375E-13	7.445E-14	
22-Jun	Hot Blank	1800	20	2.628E-09	3.683E-12	4.573E-12	1.823E-13	5E-14	
8-Jul	Hot Blank	1700	20	2.151E-09	3.59E-12	4.492E-12	1.697E-13	1.015E-13	
15-Jul	Hot Blank	1700	20	2.387E-09	3.14E-12	2.622E-12	7.909E-14	2.585E-14	
24-Aug	Hot Blank	1850	20	3.381E-09	3.95E-12	2.887E-12	3.002E-14	1.784E-14	
1-Sep	Hot Blank	1850	20	3.408E-09	8.906E-12	1.147E-11	3.944E-13	8.991E-14	
19-Sep	Hot Blank	1850	20	2.617E-09	4.538E-12	4.22E-12	1.279E-13	8.005E-14	
25-Sep	Hot Blank	1850	20	2.454E-09	1.856E-11	3.334E-11	9.681E-13	1.603E-13	
Crushing									
8-Jun	Crushing Blank				N.D.	6.79E-13	1.137E-12	2.247E-14	1.338E-14
8-Jul	Crushing Blank				N.D.	1.264E-12	2.418E-12	2.631E-14	1.731E-14
19-Jul	Crushing Blank				N.D.	8.473E-13	8.307E-13	N.D.	1.066E-14
2-Sep	Crushing Blank				N.D.	1.926E-12	1.782E-12	N.D.	6.281E-15
5-Sep	Crushing Blank				N.D.	1.917E-12	1.72E-12	N.D.	7.245E-15
11-Sep	Crushing Blank				N.D.	1.477E-12	4.854E-13	N.D.	N.D.
13-Sep	Crushing blank				N.D.	1.418E-12	1.449E-12	N.D.	7.005E-15
18-Sep	Crushing Blank				N.D.	2.019E-12	1.105E-12	N.D.	4.039E-15
27-Sep	Crushing Blank				N.D.	1.381E-12	9.177E-13	N.D.	5.518E-15

Table D-9. (Continued)

ISEI, Okayama

Date (1994)	Sample	Heating Temp.	Heating Time	abundance cm ³ STP/g	4He	20Ne	36Ar	84Kr	132Xe
Misasa 700deg									
9-Nov	Hot Blank	700	60	4.34E-10	1.18E-12	1.05E-12	1.91E-14	7.47E-15	
14-Nov	Hot Blank	700	60	3.53E-10	2.74E-12	4.71E-13	3.96E-14	1.05E-14	
16-Nov	Hot Blank	700	60	6.09E-10	1.17E-12	1.63E-12	4.42E-14	7.79E-15	
21-Nov	Hot Blank	700	60	6.50E-10	3.61E-12	1.16E-12	4.07E-14	7.53E-15	
Misasa 1850 deg									
9-Nov	Hot Blank	1850	20	3.53E-10	2.23E-12	7.54E-12	1.30E-13	2.43E-14	
11-Nov	Hot Blank	1850	20	4.32E-10	1.79E-11	4.35E-11	8.29E-13	4.96E-14	
15-Nov	Hot Blank	1850	20	4.24E-10	2.94E-12	6.94E-12	1.62E-13	2.15E-14	
21-Nov	Hot Blank	1850	20	4.65E-10	3.69E-11	8.04E-11	1.94E-12	9.58E-14	



Kodak Color Control Patches

© Kodak, 2007 TM-Kodak

Blue

Cyan

Green

Yellow

Red

Magenta

White

3/Color

Black



Kodak Gray Scale



© Kodak, 2007 TM-Kodak

A

1

2

3

4

5

6

M

8

9

10

11

12

13

14

15

B

17

18

19

